ISTANBUL TECHNICAL UNIVERSITY ★ GRADUATE SCHOOL

EXPLORING DRUG LOADING AND RELEASE CAPACITIES OF HEXAGONAL BORON NITRIDES (hBNs) IN CANCER TREATMENT

M.Sc. THESIS

Mısra YAMANSAVAŞÇILAR NAGANLU

Department of Chemical Engineering

Chemical Engineering Programme

JANUARY 2023

ISTANBUL TECHNICAL UNIVERSITY ★ GRADUATE SCHOOL

EXPLORING DRUG LOADING AND RELEASE CAPACITIES OF HEXAGONAL BORON NITRIDES (hBNs) IN CANCER TREATMENT

M.Sc. THESIS

Mısra YAMANSAVAŞÇILAR NAGANLU
(506191020)

Department of Chemical Engineering

Chemical Engineering Programme

Thesis Advisor: Prof. Dr. F. Seniha GÜNER

JANUARY 2023

İSTANBUL TEKNİK ÜNİVERSİTESİ ★ LİSANSÜSTÜ EĞİTİM ENSTİTÜSÜ

HEGZAGONAL BOR NİTRÜRLERİN KANSER TEDAVİSİ İÇİN İLAÇ YÜKLEME VE SALIM KAPASİTELERİNİN ARAŞTIRILMASI

YÜKSEK LİSANS TEZİ

Mısra YAMANSAVAŞÇILAR NAGANLU
(506191020)

Kimya Mühendisliği Anabilim Dalı

Kimya Mühendisliği Programı

Tez Danışmanı: Prof. Dr. F. Seniha GÜNER

OCAK 2023

Mısra YAMANSAVAŞÇILAR NAGANLU, a M.Sc. student of İTU Graduate School student ID 506191020, successfully defended the thesis/dissertation entitled "EXPLORING DRUG LOADING AND RELEASE CAPACITIES OF HEXAGONAL BORON NITRIDES (hBNs) IN CANCER TREATMENT", which she prepared after fulfilling the requirements specified in the associated legislations, before the jury whose signatures are below.

Thesis Advisor :	**Prof. Dr. F. Seniha GÜNER** Istanbul Technical University	.....
Jury Members :	**Prof. Dr. Yüksel AVCIBAŞI GÜVENİLİR** Istanbul Technical University	.....
	Asst. Prof. Banu İYİSAN Boğaziçi University	.....

Date of Submission : 29 December 2022
Date of Defense : 24 January 2023

To my mom,

FOREWORD

First of all, I would like to express my sincere gratitude to my precious advisor Prof. Dr. F. Seniha GÜNER, who allowed me to be a part of her laboratory. She has always provided me with moral support at every moment of my life and always guided me with her very valuable knowledge and experiences.

I would like to thank Dr. Banu KOCAAĞA, whose ideas and knowledge I have benefited from in all my experimental studies. I am lucky to be able to share everything with her as she was just a phone call away from me.

I would like to thank Dr. Hülya YILMAZ for always listening to me, being ready to answer my never-ending questions, and for her support since we met. I would like to thank Dr. Zehra ÇOBANDEDE and Dr. Hülya YILMAZ, who synthesized hBN, for all their help.

I would like to thank Burak TÜRÜDÜ who has been with me in every condition since we started our MSc journey together. I would like to thank Ceren KURÇİN for being with me every moment, and Arçelik lab was full of fun and milestones with her. I also would like to thank Zeynep GÜNER YILMAZ, Anıl YILMAZ, Karya AKBIYIKOĞULLARI, and Berkcan ARSLAN for their friendship and support.

I also give my greater thanks to my dear family, including my mother, Nuray ÖZYAVAŞ, and my brother Dr. Barış YAMANSAVAŞÇILAR for supporting me in every decision I have made throughout my life. I am fortunate to feel their love and support in every step I have taken. Without their support, I would never have come to this day.

Finally, I am appreciative to my dear husband, Taha NAGANLU, for his endless love, patience, and understanding he has shown me during my thesis process. I am very lucky that he motivates me every time I feel sad and gets me back up whenever I fall. Thanks him for always being by my side.

This thesis was funded by Istanbul Technical University Scientific Research Projects (BAP) with project number MGA-2021-43475.

December 2022

Mısra YAMANSAVAŞÇILAR NAGANLU
(Chemical Engineer)

TABLE OF CONTENTS

Page

ABBREVIATIONS

0D	**:** Zero-dimensional
1D	**:** One-dimensional
2D	**:** Two-dimensional
3D	**:** Three-dimensional
AFM	**:** Atomic Force Microscopy
B	**:** Boron
BN	**:** Boron Nitride
BNNR	**:** Boron Nitride Nanoribbon
BNNS	**:** Boron Nitride Nanosheet
BNNT	**:** Boron Nitride Nanotube
C	**:** Carbon
cBN	**:** Cubic boron nitride
CHO	**:** Chinese hamster ovary cell line
CNT	**:** Carbon nanotube
CRL 2120	**:** Human normal skin fibroblast cell line
CVD	**:** Chemical Vapor Deposition
ddH_2O	**:** Double distilled water
DFT	**:** Density Functional Theory
DLS	**:** Dynamic Light Scattering
DOX	**:** Doxorubicin
DPPH	**:** 2,2-diphenyl-1-picrylhydrazyl
DU145	**:** Androgen-independent human prostate adenocarcinoma cell line
EPR	**:** Enhanced Permeability and Retention
FA	**:** Folic acid
FA-BNMS	**:** Folate-conjugated mesoporous silica-functionalized BNNS
FDA	**:** Food and Drug Administration
FT-IR	**:** Fourier Transform Infrared
FU	**:** 5-Fluorouracil
GNR	**:** Graphene Nanoribbon
GO	**:** Graphene oxide
H	**:** Hydrogen
H_3BO_3	**:** Boric acid
HA	**:** Hyaluronic acid
hBN	**:** Hexagonal boron nitride
HCl	**:** Hydrochloric acid
HDFa	**:** Human dermal fibroblast cells
HEK 293	**:** Human embryonic kidney cells
HeLa	**:** Human cervical cancer cell line
HUVECs	**:** Human umbilical vein endothelial cells
ICG	**:** Indocyanine green
KB	**:** Human epithelial carcinoma cell
KCN	**:** Potassium cyanide

LDH : Lactate dehydrogenase
LNCap : Androgen-sensitive human prostate adenocarcinoma cell line
MCF-7 : Human breast adenocarcinoma cell line
MD : Molecular dynamics
MDCK : Madin-Darby canine kidney cell line
MEC : Minimum effective concentration
MS : Multiple sclerosis
MTC : Minimum toxic concentration
MTS : 3-(4,5-dimethylthiazol-2-yl)-5-(3-carboxymethoxyphenyl)-2-(4-sulfophenyl)-2H-tetrazolium
MTT : 3-(4,5-dimethylthiazol-2-yl)-2,5-diphenyltetrazolium bromide) tetrazolium
MTX : Mitoxantrone
MWBNNT : Multi-walled boron nitride nanotube
MWCNT : Multi-walled carbon nanotube
N : Nitrogen
NH_3 : Ammonia
NIH/3T3 : Mouse embryonic fibroblast cells
NRU : Neutral red uptake
O : Oxygen
OH : Hydroxyl
PAH-cit : Poly(allylamine hydrochlorid)-citraconic anhydride
PBS : Phosphate buffer saline
Pd : Palladium
PEG : Polyethilene glycol
PDI : Polydispersity index
rBN : Rhombic boron nitride
RMS : Root mean square
SaOS2 : Human osteosarcoma cell line
SEM : Scanning Electron Microscopy
SRB : Sulforhodamine B colorimetric assay
SWBNNT : Single-walled boron nitride nanotube
SWCNT : Single-walled carbon nanotube
TEM : Transmission Electron Microscopy
TGA : Thermogravimetric Analysis
UV/Vis : Ultraviolet/Visible
wBN : Wurtzite boron nitride
WHO : World Health Organization

SYMBOLS

Å	**:** Angstrom
µg	**:** Microgram
µm	**:** Micrometer
cm	**:** Centimeter
cm^{-1}	**:** Wavenumber
eV	**:** Electronvolt
F	**:** Fraction of drug released
g	**:** Gram
k	**:** Release constant
L	**:** Liter
m	**:** Meter
mg	**:** Milligram
mL	**:** Milliliter
mV	**:** Millivolt
n	**:** Exponent of release
nm	**:** Nanometer
t	**:** Time
u	**:** Particle mobility
v	**:** Volume
w	**:** Weight
ζ	**:** Zeta potential
η	**:** Viscosity of the medium
π	**:** Pi
σ	**:** Sigma
ε	**:** Dielectric constant of water
°C	**:** Degrees celsius
%	**:** Percentage

LIST OF TABLES

Page

LIST OF FIGURES

Page

EXPLORING DRUG LOADING AND RELEASE CAPACITIES OF HEXAGONAL BORON NITRIDES (hBNs) IN CANCER TREATMENT

SUMMARY

Cancer disease is one of the most common and severe diseases caused by uncontrollable cell division, one of the leading causes of death worldwide. Cancer is as old as human history, and no matter how advanced the current treatment methods are, they are still insufficient. The biggest reason for inadequate treatment methods is that cancer is a disease specific to the individual, so appropriate treatment is required. Various nanocarrier systems were used for reducing the side-effects of cancer treatment, to ensure that the drug reaches the targeted area instead of healthy tissues, and to increase the healing rate of patients. This study it is aimed to design a new nanosystem that can be used in cancer treatment. For this purpose, an anticancer drug's loading, and release performance on hexagonal boron nitrides (hBNs), which are small in size, unique in physicochemical, biocompatible, and attract attention in the biomedical field, were investigated under suitable conditions.

In the study, after synthesizing hBNs by a Chemical Vapor Deposition (CVD) method with boric acid, a boron precursor, the spectroscopic and morphological characterization of hBNs were accomplished by using Ultraviolet/Visible (UV/Vis), Fourier Transform Infrared (FT-IR), Transmission Electron Microscopy (TEM), Scanning Electron Microscopy (SEM), Dynamic Light Scattering (DLS), Atomic Force Microscopy (AFM), and Thermogravimetric Analysis (TGA) techniques. According to these characterization techniques, hBNs were obtained with high purity, uniformity, and similar to thrombocytes. In the next step, the drug-hBN interaction was performed as a non-covalent interaction in different pH mediums (6.0 and 9.0) to determine the optimum loading condition. Moreover, drug loading experiments were examined with various drug:hBN ratio (1.25/3.0, 2.5/3.0, 5.0/3.0) in each pH medium. It was found that the most efficient loading conditions occurred at pH 9.0 with a drug:hBN = 5.0/3.0 ratio. According to the results, the maximum loading capacity (32.8%, 0.657 mg/mg) proves that this study achieved an extremely high drug loading efficiency compared to other studies reported in literature. Efficient drug loading has also been established by UV/Vis, FT-IR, SEM, size distribution, and Zeta potential techniques, and all results support each other.

In the study, drug release experiments were achieved by UV/Vis. It was performed in two different pH mediums (4.5 and 7.4) according to the pH of cancer cell tissue (4.5-6.5) and the pH of healthy cell tissues and the bloodstream (7.4). It is desirable from drug delivery systems that the cancer drug should be as stable as possible in the nanocarrier and not be released into the bloodstream except for "minimum drug leakage". In this study, the optimum efficiency of drug release at pH 7.4 medium was obtained by the drug-hBN system with a ratio of 2.5/3.0. Furthermore the amount of drug release was 0 mg/mg in the first 5 minutes and 0.005 mg/mg in the first 24 hours demonstrates that this thesis is a very promising study. In addition, these release results at pH 7.4 were whereas the strong π-π interactions between drug-hBN nanosurfaces,

thus proving that hBNs have significantly superior drug-loading capacity. Moreover, the highest amount of release in pH 4.5 medium was performed as 0.033 mg/mg in the first 5 hours. Once and for all, release kinetic models and drug release kinetics were investigated to support drug release studies. Therefore, Zero Order, First Order, Korsmeyer-Peppas, Higuchi, and Hixson-Crowell Models were used, and the drug release mechanism of each model was explained in detail. In conclusion, it is predicted that the drug-hBN nanosystem designed in this study will be significantly successful in cancer treatment.

HEGZAGONAL BOR NİTRÜRLERİN KANSER TEDAVİSİ İÇİN İLAÇ YÜKLEME VE SALIM KAPASİTELERİNİN ARAŞTIRILMASI

ÖZET

Kanser, dünyadaki ölüm nedenlerinden biri olan, kontrolsüz hücre bölünmesi ile oluşan en ciddi ve yaygın hastalıklardan biridir. Kanser hastalığı, insanlık tarihi kadar eskidir ve mevcut tedavi yöntemleri ne kadar gelişse de hâlâ yetersiz kalmaktadır. Tedavi yöntemlerinin yetersiz kalmasının en büyük sebebi, kanserin kişiye özgü bir hastalık olmasıdır, dolayısıyla etkili bir kanser tedavisi için kişiye özgü uygun bir tedavi gerekmektedir. Ancak tedavi yöntemlerinin birçoğu tümörlü bölgeyi onarırken, aynı zamanda sağlıklı dokulara da zarar verdiği için tedavi süreci hem hasta hem de hasta yakınları açısından zorlaşmaktadır. Dünya Sağlık Örgütü'nün öngördüğü bilgilere göre, 2030 yılına kadar 11,5 milyon kişinin kanser yüzünden hayatını kaybedeceği ve yeni kanser vakalarının çıkabileceği tahmin edilmektedir. Bu doğrultuda kanser tedavisinin yan etkilerini azaltmak, ilacın sağlıklı dokular yerine doğrudan hedeflenen bölgeye ulaşmasını sağlamak ve hastaların iyileşme oranını artırmak amacıyla çeşitli nanotaşıyıcı sistem tasarımları yapılmaktadır. Bu çalışmada, kanser tedavisinde kullanılabilecek yeni bir nanotaşıyıcı sistem tasarlamak amaçlanmıştır. Bu amaç doğrultusunda, küçük boyutlu, eşsiz fizikokimyasal yapılı, biyouyumlu ve biyomedikal alanda her geçen gün daha çok ilgi çeken, bor ve azot atomlarının eşdeğer sitokiyometrisinden oluşan, altıgen yapılı hegzagonal bor nitrürlere (hBN), bir antikanser ilacının uygun koşullarda yüklenme ile salım performansları incelenmiştir.

Çalışmada, kimyasal buhar biriktirme yöntemine göre borik asit bor öncüsü ile sentezlenen hBN'lerin spektroskopik ve morfolojik karakterizasyonu, Ultraviyole/Görünür Spektroskopisi (UV/Vis), Fourier Dönüşümlü Kızılötesi Spektroskopisi (FT-IR), Geçirimli Elektron Mikroskobu (TEM), Taramalı Elektron Mikroskobu (SEM), Dinamik Işık Saçılımı (DLS) ve Atomik Kuvvet Mikroskobu (AFM) ve Termogravimetrik Analiz (TGA) teknikleri ile detaylı bir şekilde incelenmiştir ve sentezlenen hBN'lerin literatürle uyumlu olarak yüksek saflıkta, tek tip ve trombositlere benzeyen yapı sergilediği saptanmıştır. Daha sonraki çalışmada, optimum ilaç yükleme koşulunu belirlemek için ilaç-hBN etkileşimi, non-kovalent etkileşim olarak iki farklı pH ortamında (6,0 ve 9,0) ayrı ayrı incelenmiştir. Aynı zamanda, her bir pH ortamında farklı ilaç:hBN oranı (1,25/3,0, 2,5/3,0, 5,0/3,0) ile hBN miktarı ve ilaç çözeltisi konsantrasyonu sabit tutularak ilaç yükleme deneyleri oda sıcaklığı koşullarında yapılmıştır. Her bir deney, en az 3 kez tekrarlanmış ve ortalamaları alınmıştır. Böylece bu çalışma kapsamında en verimli yükleme koşulları (pH ortamı 9,0 ve ilaç:hBN = 5,0/3,0) bulunmuştur. Sonuçlara göre, hesaplanan maksimum ilaç yükleme kapasitesi 0,657 mg/mg'dir. Bu sonuç, literatürde hBN nanomalzemesi ile yapılan diğer çalışmalara göre son derece yüksek bir ilaç yükleme verimi elde edildiğini kanıtlamaktadır. İlacın verimli bir şekilde yüklendiği, UV/Vis,

FT-IR, SEM, DLS ve Zeta potansiyeli teknikleriyle de kanıtlanmıştır. Karakterizasyon analizlerinin tüm sonuçları birbirini destekler niteliktedir.

Çalışmanın devamında, ilaç salım deneyleri yapılarak hBN nanomalzemelerinin ilaç salım performansı detaylı bir şekilde incelenmiştir. UV/Vis ile hesaplanan ilaç salım deneyleri, kanser hücre dokusu pH'ı (4,5-6,5) ve sağlıklı hücre dokuları (7,4) ile kanın pH'ına (7,4) göre iki ayrı pH ortamında (4,5 ve 7,4), vücut sıcaklığı temel alınarak 37 °C'de gerçekleştirilmiştir. Bu çalışmadaki ilaç salım deneyleri, ilaç yükleme kapasitesi en yüksek olarak saptanan 2,5/3,0 ile 5,0/3,0 ilaç:hBN oranlarındaki nanosistemler üzerinde yapılmıştır. Kanser ilacının nanotaşıyıcı içinde mümkün olduğunca stabil olması ve kan dolaşımında sadece "minimum ilaç sızıntısı" dışında salınmaması, ilaç taşıyıcı sistemlerden istenilen durumdur. Bu koşul sağlandığı takdirde tasarlanan ilaç taşıyıcı sistemin başarılı olacağı öngürülmektedir. Bu doğrultuda, çalışmanın pH 7,4 ortamındaki ilaç salımının maksimum verimi, ilaç:hBN oranı 2,5/3,0 olan nanosistemde elde edilmiştir. İlaç salım miktarının ilk 5 dakikada 0 mg/mg ve ilk 24 saatte 0,005 mg/mg olması, sistemin kontrollü ilaç taşıyıcı olduğunu ve çalışmanın son derece umut vaat ettiğini göstermektedir. Ayrıca bu sonuç, ilaç-hBN nanoyüzeyleri arasındaki güçlü π-π etkileşimlerinden de kaynaklıdır, böylece hBN'lerin son derece üstün ilaç yükleme kapasitesine sahip olduğu bir kez daha kanıtlanmıştır. pH 4,5 ortamındaki en yüksek salım miktarı ise ilk 5 saatte 0,033 mg/mg olarak kaydedilmiştir. İlaç salım deneylerinin her biri, en az 3 kez tekrarlanmış ve ortalamaları alınmıştır. İlaç salım çalışmalarını desteklemek amacıyla, salım kinetiği modelleri ile ilaç salım kinetikleri matematiksel olarak incelenmiştir. Bunun için Sıfırıncı Mertebe, Birinci Mertebe, Korsmeyer-Peppas, Higuchi ve Hixson-Crowell modelleri kullanılmış ve her bir modelin ilaç salım mekanizması detaylı bir şekilde açıklanmıştır. Uygun ilaç salım kinetiği modeli, matematiksel olarak korelasyon katsayısının (R^2) 1'e en yakın sonuç veren modelinin seçilmesi ile yorumlanmaktadır. Böylece 2,5/3,0 ilaç:hBN oranındaki nanosistemin pH 4,5'daki ilaç salım modeli, Higuchi (R^2=0,94) modeli ile açıklanmaktadır. 2,5/3,0 ilaç:hBN oranındaki nanosistemin pH 7,4'teki salım modeli ise, en yüksek R^2 değerinin 0,41 olmasından dolayı bu tez kapsamında incelenen hiçbir kinetik model ile uyumlu değildir. 5,0/3,0 ilaç:hBN oranında hazırlanan nanosistem için ise hem pH 4,5'daki hem de pH 7,4'deki salım modellerinin her ikisi de Korsmeyer-Peppas modeli ile açıklanmaktadır (sırasıyla R^2=0,92 ve 0,90).

Elde edilen tüm veriler değerlendirildiğinde, kanser hastalığı için alternatif bir tedavi yöntemi olarak tasarlanan MTX-hBN nanosisteminin önemli ölçüde umut verici olduğu ve özellikle hedefe yönelik kanser tedavisinde çok önemli bir rol oynayacağı öngörülmektedir.

Gelecekteki çalışmalarda ise, ilaç yükleme kapasitesini artırmak ve hBN'lerin biyouyumluluğu üzerindeki az sayısa sınırlı belirsizliği tamamen ortadan kaldırmak amacıyla uygun biyomalzemeler ile fonksiyonelleştirme işlemi yapılması önerilebilmektedir. hBN'nin nanotaşıyıcı olarak kullanımında herhangi bir fonksiyonelleştirme şartı olmamakla birlikte, yapısını güçlendirmek, hBN'lerin dağılım özelliğini iyileştirmek, yükleme-kapasitesini ve asidik koşullardaki ilaç salım miktarını artırmak ve uygun hedefleme ajanı eklemek amacıyla çeşitli biyomalzemeler ile fonksiyonelleştirme yapılabilmektedir. Bu çalışmanın devam niteliğinde olacak diğer çalışmalar için, hBN'lerin sonikasyon ile fonksiyonelleştirilmesi, diğer yöntemlere göre daha ucuz olması ve saflaştırma için herhangi bir ek işlem gerektirmemesi sayesinde önerilebilir. Diğer bir öneri ise literatürdeki çalışmalara göre hedefleme ajanı olarak seçilen Folik asit biyomolekülü ile fonksiyonelleştirilme

işleminden sonra ilaç yükleme kapasitesinin yaklaşık 3 kat artması, Folik asite benzer biyomoleküller seçilmesi durumunda fonksiyonelleştirme çalışmalarının umut vaat ettiğini kanıtlamaktadır.

Sonuç olarak hem kanser tedavisinde kullanılan tedavi yöntemlerinin zararlı yan etkilerini en aza indirgemek hem de ilacın kanda ihmal edilebilir düzeyde salınması sayesinde, ilacın hedeflenen bölgeye taşınırken sağlıklı hücrelere zarar vermemesi açısından umut verici bir nanotaşıyıcı sistem tasarlandığı için bu çalışma son derece önem taşımaktadır ve gelecek çalışmalar için öncü olacaktır.

1. INTRODUCTION

Cancer is a disease defined as uncontrolled cell growth due to mutation in cell DNA, tissue or organ. Although cancer disease is as old as the history of humanity, it is seen that the current treatments are insufficient as it is one of the diseases in which the most deaths occur today. The death of 1 out of every 10 human diagnosed with cancer indicates how severe this disease is. It has been stated in studies that if early diagnosis and appropriate treatment methods are not provided, deaths will be increased even more than the present. On the other hand, unfortunately, drugs used in cancer treatment kill healthy cells and even weaken the body's immune system, which is the most significant disadvantage of chemotherapy. Besides, nanotechnological developments and drug delivery systems are used to ensure that the cancer drug only reaches the targeted cancerous area; therefore, healthy cells are not damaged. For this purpose, studies on the design and progress of drug delivery systems capable of targeted controlled drug release are increasing. In addition to graphene and carbon nanotubes, the most known carbon-based nanocarriers in recent years, the non-toxicity of hexagonal boron nitrides (hBN), consisting of boron (B) and nitrogen (N) atoms, the structural analog of graphene, is a highly superior feature compared to other nanocarriers. Thus, the use of hBNs as nanocarriers will be a promising study. Moreover, the interest in hBNs in the biomedical field is increasing whereas their small size, high surface area, unique physicochemical structures such as slow degradation in aqueous environments, high mechanical and chemical durability, biocompatibility and pH-dependent drug release. In this study, hBN nanomaterials were used for the drug-nanocarrier system designed to develop an alternative treatment method for cancer treatment (Figure 1.1). The synthesis of hBNs has been explained in detail by various characterization analyses. Then, the optimum loading condition of Mitoxantrone Dihydrochloride, an efficient drug in cancer treatment, was determined at different pH and drug:nanocarrier (mg:mg) environments. After performing *in vitro* drug release experiments in cancerous tissue (pH 4.5) and healthy cell tissue and bloodstream (pH 7.4), these data were evaluated kinetically by various kinetic models. The motivation

of the study is to design a new nanosystem that will deliver the Mitoxantrone used in breast and liver cancer and leukemia, which are the most common cancers today.

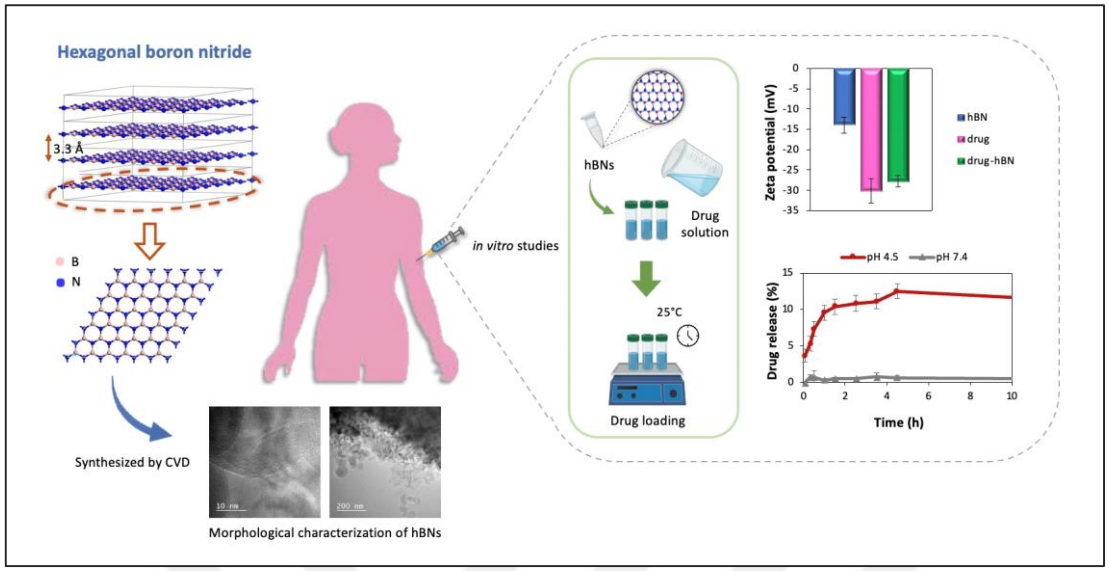

Figure 1.1 : Graphical abstract of this study.

2. THEORETICAL STUDY

2.1 Cancer Disease

Cancer disease is one of the oldest diseases known in human history, has been caused the millions of people death. Cancer, in which genetic and environmental factors are also effective, is caused by an abnormal growth and uncontrolled proliferation of cells. Today, one in every five people is diagnosed with it [1-6]. It can be estimated by looking at the data from the World Health Organization (WHO) that 11.5 million people will be probably dead by 2030 due to cancer [1]. Figure 2.1 shows the statistics worldwide and in Turkey, demonstrating the most common cancer types and incidences of them.

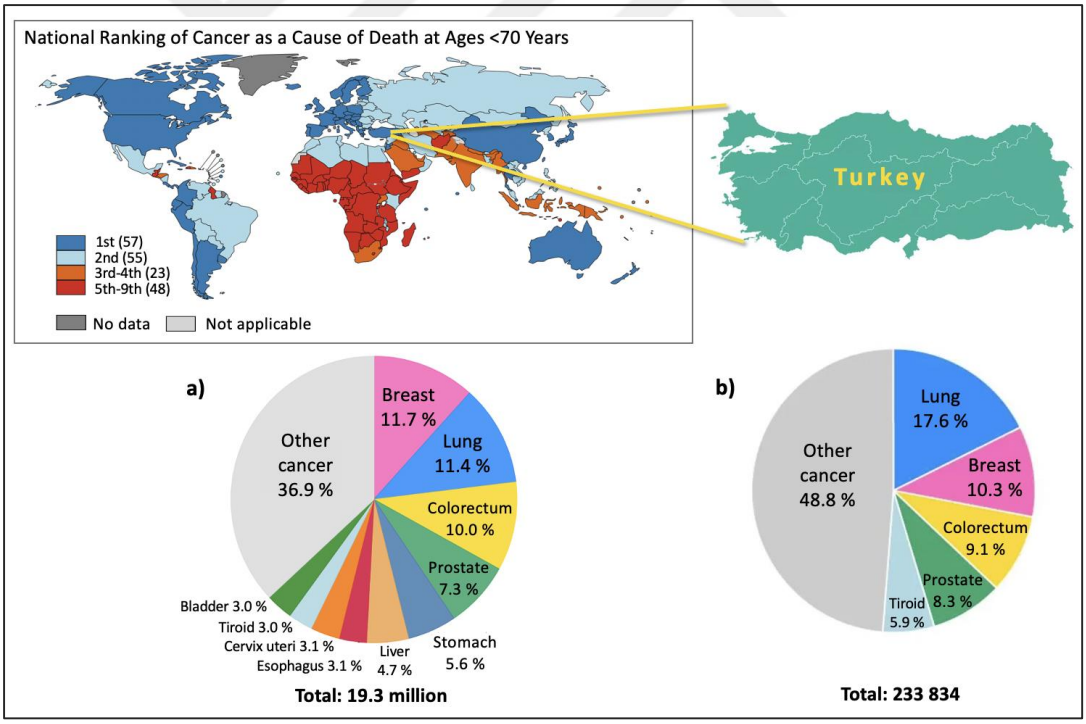

Figure 2.1 : Cancer statistics in 2020 for people of both sexes and all ages: a) incidence worldwide according to WHO [6]; b) incidence in Turkey [7].

Many treatment methods, for instance surgery, chemotherapy, radiotherapy, and hormone therapy, have been developed to treat cancer. Each method has its advantages and disadvantages; however, since cancer is an individual disease and the treatment will be particular, it is impossible to discuss a definitive treatment yet.

Although many of the treatment methods used in cancer treatment continue to be applied today, there are some difficulties encountered during the application. Current cancer drugs cannot significantly different between healthy and cancerous cells [4]. Therefore, although the primary purpose is to destroy the cancerous cell, the healthy cells are also damaged [2]. Cancer drugs contain serious side effects such as bruises and bleeding on the skin, heart failure, nausea, and infertility. These can negatively affect the patient and their relatives in the treatment process, both physically and psychologically. Another difficulty encountered is that the amount of medication to be given to the patient is limited because the drugs have severe side effects. Chemotherapy drugs, one of the most common treatment in cancer, are generally hydrophobic and therefore have low solubility in water. For this reason, chemotherapy drugs can only be given to the body by vascular access (intravenous) thanks to some solvents. Solvents used have many side effects. For example, they can reduce the efficiency of the drug and cause cytotoxicity. The resistance of tumor to cancer drugs over time and their spread to different tissues or organs by metastasis are among the negativities that make treatment difficult [2-5].

The treatment against cancer is aimed to achieve high efficiency in a short time, obtain maximum bioavailability from the drugs with the desired drug concentration, and destroy only the target tumor cells without adversely affecting the healthy cells [5]. Nanotechnology aims to provide significant benefits to cancer patients by providing a targeted approach to cancer treatment. In cancer nanotechnology, the use of nanomaterials is probably one of the most powerful and promising applications in drug delivery and targeting systems [4].

2.2 Nanotechnology and Nanomaterials

Nanotechnology is the science of designing tools or systems that examine nanoscale materials in the range of about 1-100 nm (Figure 2.2), including biotechnology, chemistry, pharmacology, polymers, and materials science [8].

Nobel award winner Richard Feynman first proposed the groundbreaking idea of nanotechnology in 1959 [8], proposing the development of molecular machines. In 1974, Norio Taniguchi's "nanotechnology" term was used for the first time to specify the elastic material properties that nanotechnology can provide. Advances in nanotechnology have led to an increase in research in various fields of use. At the same

time, the advancement of science and technology enables improvements in the design and synthesis of new nanomaterials. In the past few years, the prevention, diagnosis, and treatment of diseases with various nanomaterials have been continuing to arouse great interest in the scientific community [9].

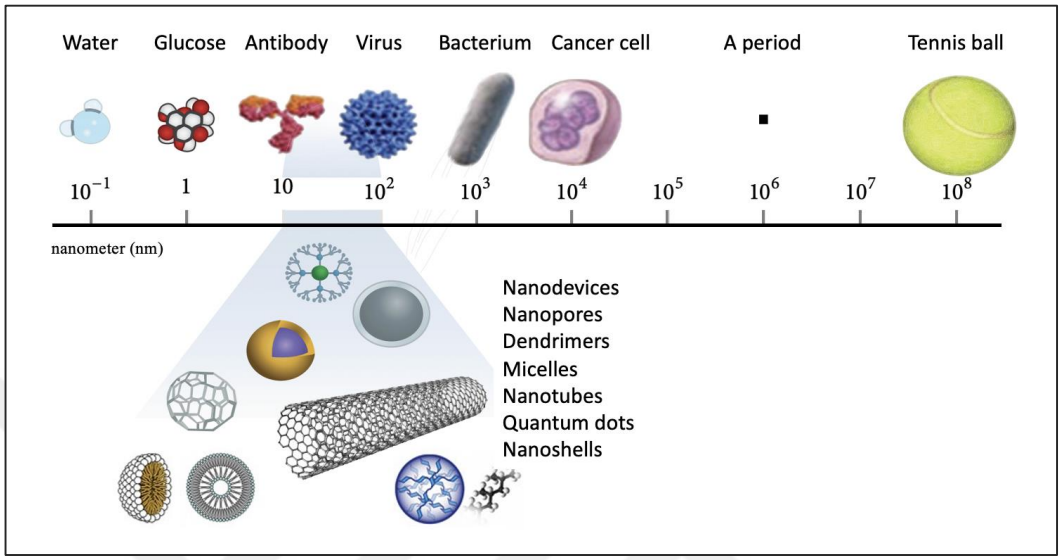

Figure 2.2 : Nanomaterials on the nanoscale line [10].

Nanomaterials are significantly smaller than biological macromolecules. Their nanosize makes them nearly 1000-times smaller than even a cancer cell, as shown in Figure 2.2 above. Nanocarriers designed for cancer treatment should be small in size, biodegradable, low toxicity, biocompatible, stable under physiological conditions, and able to circulate freely in the blood vessels [11].

The main advantages of nanocarriers [11-14] are as follows:

- It can overcome the limitations of traditional cancer treatments.
- It can make the drug direct tumor site, thereby preventing damage to healthy cells.
- The drug level can be maintained in the desired amount and time so that side effects can be greatly reduced.
- Thanks to its small size, it has the potential to overcome biological barriers. An advantage of their small size is their extensive surface area. Thus, more significant amounts of drug can be added and delivered to the target location.
- Thanks to the permeability feature of tumor cells, nanocarriers can be retained in tumor cells instead of healthy cells.

To eliminate the problems encountered in current treatment methods, interest in nanocarrier systems as an alternative method has increased tremendously. Recently, the number of studies with nanocarriers for cancer treatment has increased rapidly (Figure 2.3). According to developing nanotechnology studies, it is predicted that nanocarriers will achieve the goals for the desired purpose.

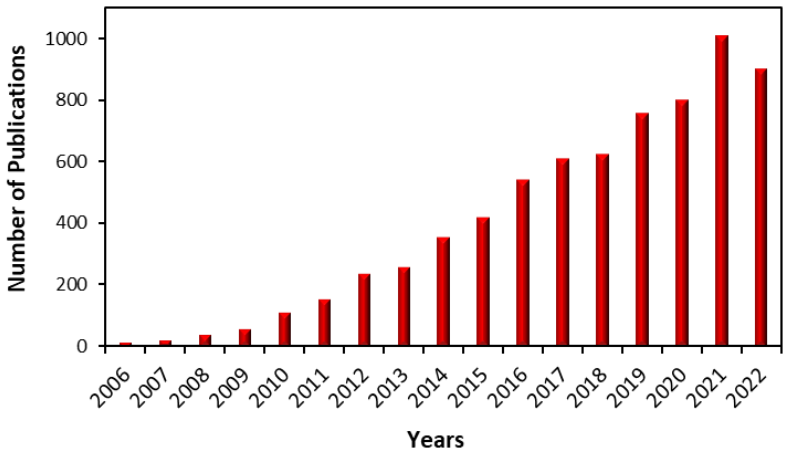

Figure 2.3 : Distribution of the number of publications by years within the scope of "nanocarriers" AND "cancer" (title, abstract, keyword), (Source: Scopus, October 2022).

2.2.1 Controlled drug release systems

Controlled drug release systems, which have about 70 years of history (Figure 2.4), are one of the most critical research areas today with the development of nanotechnology. The primary purpose of controlled drug release is to prevent long-term drug use and, thus, decreasing the side-effects of the drug. For the drug to be effective in such systems, it must first adhere to the nanocarrier, mix safely and effectively into the blood after it is injected into the body, diffuse into the tissues, go to the targeted area and release the drug. Finally, it must be expelled from the body [15].

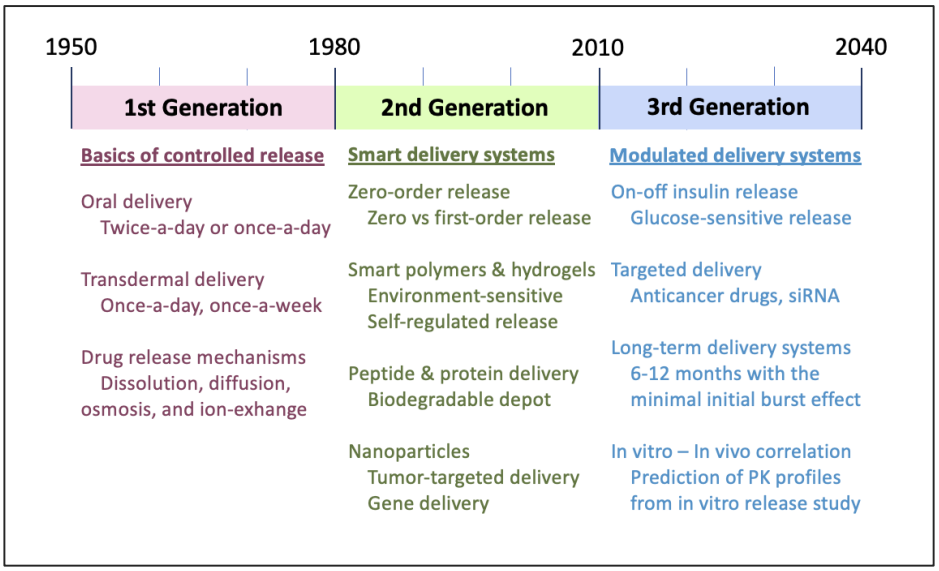

Figure 2.4 : Development of controlled drug delivery systems from 1950 to 2040 [15].

Controlled release systems are affected by factors that create physiological conditions such as ionic strengths, pH, temperature, and enzymes [16,17].

Understanding the various techniques to develop nanocarriers with desired release kinetics is necessary. The interaction of drug and nanocarrier and the way it is encapsulated, the mechanism of drug release, and the effects of the chemistry and morphology of the nanocarrier on drug release kinetics are some examples of these techniques to know [18].

The main purpose of controlled release is to maintain the drug level in the blood between minimum effective concentration (MEC) and minimum toxic concentration (MTC). As Figure 2.5 below, the range between MEC and MTC demonstrates the therapeutic window where the drug has an effectivity without showing toxicity. If the drug is given in a single large dose, the blood drug level increases above the MTC causing toxic effects, then rapidly decreases below the MEC. To prevent this situation, drug delivery systems that provide controlled release of the drug are needed. Thus, it is aimed to have a constant release rate (Zero Order profile [19]). The material to carry the drug must be biocompatible with the body but a non-toxic material. Biomaterials are used to prepare controlled release systems consisting of natural or synthetically obtained polymers [18-20].

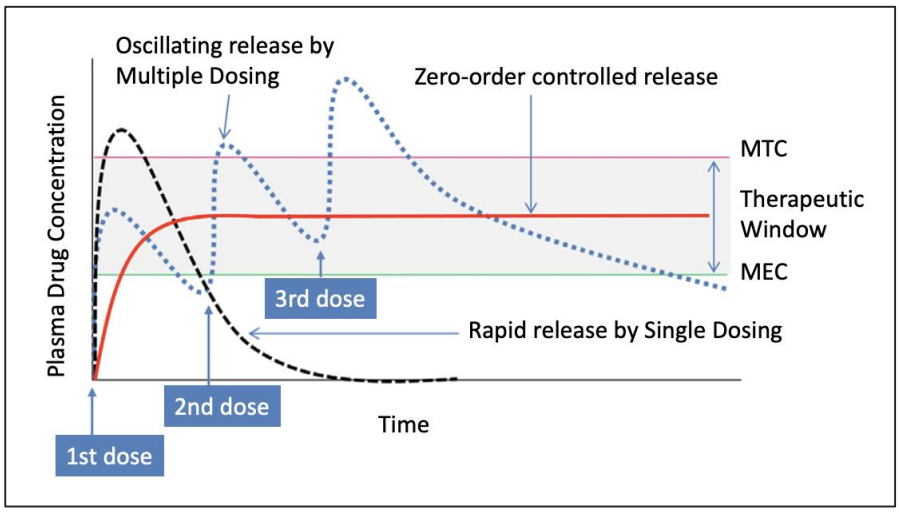

Figure 2.5 : Plasma drug concentration profiles related to time (MEC: minimum effective concentration; MTC: minimum toxic concentration) [18].

From the past to the present (Figure 2.4), several nanocarrier types designed drug delivery mechanisms (Figure 2.6) for controlled drug release systems. Nanocarriers are generally classified into inorganic [21] and organic [22]. Examples of inorganic nanocarriers are quantum dots [23,24], carbon nanotubes [25-27], and magnetic nanoparticles [28], while organic nanocarriers are liposomes [29,30], micelles [31,32], polymeric nanoparticles [33,34], and dendrimers [35,36].

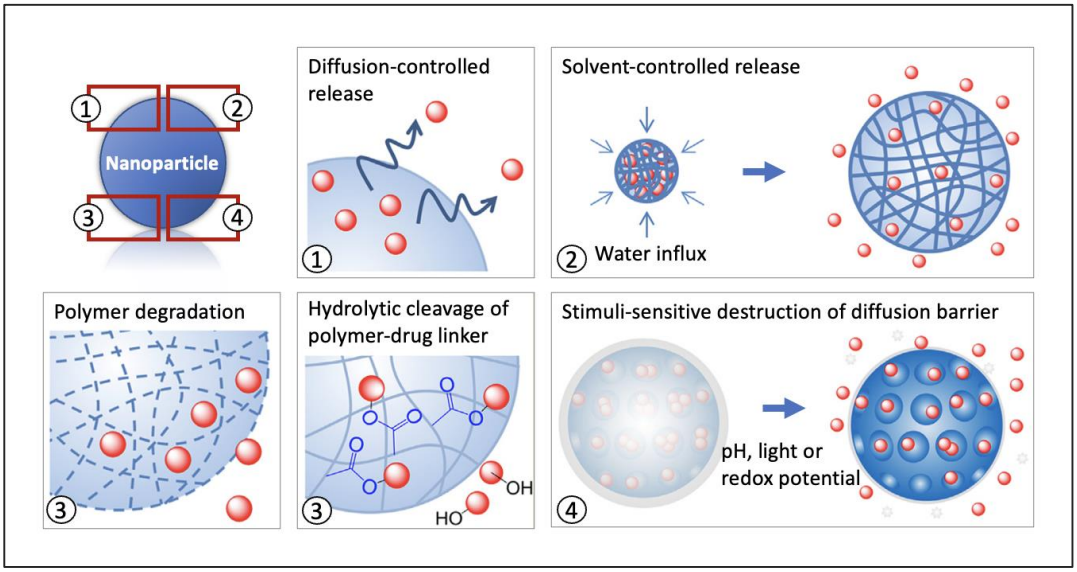

Figure 2.6 : Drug release mechanisms used in nanocarriers [37].

There are four common mechanisms for drug release from carriers. These mechanisms can be explained in the given Figure 2.6 as diffusion (the drug is dispersed in the nucleus by the polymeric membrane surrounded), solvent (occurs with the principle of osmosis and swelling), chemical reaction (occurs by hydrolytic and/or enzymatic

degradation of nanocarriers containing biodegradable polymers bonds), and stimuli-controlled release (control with stimulants such as temperature, ionic strength, pH) [37].

Although nanocarriers in the controlled release areas have many advantages for instance large surface area, drug loading efficiency, and easy structural modification, the search for new nanocarriers with superior properties continues as problems such as biocompatibility and toxicity persist. In addition, there are several advantages and challenges related to the properties and types of nanoparticles as Table 2.1 given below is summarized.

Table 2.1 : Advantages and challenges related to properties of nanoparticles [22].

Nanoparticle Types	Advantages	Challenges
Polymer-based	Outstanding stability and storage capacity	Capsuling of proteins and burst release
Lipid-based	Very good biocompatibility	Storage stability (limited), drug-loading with a wide diversity
Protein-based	Functional nanomaterial	Stability and potential immunogenicity problems
Coatings (PEG)	Proven stealth properties render colloidal stability	Potential immunogenicity compromises targeting
Agents (antibodies, peptides, aptamers) for targeting	Enlarged accumulation in target areas	Compromises circulation
Size-based (small)	Enlarged circulation, enhanced EPR effect	Limited sustained release, the enlarged potential for aggregation
Non-spherical shape	More prolonged circulation, enhanced targeting, increased specificity	Potential for complex manufacturing process
Compartmentalization	Multiple drug-loading simultaneously, independent drug-release control	Potential for complex manufacturing process

Moreover, considering the summarized challenges that nanoparticles have (Table 2.1), the search for new nanocarriers with superior properties and fewer challenges is increasing day by day, while the interest in drug delivery system design has been also growing simultaneously.

2.2.2 Active and passive targeting

After biologically active molecules are processed in the body, they must pass some biological barriers such as epithelium, endothelium, cell membrane, and enzymatic barriers. Therefore, a new drug delivery system should be designed and developed with different application ways [38]. Delivery of nanocarriers to the tumor site via systemic circulation is based on two basic targetings: active and passive targeting (Figure 2.7) [5].

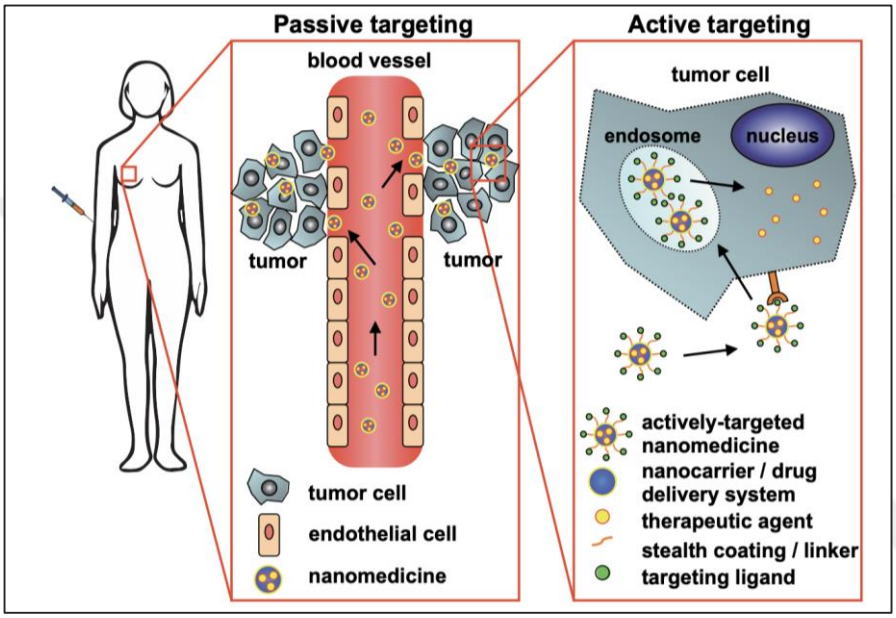

Figure 2.7 : Targeted drug delivery contains passive and active targeting [39].

In passive targeting, further selective accumulation of nanocarriers is facilitated by the enhanced permeability and retention (EPR) response due to tumor vasculature [5]. On the other hand, active targeting occurs when the nanocarrier is coated with specific targeting ligands that will recognize receptors that are more abundant on tumor cell surfaces or in the vascular region than in healthy cells. In active targeting, the cytotoxic effect of the anticancer agent is increased and the side effects on healthy tissue are minimized. Notwithstanding, active targeting has further advantages in nano-targeting to tumor tissue. Active targeting can overcome biological barriers by adding antibodies or ligands to nanocarriers. In addition, the amount of drug delivered to the cell can be increased by active targeting [5,40].

2.2.3 pH-sensitive nanomaterials

Smart drug delivery systems are be able to stimulated by several parameters (light, temperature, pH, mechanical forces, electromagnetic fields, etc.). Moreover, nanocarriers are adaptable for the targeted site and can provide controlled release or delayed of drugs. pH-sensitive nanocarriers are one of the most important nanocarrier groups researched in recent years [41].

Since pH values tremendously differ in varied tissues and cells (blood pH is neutral at 7.34-7.45; environments of tumor tissues and inside endosomes or lysosomes are acidic at 4.5-6.0 because of the lactic acid accumulation [42], pH-sensitive drug delivery systems are being developed (Figure 2.8). After targeting the nanocarriers to the tumor area, drug release starts in the acidic microenvironment of the tumor tissue. Thanks to pH-sensitive nanomaterials, the drug release rate will accelerate at low pH values; therefore, it is anticipated to have a practical release feature in the tumor microenvironment. However, since some organelles (for instance endosomes and lysosomes) are acidic, drug release continues in acidic intracellular organelles. Thus, nanocarriers injected into the body can accumulate in cancerous tissues with EPR and reduce undesirable risks for healthy cells during circulation [43,44].

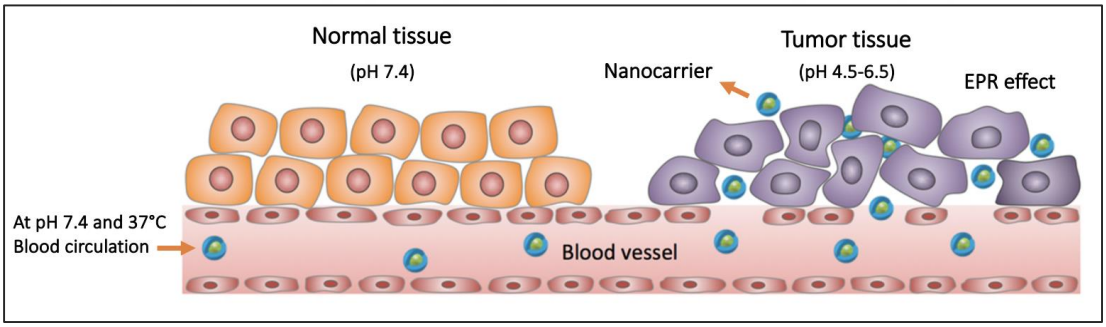

Figure 2.8 : Display of tumor and healthy tissues through the EPR effect [45].

The search for alternative treatments for serious diseases such as cancer has increased the interest in drug delivery nanotechnology-based. Nowadays, the progress of nanoparticle-based systems constitutes an exciting research area in cancer therapy. Although carbon-based nanomaterials (fullerenes, carbon nanotubes (CNTs), graphene oxide) are the most used nanocarriers in the literature, boron-based nanomaterials (boron nitride nanosheets, hexagonal boron nitride, boron nitride nanotube) have attracted more attention in these days owing to their superior properties [41].

2.2.4 Carbon-based nanomaterials

Fullerenes, also called buckyballs, are hollow spheres with carbon that can vary in size and were first discovered in 1985. Fullerenes became the subject of intense research in the 1990s thanks to their application in many nano-fields from materials science to electronics [46].

Carbon nanotubes (CNTs) discovered in 1991 [47] are one of the most researched nanomaterials these days, thanks to their various mechanical, electrical, and thermal properties. Carbon nanotubes can also be defined as cylindrical wrapping of a graphene sheet made from carbon atoms [48]. Some of their properties change according to the number of layers. To consist of a single layer, CNTs are called single-walled CNTs (SWCNTs), and to consist of multiple layers, they are called multi-walled CNTs (MWCNTs) [49]. Both types can be used in several fields like materials science, biotechnology, and electronic devices, thanks to their large surface areas and rich surface chemical functions [50].

Hexagonal graphene, consisting of a single layer of carbon (C) atoms, was found in 2004 by Andre Geim and Konstantin Novoselov, who won the Nobel award in 2010 [46]. Although a rapid field of research emerged after the discovery of graphene, it was surprising that until 2008 attention was not paid to the potential biomedical applications of graphene [51].

Even though graphene (Figure 2.9), which has a wide application area from biosensors to cancer treatment thanks to its various properties, is one of the most researched nanomaterials today. However, debates on its disadvantages have been continuing [51].

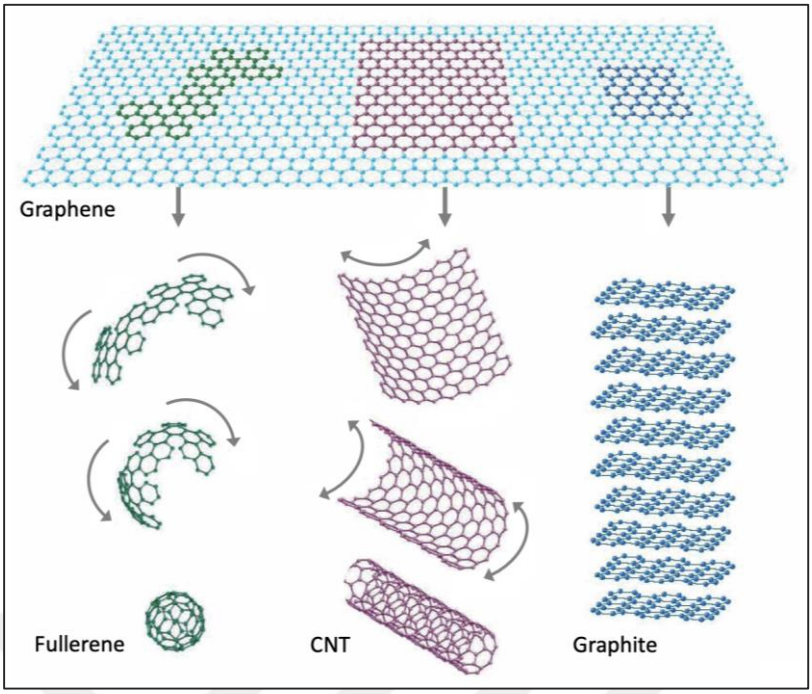

Figure 2.9 : Chemical structures of fullerene, CNT, and graphite [52].

2.2.5 Boron-based nanomaterials

Boron nitride (BN) is a promising crystalline nanomaterial consisting of the equivalent stoichiometry of boron (B) and nitrogen (N) atoms. It is produced synthetically because it is not found in nature. With the development of nanotechnology, various Boron-based nanomaterials have been discovered [53].

BN nanomaterials are the most promising materials ever discovered [54]. Interestingly, all BN nanomaterials are based on hexagonal form. B-N bonds in the structure of BN nanomaterials are isoelectronic, with C-C bonds in carbon-based nanomaterials. In this way, graphene nanoribbons (GNR), graphene, and carbon nanotubes (CNTs) are structurally similar to boron nitride nanoribbons (BNNR), boron nitride nanosheet (BNNS), and boron nitride nanotubes (BNNT), respectively [53].

Since the thermoelectric properties of graphene nanomaterials are weak, BN nanomaterials have been the focus of attention in all respects, thanks to both structural similarity and various superior properties (high chemical and thermal stability, adsorption, etc.) [55]. Boron nitrides can be in the form of lattice (0D), nanotube (1D), monolayer (2D) diamond-like crystal structure (3D), as shown in Figure 2.10 [56]. Moreover, BN does not oxidize unless heated above 800°C [57].

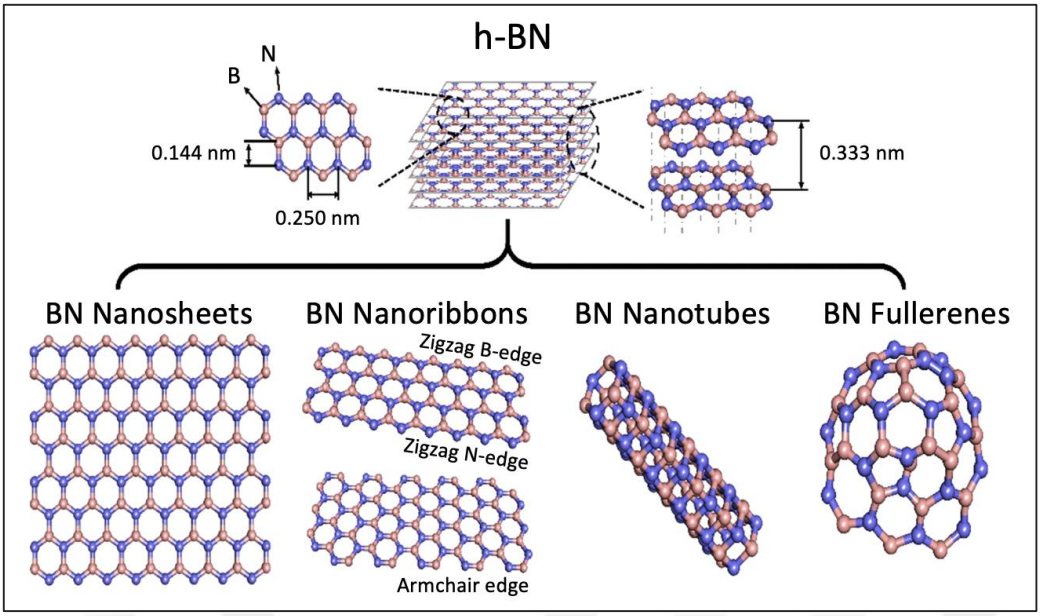

Figure 2.10 : Structures of hBN nanomaterials such as BN Nanosheets, BN Nanoribbons, BN Nanotubes, and BN Fullerenes [58].

A single and separate layer of hBN is called a BNNS, and BNNRs are also included in this definition due to their different structural properties. BNNSs are considered biocompatible because they are water dispersible and non-toxic [57].

BNNSs are used in nanomedicine because they are biocompatible and can also be used as additives to improve various polymeric composite properties [59].

BNNRs are semiconductor nanomaterials with a wide band gap that varies in size and chirality [55].

The presence of BNNTs was first estimated in 1994 and was first synthesized experimentally in 1995. BNNTs, the structural analogs of CNTs, an electrical insulator nanomaterial compared to CNTs with a band gap of approximately 5 eV. BNNTs, like BNs, have many superior properties, such as excellent mechanical and chemical stabilities, and high thermal conductivity. Thanks to these outstanding properties, BNNTs are a promising nanomaterial with the possibility of use in diverse fields. BNNTs can be single-walled or multi-walled; just like CNTs, difficulties have continued in synthesizing single-walled BNNTs compared to single-walled CNTs [60].

Many of the production methods used in CNT production (for instance chemical vapor deposition, arc discharge, and ball milling) are also used in BNNT production. In addition, although various methods, such as continuous laser heating at super high

pressures and pressurized steam condensation, have been developed, research for an effective way to synthesize small-scale and high-purity BNNT continues today [60].

2.2.5.1 Hexagonal boron nitride

BN has different polymorphisms such as hexagonal (hBN), wurtzite (wBN), rhombic (rBN), and cubic (cBN) boron nitride since it is able to crystallize in different ways dependent on pressure and temperature; however, at the room temperature conditions, its most stable form is hexagonal form. While hBN and rBN maintain the dense structure by sp^2 hybridization, a loose structure is formed by sp^3 hybridizing wBN and cBN (Figure 2.11). The most studied systems are cubic and hexagonal forms [61-63]. hBN has superior chemical and thermal stability because of its different ionicity in the B-N bond (Figure 2.12), which is different from the covalent C-C bond in graphene. Therefore, hBN is an oxidation-resistant and high-performance nanomaterial [56].

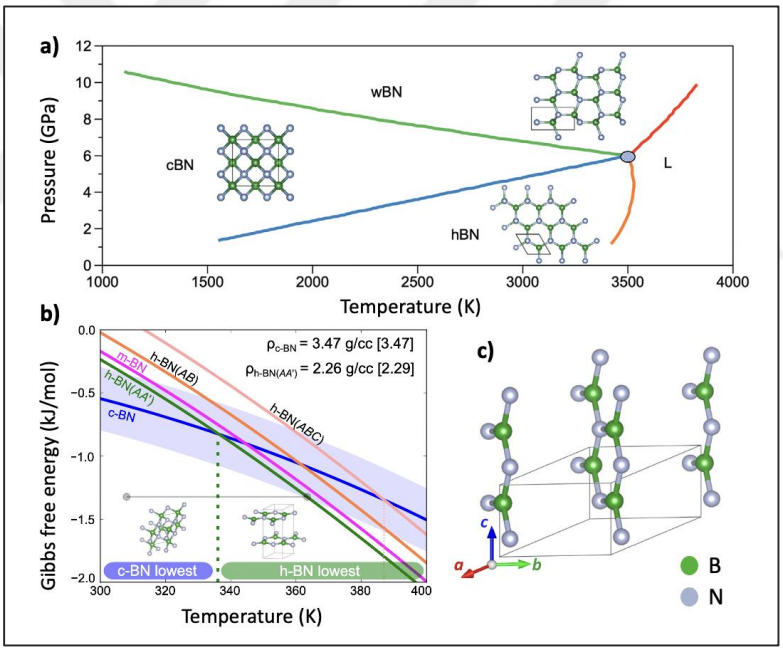

Figure 2.11 : a) Example phase diagram of the BN system [64], b) Gibbs free energy of BN polymorphs at zero pressure stated as a function of temperature [65], c) Monoclinic phase of hBN.

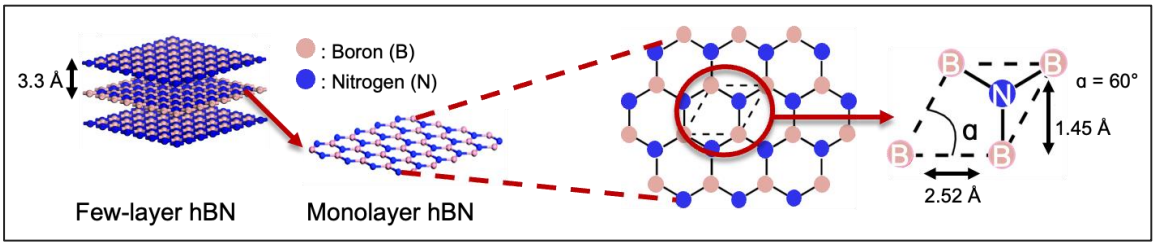

Figure 2.12 : Detailed chemical structure of hexagonal boron nitrides.

hBN, as a structural analog of graphene (Figure 2.13), is a two-dimensional (2D) layered nanomaterial, and it is also called “white graphene” because the form of hBN is very similar to conventional graphene [61-63]. Table 2.2 indicates the properties of hBNs in comparison to graphene.

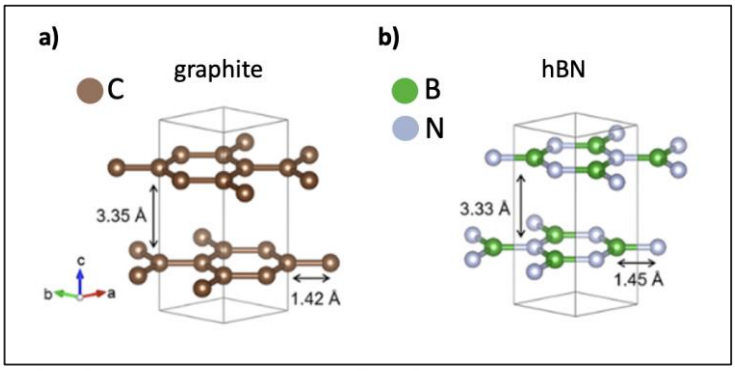

Figure 2.13 : The crystal structures of a) graphite and b) hBN [66].

Table 2.2 : Comparison properties of hBN and graphite [54,67,68].

Properties	2D Nanomaterials	
	hBN	graphite
Appearance color	White	Black
Crystal structure	Hexagonal	Hexagonal
Lattice parameters (nm)	a: 0.250 c: 0.666	a: 0.246 c: 0.670
Density (g/cm^3)	2.34	2.2
Bond length (nm)	0.144	0.142
Bond energy (eV)	4	3.7
Interlayer spacing, by diffraction (nm)	0.333	0.335
Thermal conductivity (Wm^{-1} K^{-1})	25.1	25-470
Dielectric constant	4	8.7
Young's modulus (Tpa)	0.81-1.3	1.1
In-plane thermal conductivity (Wm^{-1} K^{-1})	400	2600
Charged transferred between neighbors (e)	~0.4	~0
Band gap (eV)	5.5-6.0	~0
Breakdown voltage (MV/cm)	~7	Conductor
Oxidation resistance	~840	~600

Although hBNs were synthesized for the first time by English chemist W.H.Balmain in 1842 by the reaction of boric acid (H_3BO_3) and potassium cyanide (KCN), the first stable forms were obtained in the laboratory for the first time in 1962, about a hundred years later [69,70]. Interestingly, in 2009, a cubic BN mineral was reported in nature in Tibet [56].

hBNs resemble honeycombs and have a crystal lattice structure, and have chemically inert, atomically thin, and smooth surface (0.1 nm RMS) properties [71]. Moreover,

there are strong intralayer covalent bonds and weak interlayer van der Waals interactions between B and N atoms [61-63].

Notwithstanding that the studies on the synthesis of hBNs have been continuing to be widely investigated in the literature, the main production methods are chemical vapor deposition, arc discharge, electrospinning, laser ablation, autoclave, carbonization of nitrogenous organic compounds, and template synthesis technique [71-73].

Since chemical vapor deposition is used to produce high-quality and high-performance materials, it is generally the most commonly used method to generate high-quality BN nanostructures [72].

Thanks to their fantastic properties, such as being biocompatible [61,62], non-toxicity [74], high chemical and thermal stabilities, excellent mechanical strength, and electrical insulation, they can be used as potential nanomaterials in many fields like pharmacy, chemistry, cosmetics, materials science, biosensors, and tissue engineering. There is currently a growing interest in hBNs so that they can be used in many fields. It is also possible to strengthen hBNs according to the area used by developing new synthesis routes or making appropriate surface functionalization [61,75].

Biocompatibility of hBN

For applying nanocarriers for drug delivery, biological safety is one of cancer treatment's most essential and critical criteria [76]. There is an interesting situation: since all boron nitride structures are based on hBN due to isoelectronic B-N bonds [77], studies on the cytotoxicity of hBN are summarized in the given Table 2.3 below.

Table 2.3 : Cytocompatibility of BN nanoparticles in detail.

Type of BN	Cell Lines	Toxicity Parameters				Ref.
		Assays	Concentration (μg/mL)	Incubation Time (h)	Results	
BNNT, hBN	HeLa and HUVECs	WST-1	5, 10, 20, 50, 100	1, 2, 4, 8, 24, 72	Nontoxic for both cell lines	[62]
BNNS	93XL-hTLR9	Cell Counting Kit-8 and Cytokine	up to 100	24	No detectable cytotoxicity	[78]

Table 2.3 (continue): Cytocompatibility of BN nanoparticles in detail.

Type of BN	Cell Lines	Toxicity Parameters				Ref
		Assays	Concentration (μg/mL)	Incubation Time (h)	Results	
BNNS	SaOS2	MTS and DPPH	Not exactly given	168	Size-dependent toxicity	[79]
BNNS	HeLa	CCK-8	up to 100	24	Nontoxic ≤ 100 μg/mL	[80]
BNNS	LNCap and DU-145	WST-8	5, 25	72, 144	Time-dependent toxicity	[81]
BNNP	IAR-6-1	MTT	20, 40	24, 48, 72	Low cytotoxicity	[82]
BNNT	planarians (animal, in vivo)	Phototactic and mitosis	100 or 200	24, 72	Arabic coated-BNNTs are nontoxic and biocompatible	[83]
hBN	L929 fibroblast and MCF-7	Cell Counting Kit-8, LDH, and NRU	3.125, 6.25, 10, 12.5, 25, 50, 100, 200	24, 48, 72	No toxicity	[84]
hBN	HEK-293T and CHO	MTT and annexin V-FITC/PI	0, 20, 40, 60, 80, 100	48	Nontoxic ≤ 100 μg/mL	[85]
hBN	KB	MTT	10, 20, 50, 100	24	Nontoxic ≤ 500 μg/mL	[86]
hBN	MDCK and CRL 2120	MTT and SRB colorimetric PicoGreen	25, 50, 100, 200, 400	24, 48	Nontoxic ≤ 100 μg/mL (for both cell lines)	[87]

Considering the differences in cell types, concentrations, exposure times, and test types used in these studies, we can say that BN nanostructures are not toxic. However, Mateti et al. [79] found that size-dependent toxicity has occurred. In another study [81], time-dependent toxicity has observed. Moreover, Ciofani et al. [88] claimed the low cytotoxicity of BNNPs could be misinterpreted as cytotoxicity due to the interaction of some tetrazolium salts with BN nanophases. However, since the toxicity of BNs depends on cell type, dose, animal model, and lateral size, Kar et al. [89] have investigated the dose-dependent biocompatibility of hBNs *in vivo*. The concentration of hBN with a diameter of 121 nm used in this study ranged

between 50-3200 μg/kg and the incubation time was 24 hours. According to the results, hBNs were non-toxic up to ≤ 800 μg/kg, and were found to be highly suitable for applications in the biomedical field.

To sum up, it is seen that BN nanomaterials do not have a significant adverse effect on cell viability. However, to have more straightforward ideas in this field, the limited number of biocompatibility studies should be increased, and more *in vivo* studies should be accomplished [77].

2.2.6 Active ingredients in cancer treatment

Drugs used in cancer treatment are toxic to all cells (tumor and healthy). Therefore, these drugs are also carcinogenic and mutagenic drugs [90]. New drug delivery systems are designed to reduce the side-effects (hair loss, nausea, vomiting, deterioration of the immune system, etc.) caused by these drugs as much as possible.

2.2.6.1 Mitoxantrone dihydrochloride

Mitoxantrone (MTX) is a dihydrochloride salt widely used in various types of cancer treatments (breast, liver, other malignant tumors, etc.) and Multiple sclerosis (MS) [91]. It is also an anthraquinone-type synthetic drug. MTX is a drug with greater antineoplastic activity than other dihydrocyanthrasendione salts [92,93].

MTX, one of the drugs that can interact with the DNA sequence and result in apoptosis (Figure 2.14), has been approved by the Food and Drug Administration (FDA) for cancer [94].

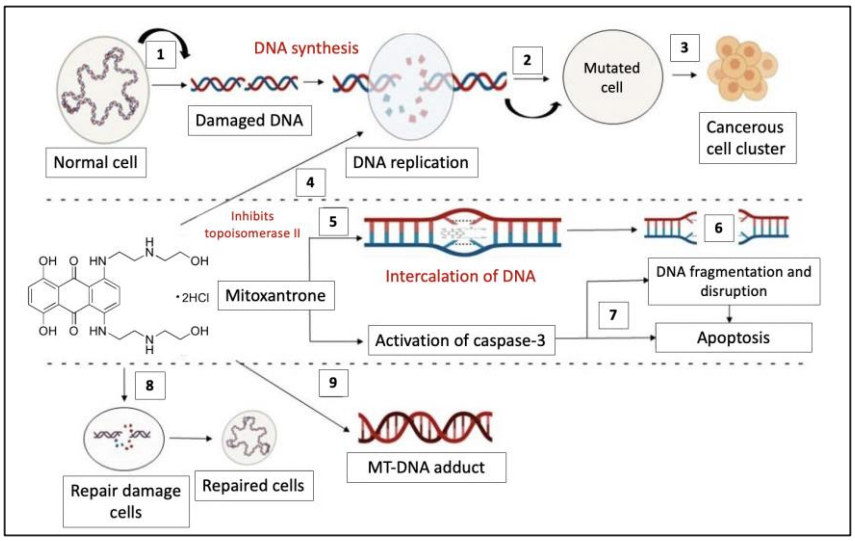

Figure 2.14 : Action mechanism of Mitoxantrone (MTX) on cytotoxicity [94].

According to the Table 2.4 given below, it is seen that the recommended treatment dose of Mitoxantrone is lower than other anti-cancer drugs. Thus, Mitoxantrone is a drug with fewer side effects, although its effectiveness is higher than other cancer drugs.

Table 2.4 : Dosage regimens for some active anti-cancer ingredients [94].

Drug	Dose (mg/m^2)
Mitoxantrone	12-14
Doxorubicin	40-60
Adriamycin	60-75
Cyclophosphamide	500
5-fluorouracil	500
Cisplatin	50-100

2.2.6.2 Use of hBNs with different anti-cancer drugs

Mitoxantrone, a structural analog of Doxorubicin [94] frequently used in the literature, demonstrates far fewer side effects than Doxorubicin [95]. The fact that hBN nanocarrier systems have not been studied with MTX in the literature makes our study innovative. A few studies in which hBN was used as a drug delivery system and studied with different anti-cancer drugs are briefly summarized below.

Weng et al. studied the interaction of hydroxylated (functionalized) hBNs with the anti-cancer drug Doxorubicin (DOX) [96]. They determined that the hydroxylated hBNs are biocompatible and can load DOX three times its weight.

Sharker et al. aimed to design a new drug delivery system in cancer therapy by loading Indocyanine Green (ICG) on hydroxylated hBNs [97]. Then, they synthesized Hyaluronic acid (dHA-DOX) conjugated with dopamine and DOX and examined its interaction with hBNI [d-HA-DOX (hBNI/d-HA-DOX)]. This innovative study determined the hBNI/d-HA-DOX nanoparticles, whose cytotoxicity studies were also performed, work as an antitumor agent with its auxiliary and therapeutic power and can prevent tumor regrowth.

Emanet et al. comparatively investigated using BNNTs and hBNs as nanocarriers in cancer therapy with the anti-cancer drug DOX [62]. Exploring the effect of drug loading pH, drug loading studies were done at different pH values (4, 7, 11) and they found that the most appropriate loading was obtained at basic pH. According to the results obtained, it was observed that BNNTs have approximately three times higher

capacity of DOX-loading than hBNs. The capacity of DOX-loading of hBNs was calculated to be 3.75%. In the next part of the study, they conjugated DOX-loaded BNNTs with folate molecules and studied cell viability experiments in HeLa cells with this system. Here, the folate molecules (F) acted as receptors. Owing to the existence of F-receptors on the cell surface, cellular encapsulation of F-DOX-BNNTs was carried out to be much higher for HeLa cells compared to DOX-BNNTs, resulting in increased cancer cell death.

Sharker et al. investigated the DOX loading efficiency after dispersing the ICG substance into the hBNs in PBS buffer using hBNs with a lateral size of 1 μm. They found a drug loading efficiency of 90% [97]. In addition, the amount of DOX release was determined in this study (92% at pH 5.5; 70% at pH 7.4). The fact that drug loading and release amounts are higher, according to the study of Emanet et al.[62] can be explained by the fact that hBNs interact with the ICG substance before interacting directly with DOX, and then drug-loading studies are performed.

Vatanparast et al. performed density functional theory (DFT) calculations and molecular dynamics (MD) simulations to examine the relationship of 5-fluorouracil (FU)/6-mercaptopurine (MP)/6-thioguanine (TG) anticancer drugs with hBNs [98]. In these simulation studies, it was determined that the adsorption of hBNs and drug molecules is exothermic, and this situation occurs spontaneously. It also confirms that the interaction energy is lower in acidic conditions than in neutral states and that the drug can be released within the targeted cancerous cells. These findings prove that using hBNs as nanocarriers in cancer treatment is promising.

Weng et al. investigated the biocompatibility and DOX loading capacity of hBNs that they functionalized by hydroxylation (hBN(OH)) [96]. The capacity of DOX-loading of hBN(OH) (from 0% to >300%, by weight) varies according to various parameters (nanocarrier concentration and ratio, type of drug used). Two different cell types (NIH/3T3 mouse embryonic fibroblast cells and LNCaP human prostate cancer cells) were used for biocompatibility-studies. The survival of more than 92% of cells in cell viability experiments performed at different concentrations proves the extremely low cytotoxicity of hBNs. Thus, the use of hBNs in medical and biological fields is promising. According to another study [99], the survival of ~70% of human fibroblast cells exposed to graphene oxide indicates the superiority of hBNs.

Yıldırım et al. aimed to design an alternative delivery system using hBN to treat Alzheimer's disease [100]. In this study, hBNs were functionalized with folic acid (FA) (hBN-FA), then the Memantine, which uses in the treatment of Alzheimer's disease, loading capacity (95%) of this system was investigated. Cytotoxicity tests were performed on HDFa human dermal fibroblast cells, and the cell viability of hBN-FA-Memantine was 94%. It was found that the designed new delivery system did not change the toxicity result even at higher concentrations.

2.3 Aim of The Study

This study aims to examine the release performance of Mitoxantrone Dihydrochloride by loading hexagonal boron nitrides (hBNs) and to synthesize them which can be used as an alternative method for cancer treatment, do not show any toxic properties, and have high drug loading capacity.

The main issues that constitute the motivation of this study are given below, respectively:

1) Why is hexagonal boron nitride used?

The use of BN-based nanomaterials in medical and biomedical fields has shown promising results and superior properties. Although hBNs are the structural analogs of carbon-based graphene, it is noteworthy that they are preferred among other nanocarriers due to their non-toxicity and biocompatibility properties. In addition, hBNs have other properties such as small size to enter the targeted cells easily, high surface area, unique physicochemical structures like slow degradation in aqueous environments, high mechanical and chemical durability, high drug loading capacities, and pH-dependent drug release. Today, these situations have made them useful as promising nanomaterials.

hBNs are used in this study because of being promising innovative nanomaterials in cancer treatment.

2) Why isn't any functionalization method done?

In drug delivery systems designed with nanocarriers, it is aimed to ensure that the drug acts on the tumor tissue in a short time and with maximum efficiency, and minimizes the damage to healthy tissues. At the same time, nanocarriers must be

non-toxic and biocompatible with the body. In addition to graphene and carbon nanotubes, the most known carbon-based nanocarriers in recent years, the non-toxicity of hBNs is a highly superior feature compared to other nanocarriers. In this way, the direct loading efficiency of the drug and the release experiments under different pH conditions are carried out without seeking any functionalization conditions in the use of hBNs as nanocarriers. However, in future studies, it may be possible to functionalize hBNs with various biomaterials in order to strengthen their structure and increase drug loading efficiency.

3) Why is Mitoxantrone Dihydrochloride used?

In some studies in the literature, hBNs were designed as nanocarriers for cancer treatment, anti-cancer drugs such as Doxorubicin [62,74,97,101,102]. Cisplatin [103], and Hyaluronic acid [97] were used. For instance, in a study by Emanet et al., the drug loading effectiveness of hBN was investigated with Doxorubicin, the structural analog of Mitoxantrone Dihydrochloride, prepared at different concentrations [62]. Doxorubicin is the most commonly used drug in cancer therapy and nanomedicine [95]; however, Mitoxantrone Dihydrochloride has fewer side effects.

Although Mitoxantrone Dihydrochloride is a potent and essential anti-cancer drug, no study performs the drug loading and release performances with hBNs. The fact that a gap in the literature will be filled in this study, which is carried out with the drug Mitoxantrone Dihydrochloride, which has fewer studies in the literature compared to other cancer drugs, and makes this study more innovative.

3. MATERIALS AND METHODS

3.1 Chemicals Used In This Study and Their Properties

Mitoxantrone Dihydrochloride, was obtained from Sigma-Aldrich. Its chemical structure is shown in Figure 3.1 and some of its chemical and physical properties are given in Table 3.1.

hBN nanomaterial was provided by Sabancı University. Other chemicals used to prepare buffer solutions were, for example, Tris, Tris HCl, disodium hydrogen phosphate were obtained from Sigma Aldrich; potassium dihydrogen phosphate was obtained from Merck, and NaCl, KCl salts were obtained from Lab-Kim.

All solutions were prepared using ultra deionized water.

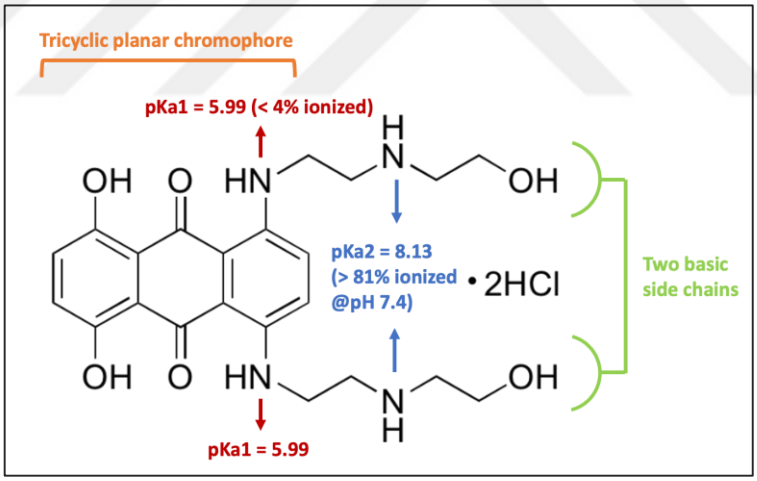

Figure 3.1 : The chemical structure of Mitoxantrone Dihydrochloride [104].

Table 3.1 : Physical and Chemical Properties of Mitoxantrone Dihydrochloride.

Description	Property
Molecular formula	$C_{22}H_{28}N_4O_6 \cdot 2HCl$
Molecular weight (g/mol)	517.40
Colour	Dark Navyblue
Physical state (25°C)	Solid (powder)
pKa	8.3-8.6
Melting point (°C)	205-205
Solubility in water (mg/mL)	5-10

3.2 Hexagonal Boron Nitride Synthesis

Since the system that can produce hexagonal boron nitrides (hBNs) used in experimental studies is located in Sabancı University Nanotechnology Research and Application Center (SUNUM) Laboratory, hBNs were produced by a chemical vapor deposition method (Figure 3.2).

In the synthesis of hBNs, boric acid (H_3BO_3) and ammonia (NH_3) were used as a source of boron and nitrogen atoms, respectively. First, 2 g of H_3BO_3 was suspended in 3 mL of 13.38 M NH_3 solution and H_3BO_3 solution was prepared. The mixture was then layered in an alumina boat and dried on a hot plate set at 100°C for about 20 minutes. The mixture in the alumina vessel was heated in a high-temperature oven up to 1300°C with a heating rate of 10°C/min under a stream of ammonia gas for 2 hours. After heating process, the alumina boat was seperated from the furnace at approximately 550°C, and hBN products were collected in a tube from the surface of the alumina boat and kept at 25°C in the desiccator [105].

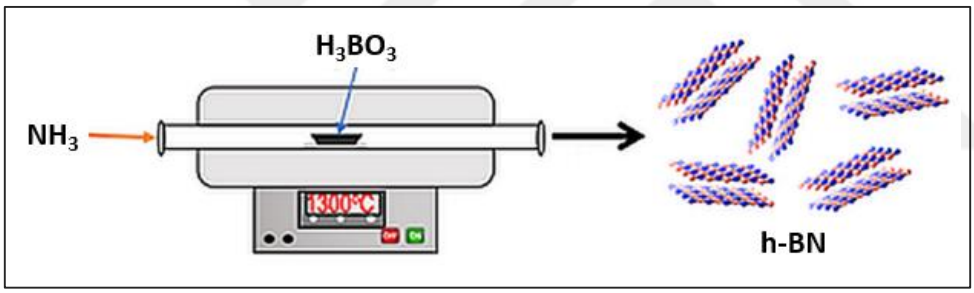

Figure 3.2 : Schematic representation of the hBN synthesis process [106].

3.3 Preparation of Buffer Solutions, Stock Drug Solutions, and Calibration Curves at Different pH Values

Drug loading experiments were prepared at two different pH (6.0 and 9.0) mediums to compare the efficiency of drug loading pH. Tris buffer solutions were prepared by using Tris Hydrochloric acid (HCl) and Tris base salts to prepare drug solutions at both different pHs. In order to keep the pH of the drug solution constant and to prevent pH change, [107] drug stock solutions were prepared with buffer solutions.

Drug stock solutions were sonicated in an ultrasonic bath for about 1 hour to dissolve the drug better; then, they were prepared by mixing in a magnetic stirrer at approximately 150 rpm for 48 hours.

Drug release experiments were carried out in two different pH (4.5 and 7.4) mediums with phosphate buffer solution (PBS).

In the literature, the maximum absorbance value of Mitoxantrone Dihydrochloride is given as 608 nm [108]. This study determines this value at 611 nm with the Perkin Elmer LS 45 branded UV/Vis spectrometer. All drug loading and drug release experiments were calculated at 611 nm, and each experiment was repeated at least 3 times. All results were averaged.

To be used in drug loading (pH 6.0 and 9.0) and drug release (pH 4.5 and 7.4) experiments, different calibration curves were prepared for each pH medium (Appendix A).

3.4 Drug Loading Studies

Drug loading experiments were carried out at constant drug loading concentration and constant amount of hBN while different amounts of drug solution was changed to determine the maximum loading conditions. Drug loading efficiency was evaluated acording to Equation 3.1.

$$\text{Drug Loading Efficiency } (\%) = \frac{a - b}{a} \text{ x } 100 \qquad (3.1)$$

where;

a: The amount of drug in the initial solution (mg)

b: The amount of drug after the drug-loading is completed (mg)

The direct interaction of Mitoxantrone Dihydrochloride with the hBN nanomaterial was performed in pH 6.0 or pH 9.0 in a Tris buffer medium. To make the hBNs dispersed, they were sonicated in an ultrasonic bath for 10 minutes with the specified volume of buffer solution.

All drug loading experiments were done in an orbital shaker at 25°C with a speed of approximately 200 rpm. The drug loading steps are shown in Figure 3.3. For calculating the amount of drug loaded at certain time intervals, samples were taken from the solutions, and the absorbances of the samples were measured at the characteristic peak value of the drug (611 nm) using the UV/Vis spectrometer. The concentration corresponding to the measured absorbance value was determined with

the help of the calibration curve. All experiments were repeated at least 3 times, and the calculations were made by taking the average value.

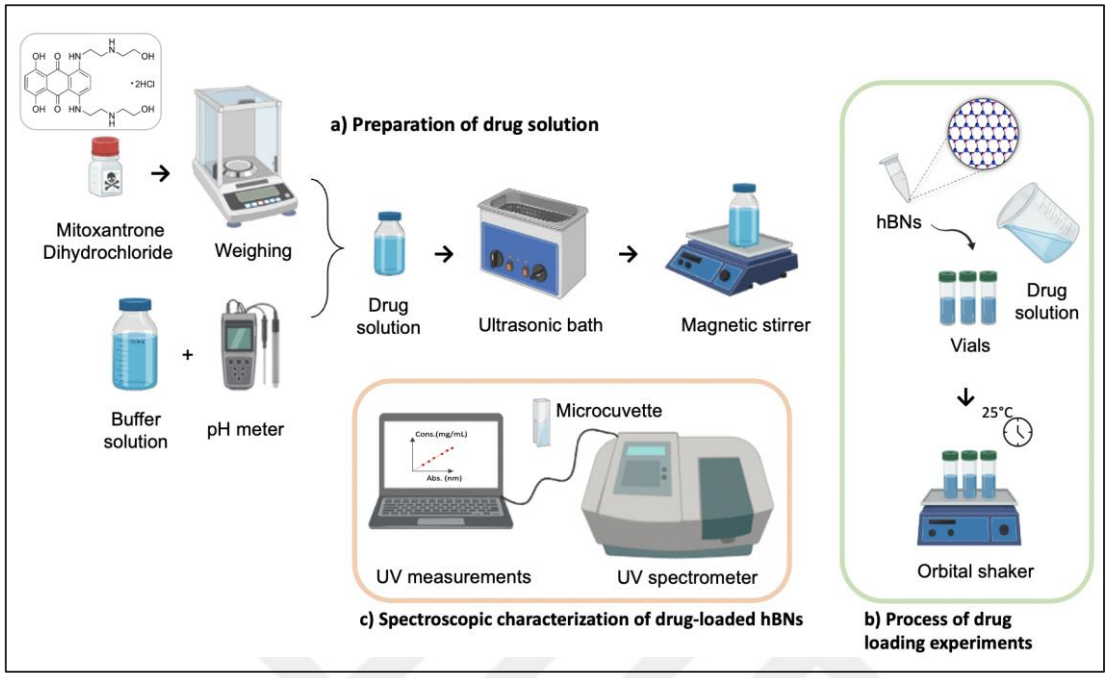

Figure 3.3 : The process of preparating buffer and drug solutions, drug loading experiments and spectroscopic characterization.

3.4.1 pH-dependent evaluation

In drug loading experiments, the pH of the solutions was measured at various time intervals before, during, and after the investigation, and it was observed whether the loading pH changed related to time. The changes in pH were compared in the experiment performed under the same conditions. It was determined that the pH of the samples, in which drug loading experiments were initiated with pH 9.0 Tris buffer solution, was fixed at approximately 8 during the experiment. Therefore, stock solutions and drug loading experiments were prepared in a pH 9.0 medium; however, for more accurate calculations, the calibration curve was designed in pH 8.0 medium (Appendix A).

3.5 Drug Release Studies

The drug release experiments were continued with drug-loaded hBNs. For determining the drug release performance of drug-loaded hBNs at different pHs, drug-loaded hBNs were left to settle in the dark at 25°C room conditions for approximately 1.5 days. The decantation process was done carefully to separate the remaining drug solution from

the precipitated nanoparticles without any loading. The solutions were centrifuged at 4,000 rpm for about 30 minutes in case of the presence of hBN in the drug solution remaining unloaded. The nanoparticles were not observed in the solutions at the end of centrifugation. Then, the nanoparticles were dried in an oven set at about 40°C for 48 hours. The dried materials were carefully washed at least 2 times to remove the remaining drug without loading on the nanoparticles.

Drug release experiments were first carried out with drug-loaded hBNs at 37°C human body temperature, in pH 4.5 PBS solution medium, in 10 mL buffer solution with an orbital shaker (Figure 3.4). The measurements were taken on the first day of drug release frequently. Then, it was continued until the drug release reached the equilibrium. Each measurement was made by recording the absorbance of the drug at the characteristic peak value (611 nm) in the UV/Vis spectrometer of the 0.88 mL samples drawn with a micropipette at different time intervals. Concentrations corresponding to absorbance values were calculated with the calibration curve. After each measurement, the amount withdrawn for measurement was returned to the experimental environment. Each experiment was repeated at least 3 times within itself and the average values of the results were recorded. The same procedures were repeated for pH 7.4 PBS medium.

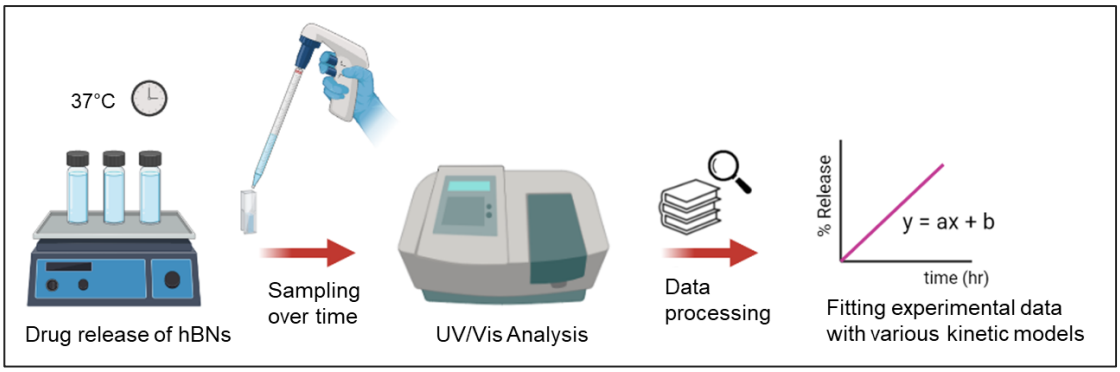

Figure 3.4 : The process of drug release experiments.

3.6 Characterization Techniques

Various characterization techniques were used in this study such as UV/Vis Spectrometer, Fourier Transform Infrared Spectroscopy (FT-IR), Transmission Electron Microscopy (TEM), Scanning Electron Microscopy (SEM), Thermogravimetric Analysis (TGA), Atomic Force Microscopy (AFM), Dynamic Light Scattering (DLS), and Zeta potential.

3.6.1 UV/Vis Spectrometer

UV/Vis spectra were performed using Perkin Elmer Lambda 35 UV/Vis Spectrometer in the 200-650 nm range for drug loading and release experiments. The measurements were obtained at least three times, then their mean values were calculated.

3.6.2 Fourier Transform Infrared Spectroscopy (FT-IR)

FT-IR spectra of hBN, Mitoxantrone Dihydrochloride, and drug-loaded hBN were obtained in the wavelength range of 4000-650 cm^{-1} using Agilent Technologies Cary 630 FT-IR measuring instrument.

3.6.3 Transmission Electron Microscopy (TEM)

TEM was carried out by using FEI TALOS F200S in SUNUM laboratories to examine the microstructure of the hBNs after their sythesis process.

3.6.4 Scanning Electron Microscopy (SEM)

The morphology of the synthesized hBNs were monitored by SEM. For SEM analysis, JEOL JSM-6390LV device was used.

3.6.5 Thermal Gravimetric Analysis (TGA)

TGA was performed at room temperature under an inert gas atmosphere, from room temperature to 550°C, with a heating rate of 10°C/min, using a Perkin-Elmer Diamond TA/TGA instrument.

3.6.6 Dynamic Light Scattering (DLS)

The particle size distributions of hBNs synthesized in aqueous media were measured by DLS analysis using Malvern Zetasizer Nano ZS in SUNUM laboratories and the hydrodynamic stability of hBNs was investigated. After the optimal distribution of hBNs sonicated in ddH_2O for 2 minutes was achieved, samples were analyzed to evaluate their colloidal stability over time.

3.6.8 Atomic Force Microscopy (AFM)

AFM analysis was performed by using Park System XE100 in SUNUM laboratories to precisely measure the forces between the molecules of the synthesized hBNs and to visualize the surface topography and morphology of the material.

3.6.9 Zeta Potential

It isn't easy to characterize the actual surface potential experimentally. Therefore, Zeta potential (ζ) measurements have been performed by using Malvern Zetasizer Nano ZS.

3.7 Kinetic Models of Mitoxantrone Loaded hBNs

For *in vivo* studies, which are the continuation of *in vitro* studies, kinetic models are used to determine biological performance. Thus, experimental data of *in vitro* drug release are evaluated, and controlled release formulations are developed. For this purpose; many models indicate drug release from nanocarriers kinetically. In this study, the Zero Order, First Order, Higuchi, Korsmeyer-Peppas, and Hixon-Crowell models [109], which are the most widely used kinetic models, were used. In addition, the kinetic constants of the models were calculated using the release data of Mitoxantrone from hBNs. Table 3.2 shows the kinetic models used and their equations to examine the drug release kinetics within the scope of this study.

Table 3.2 : Drug release kinetic models used in this study.

Model Name	Mathematical Model
Zero Order	$F = k_0 t$
First Order	$\ln(1–F) = – k_f t$
Higuchi	$F = k_H t^{1/2}$
Korsmeyer-Peppas	$F = k t^n$
Hixson-Crowell	$W_0^{1/3} – W_t^{1/3} = k_S t$

Where, W_0 is initial amount of drug in the solution, W_t is amount of drug released in time t, F is fraction of drug released at time t, t is time, k_0 is Zero Order release constant, k_F is First Order rate constant, k_H is Higuchi dissolution constant, k_P is Korsmeyer-Peppas constant, k_S is Hixon-Crowell constant, and n is exponent of release.

The release profile of each drug system can be mathematically modeled and described (Figure 3.5). By using these models, a controlled and adjustable drug delivery system can be designed for various applications. The correlation coefficient (R^2) is used to validate the experimental data to check the accuracy of the kinetic model.

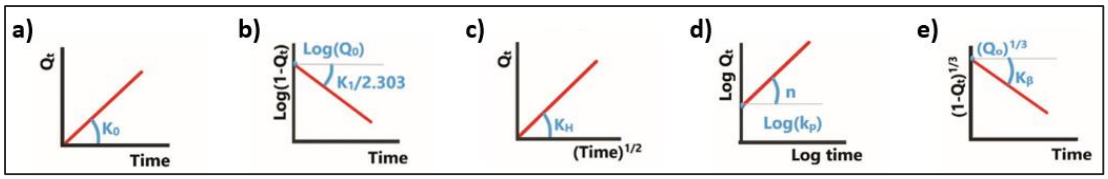

Figure 3.5 : Linearized plots of most common kinetic models; a) Zero Order, b) First Order, c) Higuchi, d) Korsmeyer-Peppas, and e) Hixson-Crowell [110].

3.8 Statistical Analysis

All experimental studies were accomplished at least three times, and each concentration was performed in triplicates in order to do independent experiments. Results were expressed as mean ± standard deviation (SD). Statistical analysis was carried out by one-way analysis of variance (ANOVA), followed by t-test with considering $p \leq 0.05$ statistically significant.

4. RESULTS AND DISCUSSIONS

In this study, the transport of Mitoxantrone drug with the synthesis of hexagonal boron nitride (hBN), which is both a new and promising nanomaterial, was investigated, and a new drug delivery system was designed to reduce the side-effects of cancer treatment and ensure that the drug reaches the targeted area safely. The experimental plan for this study is as follows:

- hBN synthesis (Performed in SUNUM Laboratory)
- Loading of MTX drug into hBNs at different pH mediums
- Release of MTX drug in different pH mediums
- Examination of drug release kinetics
- Characterization studies

The methods followed in each step, and the results of the studies are explained in detail in the relevant sections below, and the results compared with the literature are interpreted.

4.1 Hexagonal Boron Nitride Synthesis

The most important step in designing a drug delivery system begins with synthesizing the nanocarrier. For this purpose, the raw materials and synthesis method to be used in hexagonal boron nitride (hBN) synthesis in this study were investigated in detail.

The characteristic property of each nanomaterial varies according to the process in which it is synthesized, and the raw materials used. For producing hBN with a honeycomb-like crystal lattice structure, boric acid was chosen as the starting boron material, and hBN synthesis was carried out according to the Chemical Vapor Deposition (CVD) method [105]. The fact that boric acid is one of the most effective starting materials has an essential effect on the morphological structure of hBNs [77]. Depending on the literature studies conducted to interpret synthesis results, both spectroscopic and morphological characterization results show that hBNs synthesized

in SUNUM laboratories exhibit high uniformity, and similarity to the thrombocyte-structure.

4.1.1 UV/Vis spectrophotometer

UV/Vis spectrophotometer is of great importance in identifying, examining, and characterizing synthesized hBNs. For this purpose, UV/Vis spectrophotometer has been used to evaluate the absorption of hBNs. First, hBNs were dispersed by sonication in ddH_2O about 2 minutes before the analysis. Each measurement was repeated at least 3 times, and the averages were taken.

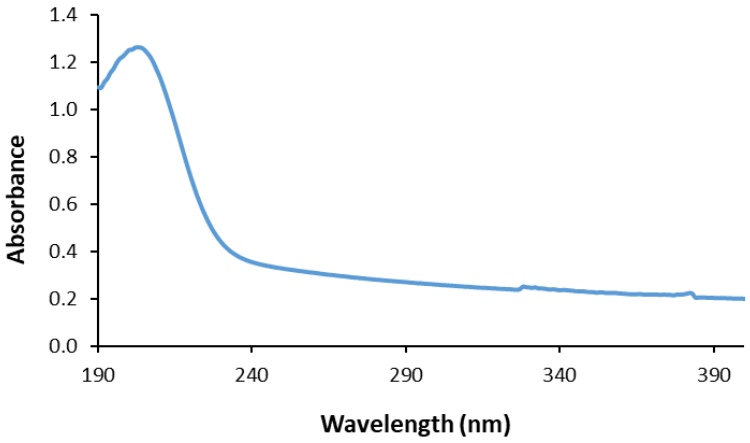

Figure 4.1 : UV/Vis spectrums of hBN.

hBNs have a maximum specific absorbance at about 200-220 nm, corresponding to the B-N bond. This absorbance value is clearly seen in the UV/Vis spectrum of the synthesized hBNs (Figure 4.1), and its characteristic peak is measured as 205 nm. This value is compatible with other studies in the literature [62]. Moreover, the absence of any other peaks in the spectrum other than this value proves the purity and successful synthesis of hBNs in this wavelength range.

4.1.2 FT-IR

FT-IR analysis was carried out to obtain structural and compositional information arising from the vibrational movement of the bonds in the boron and nitrogen containing the structure of the synthesized hBNs. According to the literature, hexagonal boron nitrides have 2 characteristic peaks. These vibratons are summarized as follows [84]:

706 - 810 cm^{-1} : out-of-plane B-N-B (bending)

1370 - 1408 cm^{-1} : in-plane B-N (stretching)

The hBN peaks in the FT-IR measurements (Figure 4.2) taken in the wavenumber range of 500 to 4000 cm^{-1} show similar behavior with the peaks obtained in the literature [62,81,105].

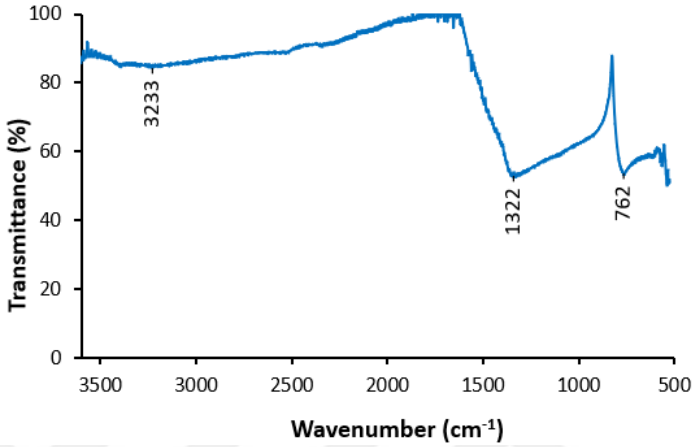

Figure 4.2 : FT-IR spectrums of hBN.

In the FT-IR spectra of the synthesized hBNs, wide peaks were detected at 762 cm^{-1} and 1322 cm^{-1} attributed to B-N-B and B-N vibrations, respectively. According to the literature, the peak at ~3200 cm^{-1}, which is attributed to the -OH stretch, indicates the -OH stretching vibration caused by the moisture the material takes from the air [111]. In the synthesized hBNs, a slight peak, is attributed to the -OH stretching vibration was observed at approximately 3233 cm^{-1}, although not very prominent. This situation clearly demonstrates that hBNs have low degradation capacities [112].

The fact that the results are compatible with the results determined in the literature proves that the hBN synthesis was carried out successfully.

4.1.3 TEM

TEM analysis was carried out to examine the microstructure of the synthesized hBNs. Based on TEM images (Figure 4.3), it was observed that the synthesized hBNs showed platelet-like structures. They have uniform size with a lateral size of about 50 nm. In addition, the absence of any impurities around the hBNs indicates that the hBN synthesis has taken place successfully and that the synthesized hBNs are produced without any contamination. The results are compatible with the literature [62,77,105].

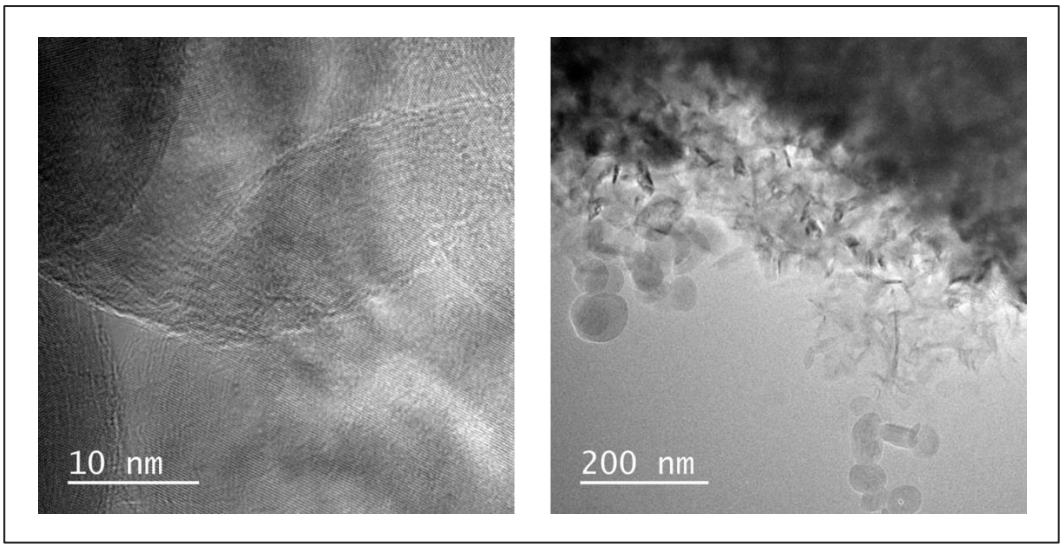

Figure 4.3 : TEM images of hBN with increasing magnification.

4.1.4 SEM

After the synthesis of hBNs, SEM analysis was performed to examine their morphological characteristics and sizes. Surfaces scanned by SEM contain high-energy electron beams. Thanks to this technique, three-dimensional morphological images of a sample less than about 1 nm are obtained [113]. The morphology and size of hBNs change depending on the preferred the method of synthesis and conditions and the type of boron precursor used as raw material [105].

The size of hBN particles synthesized with boric acid precursor is variable, and their morphological structure resembles platelets, as in Figure 4.4 [114]. The hBNs synthesized in this study are similar to platelets, as in Figure 4.5. The results show that the synthesized hBNs do not contain any impurities. The SEM images support the TEM results and the results are compatible with both each other and the literature [77,105,114].

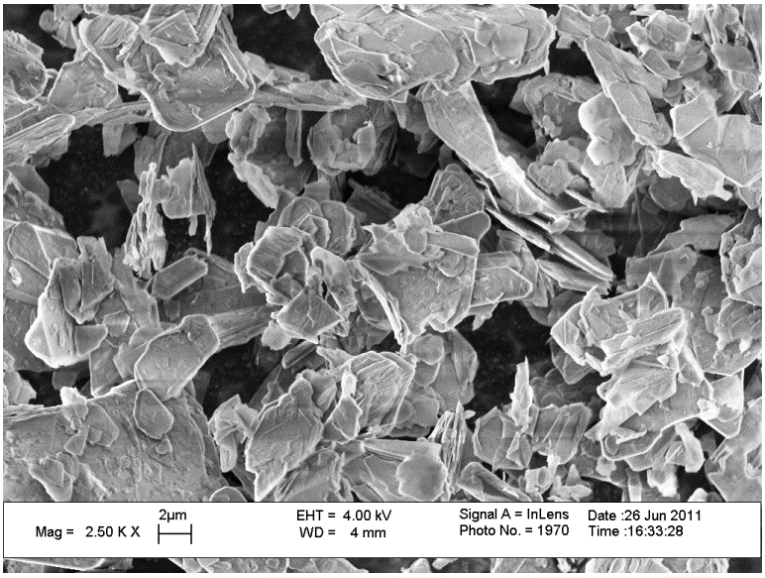

Figure 4.4 : SEM image of hBN in the platelet structure [114].

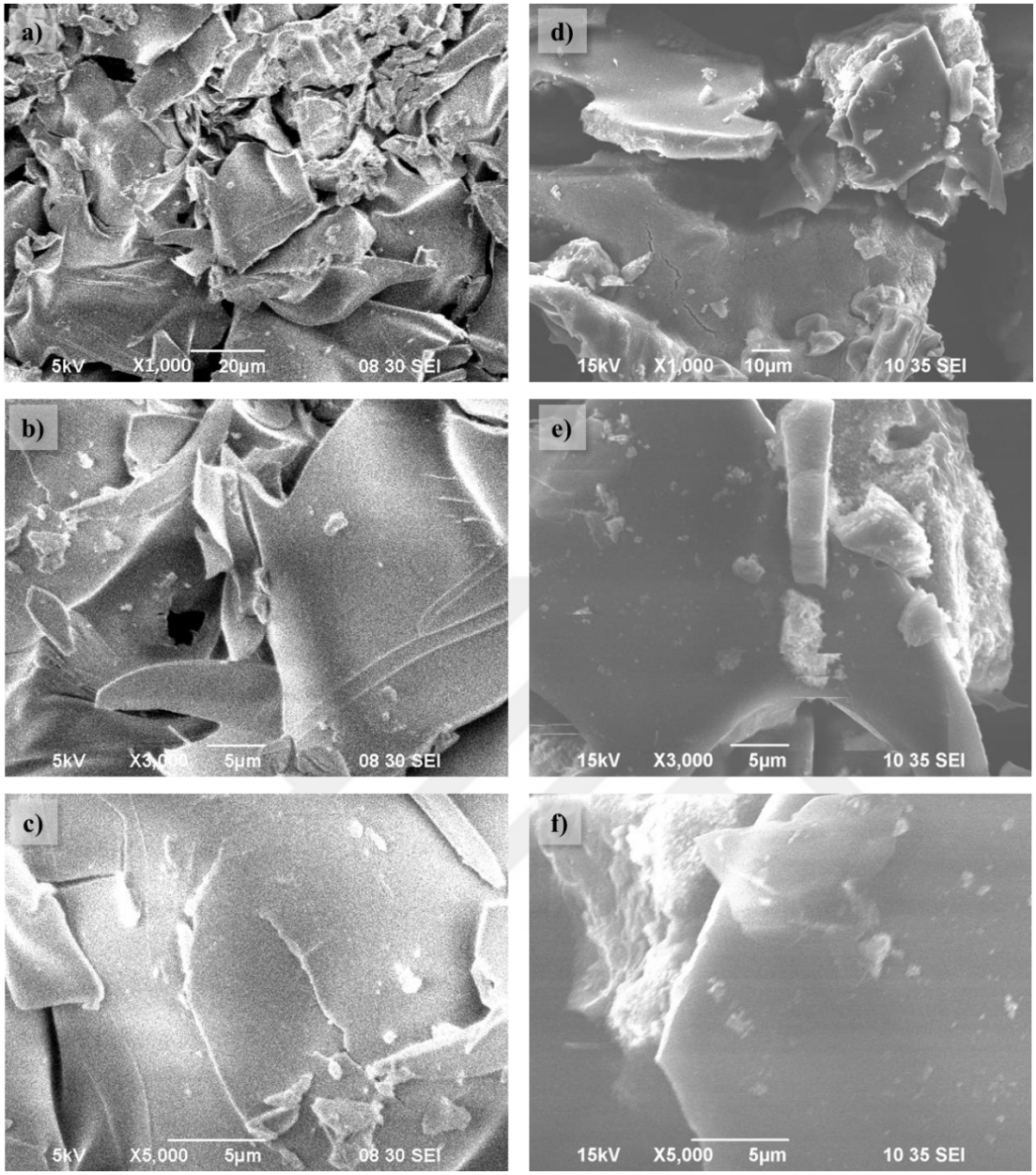

Figure 4.5 : SEM images of pure hBN.

Figure 4.6 shows SEM images of hBN surfaces with Mitoxantrone dihydrochloride (MTX). SEM images of pure hBNs without Mitoxantrone dihydrochloride (Figure 4.5) have different morphology compared to hBN images loaded with MTX (Figure 4.6). In Figure 4.6, it is clearly seen that the drug molecules cover the hBNs surfaces. The homogeneous MTX particles prove the successful drug-loading.

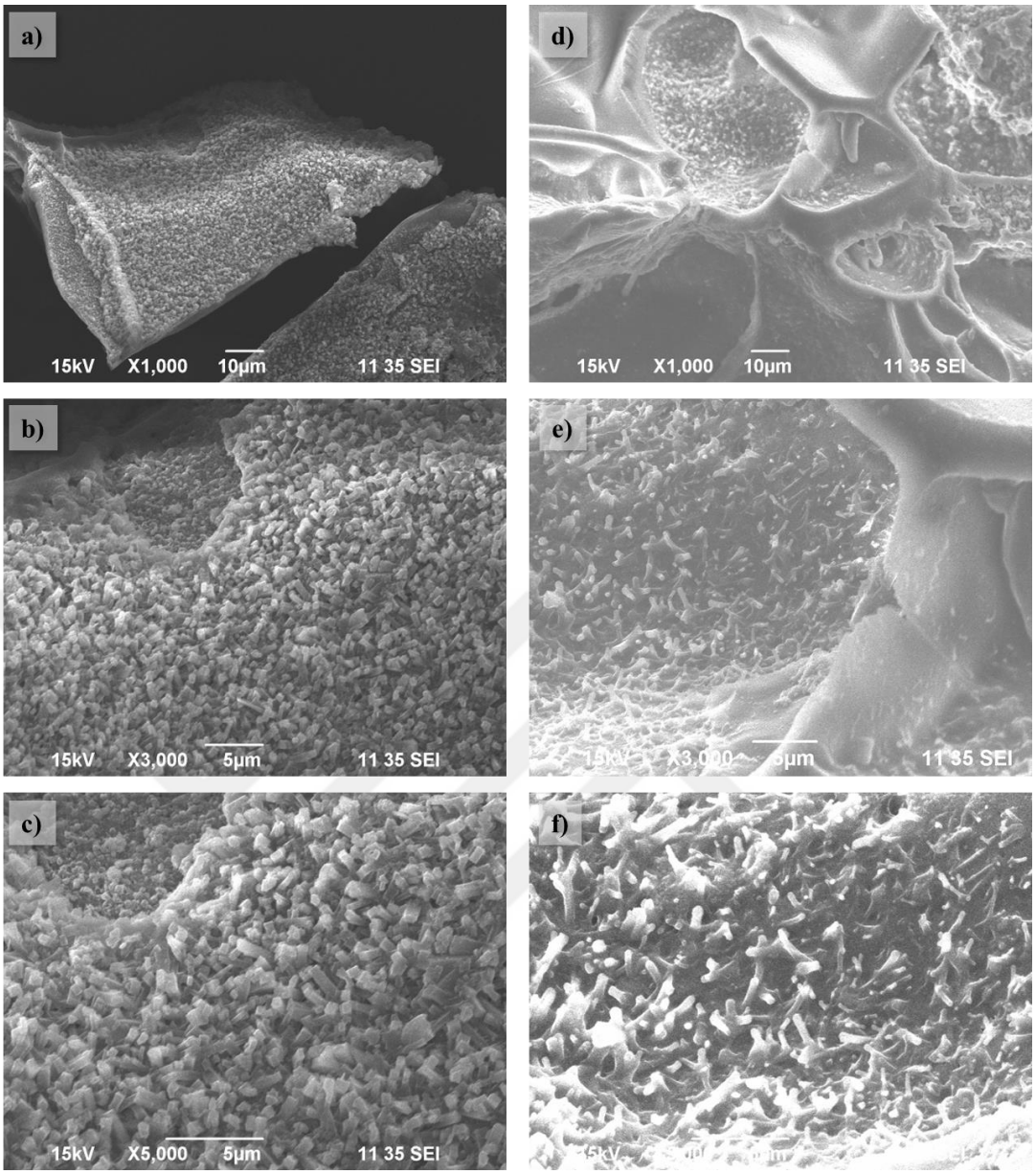

Figure 4.6 : SEM images of Mitoxantrone dihydrochloride loaded on hBN.

4.1.5 TGA

TGA analysis was performed to specify the impurity percentage of the synthesized hBNs. Thus, oxidation of hBNs was ensured by increasing the temperature in the air environment with TGA analysis. The remaining amount in weight loss indicates impurities. According to TGA analysis, the amount of impurities in hBNs was found to be approximately 5.8% (Figure 4.7). This is an acceptable value and shows that the hBNs are produced quite purely.

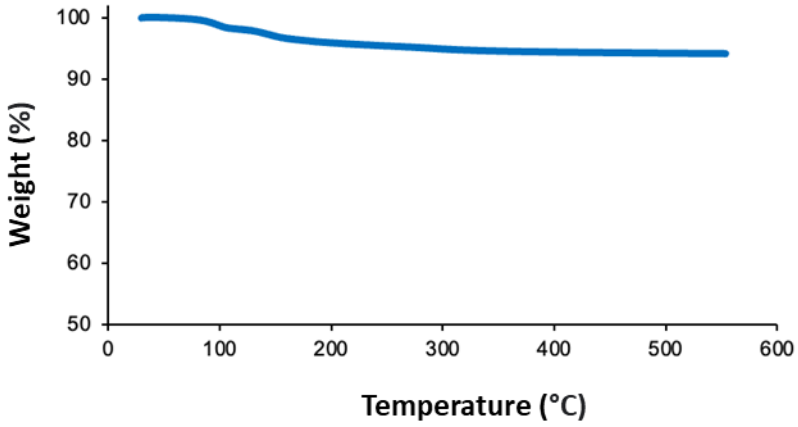

Figure 4.7 : TGA measurements of hBN.

4.1.6 DLS

With the DLS analysis, which is used to characterize nanoparticles and to obtain information about the particle size in solution, the particle size distributions of the synthesized hBNs in the aqueous medium were measured, and their hydrodynamic stability was investigated.

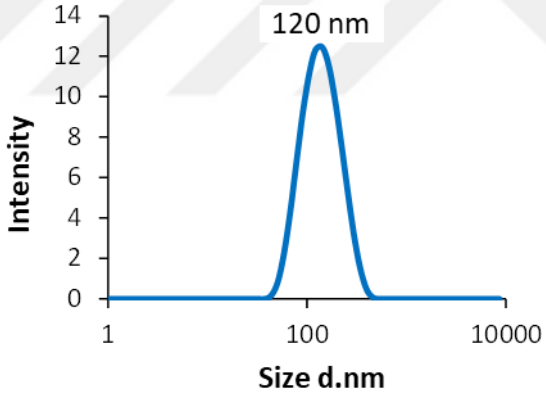

Figure 4.8 : DLS spectrums of hBN.

Time-dependent modification in the hydrodynamic size of hBNs demonstrates their colloidal stability. To measure the hydrodynamic size of hBNs, DLS analysis was performed in incubation in an aqueous medium. The hydrodynamic size of the synthesized hBNs was recorded as a maximum 120 nm after incubation (Figure 4.8). According to the results, the hBNs are dispersed efficiently in water and exhibit narrow size distribution even after incubation, corroborating their high colloidal stability. In addition, the thinner the size distribution of hBNs, the more regular their structure and higher uniformity [105]. The results of the DLS analysis are compatible with the literature [81,105] and the colloidal stability of the synthesized hBNs is relatively high.

4.1.7 AFM

AFM analysis was performed to precisely measure the forces between the molecules of the synthesized hBNs and to visualize the surface topography of the material. The results show that the synthesized hBNs have uniform structures (Figure 4.9) and are compatible with the literature [71,84]. In this way, it is understood that hBNs were synthesized with high efficiency and well-purified.

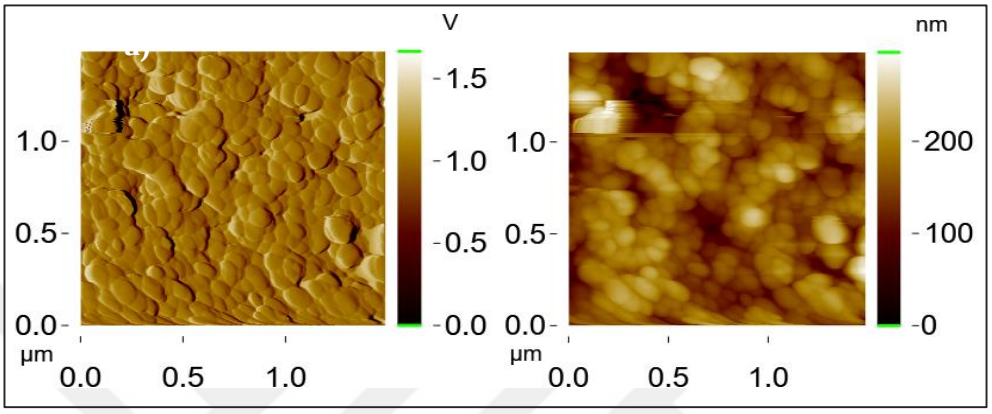

Figure 4.9 : Topography images of hBN with AFM analysis.

The general results of the characterization studies of synthesized hBNs are summarized as follows:

- Nano-sized hBNs have been produced.

- Structural and morphological properties of the synthesized nanomaterials were investigated, and various analyses were made in this direction.

- The synthesized hBNs have a significantly high purity.

- The characteristic peak was measured as 205 nm by UV/Vis. The lateral size dimension was around 50 nm. The hydrodynamic size was also measured as 120 nm which proved its high stability.

- The results are extremely compatible with the literature. At the same time, the purity of the material, its honeycomb, and its layered structure also support the results.

4.2 Drug Loading Studies

In this study the potential of hBN was investigated as a nanocarrier in cancer treatment. First, the interaction of hBN with MTX (MTX-hBN) was investigated as a non-covalent interaction at different pH mediums to determine the most efficient loading

condition. At the same time, drug loading was performed with different MTX/hBN ratios, and the most efficient loading condition was determined.

Mitoxantrone, which is a weakly basic drug, has pKa1 and pKa2 values of 5.99 and 8.13, respectively, as shown in Figure 3.1 and there are two ionizable amine groups in its structure. If the pH is higher than pKa2 = 8.13, MTX loses protons. In another words, amine groups makes MTX more hydrophobic at highes pH values. The UV absorption value for drug loading kinetics in the UV/Vis spectrum of MTX is 611 nm [115-117].

According to a study in the literature [108], the effect of Mitoxantrone on drug loading efficiency for carbon nanotubes at optimum pH was explored, and it was found that the optimum drug loading efficiency was at pH 9 (Figure 4.10). In the study, the reason for this was explained as the pKa value of the drug being between 8.3-8.6. It has also been demonstrated that in this pH range, specified as the optimum condition, most amine groups are deprotonated and become more hydrophobic so that they can bind to the nanotube surface by π–π interactions.

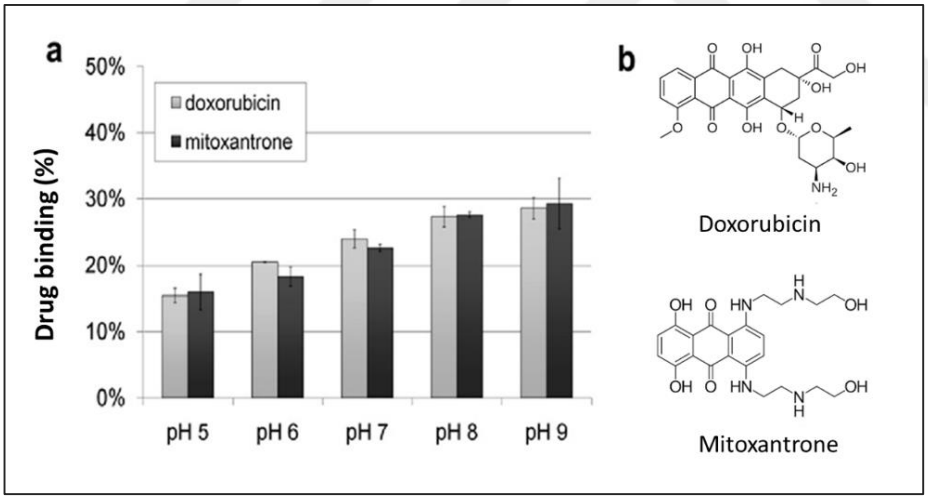

Figure 4.10 : a) pH-dependent interaction of Doxorubicin and Mitoxantrone with carbon nanotubes (at pH ranging from 5 to 9), b) chemical structures of DOX and MTX [108].

On the other hand, when the studies with Doxorubicin (DOX), which is the structural analog of Mitoxantrone anti-cancer drug and for which there are more studies in the literature compared to MTX, are examined, it is emphasized that the drug loading efficiency can vary according to the type of nanomaterial. In the literature, studies on the loading pH of DOX drug have reported that the most stable loading is at pH 7.0, according to its pKa values [pKa1= 7.34 (phenol); pKa2=8.46 (amine); pKa3=9.46];

however, since the optimum drug loading efficiency can alter depending on the type of nanomaterial and drug, the optimum loading pH has been investigated by loading at different pHs (4; 5.5; 7.4; 8.5; 9.4; 10.5; 11) in various studies Table 4.1. In this case, it would not be correct to determine the drug loading pH by only looking at the pKa value used in the study. Some of the studies on this subject are summarized in Table 4.1.

Table 4.1 : pH-dependent drug loading studies.

Nanocarrier type	Loading pH and loading solution	Notes (if necessary)	Ref.
hBN and BNNT	First fixed 7; then 4, 7, 11	The strongest interaction was observed at pH 7 and pH 11. Higher pH (pH 7 or pH 11) drug loading is appropriate for DOX–BNNTs and DOX–hBNs	[62]
Polymeric micelles	7.4 PBS	-	[118]
Mesoporous silica functionalized with Poly-L-Histidine and Tamoxifen	5 PBS	-	[119]
Poly(trimethylene carbonate)-b-poly(L-glutamic acid) (PTMC-b-PGA)	7.4 Tris; 10.5 Carbonate	The maximum DOX-loading content in polymerosomes is pH dependent: 23% (235 μg drug/mg polymer) at pH 7.4 and 47% (472 μg/mg) at pH 10.5.	[120]
SWCNT (PEG-SWCNT, PEG-PEI-SWCNT)	5.5; 7.4; 8.5 PBS	The amount of DOX loaded on SWCNTs depends on pH parameter. The loading factor was reduced from 100 to 19.5 to 11 as the pH was lowered from 8.5 to 7.4 and 5.5, respectively.	[121]

Considering all these studies, since the interactions of hBN and MTX have not been investigated before, drug loading experiments were carried out with this new nanomaterial with different drug amounts in both pH 6.0 and pH 9.0 mediums to determine the max drug-loading efficiency under optimum conditions. Within the scope of this study, the amount of hBN (3.0 mg) was kept constant, and the amount of the drug was determined in three different conditions such as 1.25 mg, 2.5 mg, 5.0 mg. The pH medium where the maximum loading was observed was selected for drug release and characterization studies.

4.2.1 pH-dependent evaluation

To investigate the optimum loading performance of Mitoxantrone on hBNs, time-dependent pH measurements were examined. After the drug loading experiment was started, the pH change during loading was explored at different time intervals. In addition, the same experiment was repeated under the same conditions, using a model drug, Procaine [122]. Since Procaine is a stable drug that has been used in many studies in our laboratory, it was chosen as a model drug in this study. In addition, the amine group in its structure is also present in Mitoxantrone (Figure 4.11).

The non-covalent interactions between hBN and drug occur with π-π bonds. Therefore, a reaction develops between the hBN and the drug, and this situation may affect the pH of the environment. In addition, some special conditions affecting the pH of the environment are due to the pKa of the drug. In another words, the type of drug, the pH of the drug, and the interaction between the drug and the nanomaterial which are the specific conditions affect the pH.

In Figure 4.11 b), the decrease in pH at pH 9.0 buffer+hBN may be due to the opening of the layers in the structure of hBN because of the sonication process. Furthermore, in Figure 4.11 c), pH stabilization at approximately 8 in hBN-Mitoxantrone and hBN-Procaine nanosystems prepared individually under all conditions including drug solution concentration is drug-dependent condition. The fact that Mitoxantrone (pKa = 8.3-8.6) and Procaine (pKa = 8.05) have similar pKa values and the pH of both drug solutions mediums stabilized to 8 over time explain that the pH of the medium is affected by the pKa of the drug.

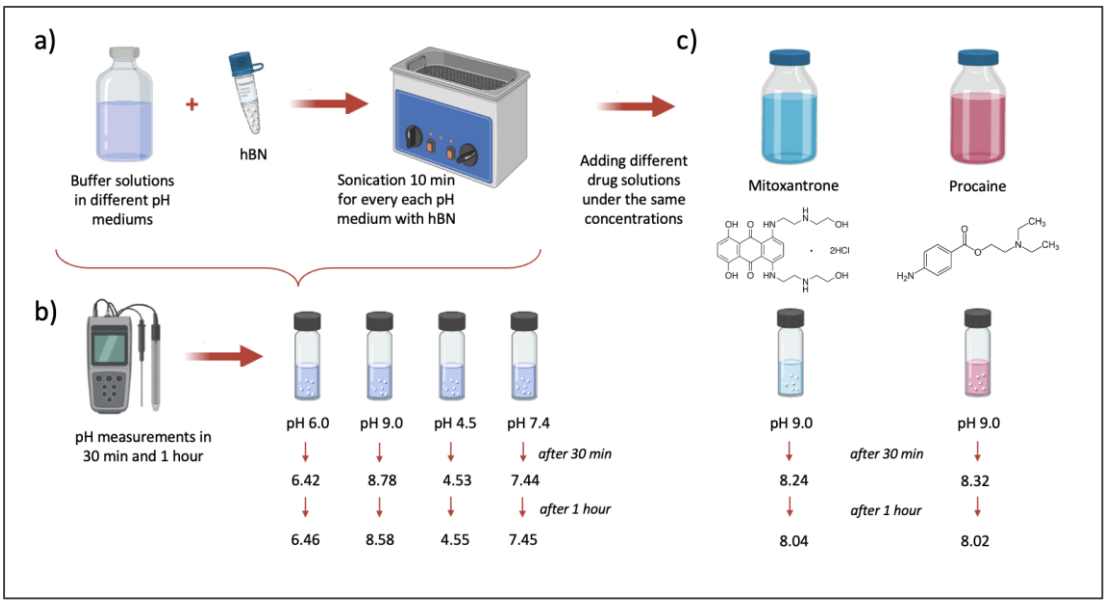

Figure 4.11 : pH-dependent measurements in detail; a) sonication process to make hBNs dispersed, b) pH measurements with only different buffer solutions in the first 30 min and 1 hour, c) pH measurements with different drug solutions under the same conditions.

Confirming to these results, we can not say that hBN nanomaterials reduce the pH of the drug solutions. In addition to the result, a calibration curve was prepared in pH 8.0 medium in order to determine more sensitive and accurate results, and the absorbance values measured in UV/Vis spectroscopy were read on the calibration curve (Appendix A) at pH 8.0 to determine the amount of drug in the solution prepared in pH 9.0 medium. Thus, it was determined that there was an improvement of about 1.5-2% compared to the values read at pH 9.0.

4.2.2 Drug loading at pH 6.0

Figures 4.12 indicates drug loading data at different drug:nanocarrier ratios in a pH 6.0 medium. According to the results obtained, depending on the MTX/hBN ratio, maximum drug-loading data were 6.0% (3rd day), 4.6% (1st day), and 6.3% (3rd day) for 1.25/3.0, 2.5/3.0, and 5.0/3.0, respectively (Figure 4.14). These data correspond to 1 mg of hBN versus 0.024 mg, 0.036 mg, and 0.102 mg of drug loading, respectively.

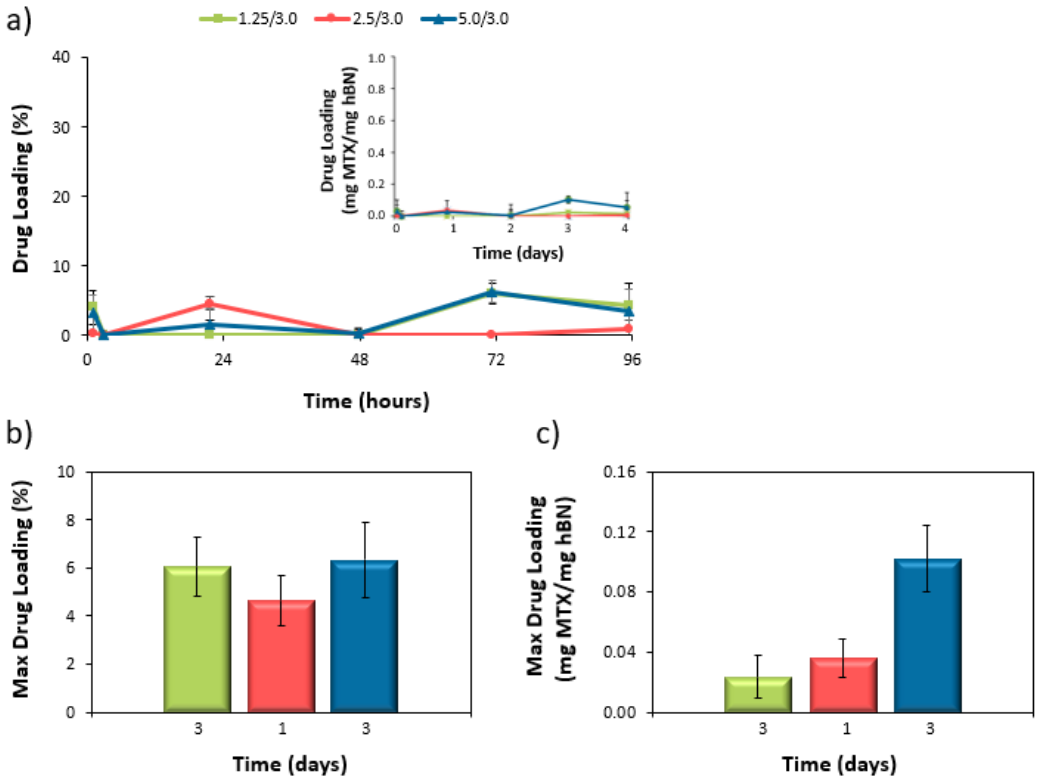

Figure 4.12 : Mitoxantrone loading at pH 6.0 medium a) efficiency (%) and amount (mg/mg); b), and c) max drug loading capacities (% and mg/mg, respectively) (The results are given as mean ±SD, $p > 0.05$).

4.2.3 Drug loading at pH 9.0

Drug loading data at different drug:nanocarrier ratios in pH 9.0 medium are shown in Figure 4.13. According to the results obtained, depending on the MTX/hBN ratio, maximum drug-loading data were 20%, 27.87%, and 32.75% in 30 minutes for 1.25/3.0, 2.5/3.0, and 5.0/3.0, respectively (Figure 4.14). These data attributed to 1 mg of hBN versus 0.111 mg, 0.284 mg, and 0.657 mg of drug loading, respectively. Interestingly, the maximum drug loading efficiency in all three MTX/hBN systems was achieved within the first 30 minutes. In addition, the stability of drug loading data observed up to 50 hours in pH 9.0 environment shows how excellent and stable nanocarriers hBNs are in terms of drug loading.

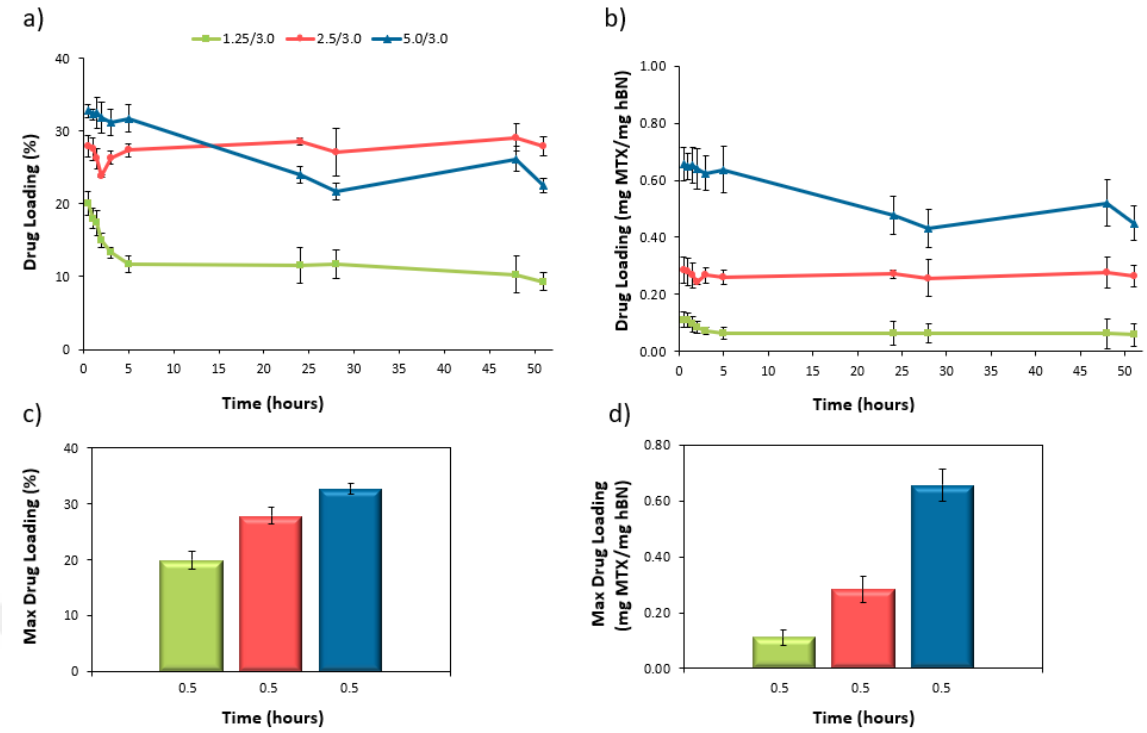

Figure 4.13 : Mitoxantrone loading at pH 9.0 medium a) efficiency (%); b) amount (mg/mg); c), and d) max drug loading capacities (% and mg/mg, respectively) (The results are given as mean ±SD, $p \leq 0.05$).

This study observed that the drug loading capacity, which was examined in pH 6.0 and pH 9.0 Tris buffer environment, was higher and more stable in pH 9.0 medium. According to a study examining the drug loading capacity of CNTs with Mitoxantrone [108], optimum drug loading efficiency was achieved at pH 5 to 9 ranges for 18 hours (Figure 4.10). It was determined that the max loading efficiency of Mitoxantrone drug was determined in the pH 8-9 range, the pKa value of the drug was in the range of 8.3-8.6, and thus higher drug loading efficiency was obtained due to the protonation of amino groups in the pH 8-9 range.

All results obtained for maximum drug-loading at pH 6.0 and pH 9.0 are given in Figure 4.14. According to the results, the maximum loading environment for Mitoxantrone and hBN nanosystem should be at pH 9.0.

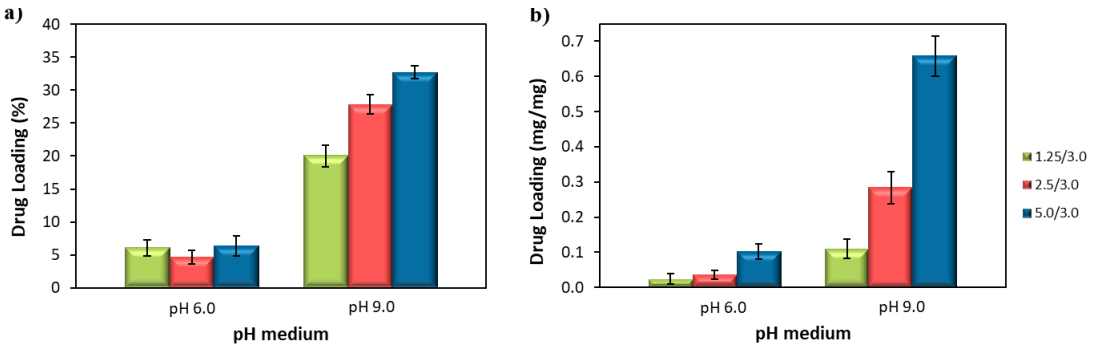

Figure 4.14 : pH-dependent drug interaction summary of MTX-hBN nanosystems; a) % loading, b) mg/mg loading (The results are given as mean ±SD, $p \leq 0.05$).

Confirming the drug loading capacity of the boron nitride nanomaterials summarized in Table 4.2, although we obtained low drug loading efficiency in the pH 6.0 medium when compared with the studies in the literature, it is seen that the loading capacity increases as the amount of drug in the drug/nanocarrier model increases. In this case, it can be interpreted that the drug-loading efficiency depends on the amount of the drug, as can be seen from the Figures 4.12, 4.13, 4.14.

According to a study [62], BNNTs have been proven once again to be superior to hBNs in terms of drug-loading capacity with having 3 times more capacity than hBNs (Table 4.2). However, MTX-hBN drug loading results in this study are higher than DOX-BNNT loading results, as can be seen from the table. Thus, except for the functionalization process, our drug loading efficiency results (especially at pH 9.0) are higher than other drug/BN nanosystems. Again, as seen from Table 4.2, the effect of functionalization on drug loading capacity is clearly seen in DOX-BN and FA-DOX-BN nanosystems. In these systems, DOX-BN has a drug loading capacity of 6.9 µg/mg prior to any functionalization; whereas functionalization with folic acid (FA), the FA-DOX-BN system reaches a drug loading capacity of 20.7 µg/mg. According to these results, functionalization has affected the loading efficiency aproximately 3 times.

In order to obtain a high drug loading capacity of Mitoxantrone on hBNs, in future studies, functionalizing the hBN nanomaterial with appropriate biomaterials will increase the drug loading capacity considerably, and a higher loading capacity will be obtained according to the literature. As an example of functionalization for future studies, the functionalization of hBNs by sonication with ddH_2O (OH-hBNs) can be recommended as it is a cheaper method and does not involve an additional process for purification. Another suggestion is that functionalization with Folic acid (FA), which

is biocompatible with the body and as indicated in the studies in Table 4.2, has been shown to increase drug loading efficiency by approximately 3 times. To make the study unique, functionalization studies with various amino acids (Fmoc-Glycine, Fmoc-Cysteine, Fmoc-Tryptophan) are also considered to increase the drug loading efficiency.

Table 4.2 : Exploring drug loading capacities related to nanocarrier types.

Nanocarrier Type	pH medium	Drug-loading capacity		Reference
		μg drug/mg nanocarrier	mol/mg nanocarrier	
MTX-hBN (1.25/3.0)	6	24	0.05	This study
MTX-hBN (2.5/3.0)	6	36	0.07	This study
MTX-hBN (5.0/3.0)	6	102	0.20	This study
MTX-hBN (1.25/3.0)	9	111	0.21	This study
MTX-hBN (2.5/3.0)	9	284	0.55	This study
MTX-hBN (5.0/3.0)	9	657	1.27	This study
DOX-hBN	4, 7, 11	110	0.20	[62]
DOX-BN	No information	55	0.10	[82]
DOX-BNNS	7.4	6.9	0.01	[77]
FA-DOX-BN	No information	20.7	0.04	[80]
DOX-BNNT	4, 7, 11	330	0.61	[62]
DOX-BNMS	No information	52.6	0.10	[119]
FA-DOX-BNMS	No information	49.2	0.09	[119]
DOX-BN	No information	7	0.01	[119]
DOX-Pd-OHBNNS	No information	862	1.59	[61]
PAHcit-BNNS	5, 6.5, 7.4, 9	72.6	0.13	[77]
MTX-CNT	9.1	510	0.99	[123]
MTX-CNT	9.0	1960	3.79	[124]

In addition, the drug-loading capacity without functionalization of Mitoxantrone and carbon nanotubes (CNTs) which is the most widely used drug delivery system from carbon-based materials, was found to be 0.51 mg/mg in one study [123] and 1.96 mg/mg in another study [124]. It should not be forgotten that CNT is a 1D material which is different from hBN (2D), so the optimum comparison should be made with BNNT (1D). BNNTs are non-toxic materials with a much higher drug-loading capacity than both CNTs and hBNs. In addition, the molecular interaction is superior to CNTs,

thanks to the spontaneous polarization of the B-N bond in BNNTs based on hBN structure.

4.2.3.1 UV/Vis

The interactions between MTX and hBNs values at pH 6.0 and 9.0 mediums were also characterized by using UV/Vis spectroscopy. The specific peak of hBN was observed at 210 nm and the specific peak of MTX was observed at 611 nm. As noted in the literature, hBN has a specific peak at 200-220 nm [62,105] and MTX has specific peaks at 247 nm, 277 nm, and 608-613 nm [108,120].

4.2.3.2 FT-IR

The structure of hBN nanosystems loaded with Mitoxantrone was analyzed by FT-IR spectrometry. The spectra for MTX, hBN andMTX-hBN are given in Figure 4.15.

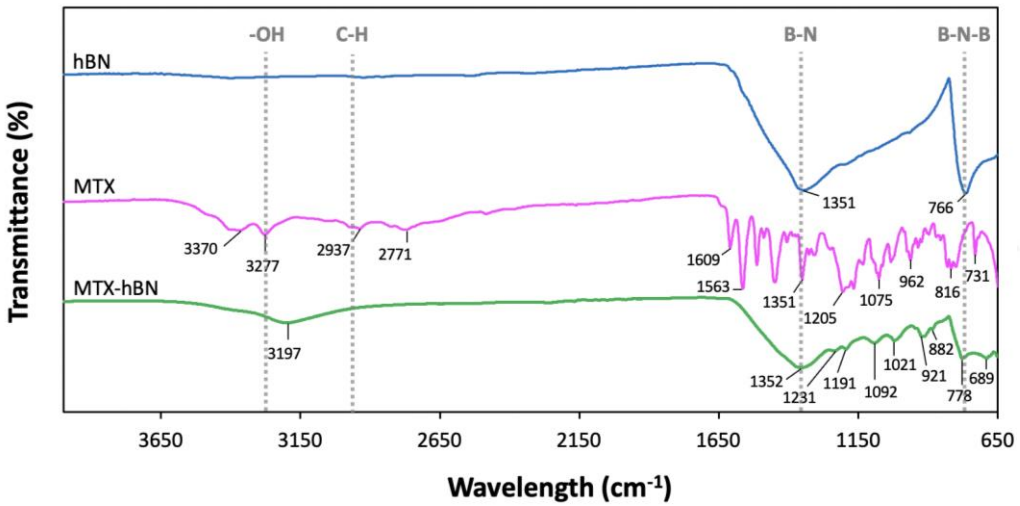

Figure 4.15 : FT-IR spectrums of hBN, MTX, and MTX-hBN.

hBN and MTX peaks show similar behavior to peaks obtained in the literature [62,81,105,121,125]. The results are consistent with the results found in the literature. Following the results of the spectra thus obtained, it is seen that the MTX drug was successfully loaded onto the hBN nanomaterials.

The 778 cm^{-1} and 1352 cm^{-1} peaks correspond to B-N-B and B-N vibrations, respectively, in MTX-hBN system. In addition, the slight peaks at 1231 cm^{-1}, 1191 cm^{-1}, 1092 cm^{-1}, and 1021 cm^{-1} belongs to the C-H bonds in the chain originating from the MTX molecule. Moreover, as reported in literature [121], a weak peak attributed to the -OH bond was observed for MTX-hBN at 3197 cm^{-1} (Figure 4.16).

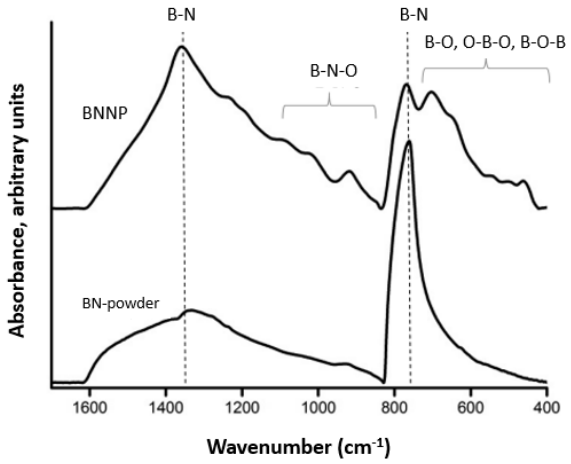

Figure 4.16 : FT-IR spectra of BNNP and BN-powder in detail [82].

The peak values of Mitoxantrone according to the FT-IR spectra in the literature are summarized below as shown in Figure 4.17 [121]:

C=C bonds in the aromatic ring : 1626-1370 cm^{-1}

C=O bonds in the aromatic ring : 1729 cm^{-1}

C-H bonds in the chain : 1217-1006 cm^{-1}

-OH bonds in the chain : 3290 cm^{-1}

C-H bonds in the amide group: : 2989 cm^{-1}

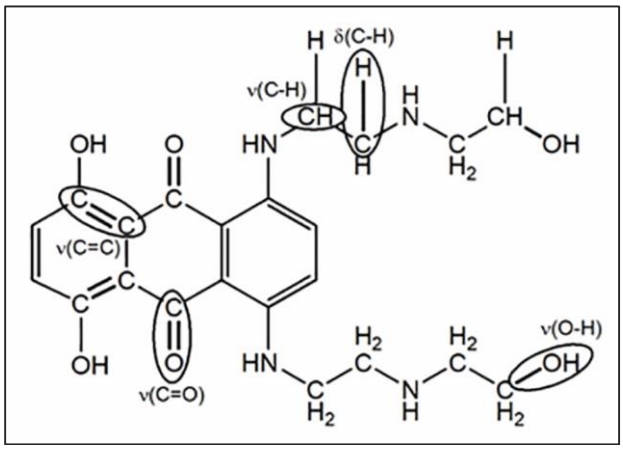

Figure 4.17 : Bonds in the chemical structure of Mitoxantrone in detail [121].

According to the FT-IR spectrum results of MTX molecule in Figure 4.15, 2987 cm^{-1} moderate peak is attributed to C-H stretching band [126], which is found as amide group in the structure. Peaks at 1609 and 1351 cm^{-1} are attributed to C=C bonds in the aromatic ring, and peaks 1205 are 1075 cm^{-1} are attributed to two chains of C-H bonds.

The absence of any peaks in the functional group region between 4000-1450 cm^{-1} in the MTX-hBN nanosystem indicates that there is no functional group in the structure.

4.2.3.3 Zeta potential and size distribution

Zeta potential is a physical property of all liquid-liquid and solid-liquid colloidal systems and is widely used to measure the charge value of the surface [127]. Zeta potential is formed between the material and the liquid containing the material. In a liquid, repulsive and attractive forces occur between particles because the particles with the same charges repel each other, and particles with opposite charges attract each other. In addition, these forces vary depending on the Zeta potential of the nanomaterial. That is why Zeta potential is also called electrokinetic potential, and measurement of Zeta potential gives critical information about the electrostatic distribution mechanism (Figure 4.18). The purpose of Zeta potential is to know about the material's colloidal stability and to comment on the surface charge, adsorbent property, and material-media relationship. Moreover, Zeta potential values alter depending on the pH of the solution, the properties of the solid surface, and the ions in the solution. A positive Zeta potential represents the net positive charge on the material surface, and a negative Zeta potential represents the net negative charge on the material surface. According to the Zeta potential value, it can be interpreted that the material with a more negative value is more hydrophobic [127,128].

Colloidal stability of hBNs with Zeta potential and Zeta size were performed by using Malvern Zetasizer Nano ZS. The average electrophoretic mobility is calculated by the Smoluchowski equation (Equation 4.1) [129].

$$u = \frac{\varepsilon \zeta}{\eta} \tag{4.1}$$

where, u, ε, and η are the particle mobility, the dielectric constant of water, and the viscosity of the medium, respectively.

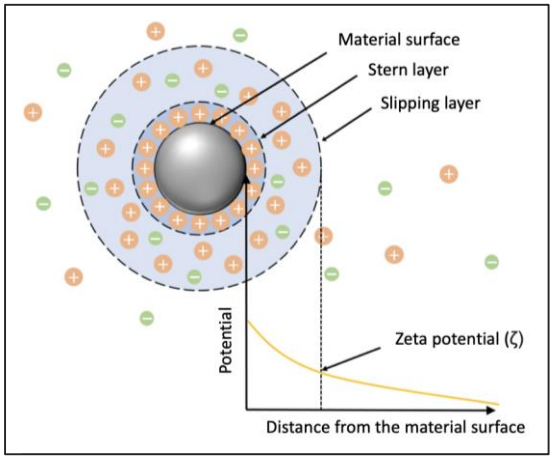

Figure 4.18 : Diagram of Zeta potential around a material in an aqueous electrolyte [127].

The surface of cancerous tissues is usually negatively charged. Generally, positively charged nanoparticles are more easily taken up by the cancerous cell and retained longer than negatively charged ones. Thanks to the Zeta potential measurement, the circulation of the nanosystems in the bloodstream and their absorption from the body membranes can be significantly adjusted and modified. In addition, drug loading efficiency to nanocarriers and drug release rate from nanosystems also vary depending on the Zeta potential. However, by looking at the drug's Zeta potential, it can be understood whether the nanomaterial protects the drug. If the Zeta potential value is close to the Zeta potential of the nanoparticle or is zero, it can be understood that the drug is protected by the nanoparticles. The nanoparticle's surface and its surface properties are essential for drug delivery systems. Surface modification is often done to allow nanosystems to stay in the bloodstream longer. Parameters such as the size and charge of nanoparticles can significantly impact the behavior of these materials in the biological environment [130].

In addition, due to studies that positively charged nanomaterials increase cytotoxicity, these materials have not been approved by the FDA. In contrast, negatively charged nanomaterials have been approved by the FDA, because they have lower cytotoxicity. On the other hand, it was found that negatively charged nanomaterials were less drug-loaded and cleared from the blood more slowly (staying longer in the blood) than positively charged nanomaterials. The surface charge density of nanomaterials should be optimally adjusted for the effective target of the drug, as there are various advantages and disadvantages for both charges [130].

The binding of the MTX molecule to hBNs has been demonstrated by its Zeta potential (Table 4.3 indicates widespread properties of Zeta potential in drug delivery literature).

Table 4.3 : Colloidal stability for Zeta potential intervals [131].

Zeta potential (mV)	Types of colloidal stabilities
0 to ± 5	Rapid agglomeration
± 10 to ± 30	Incipident
± 30 to ± 40	Moderate
± 40 to ± 60	Good
> ± 60	Excellent

As seen in Figure 4.19, hBN and MTX molecules are negatively charged, which indicates that both molecules are stable. The fact that MTX molecule is more negative than hBN shows that MTX is more stable than hBN.

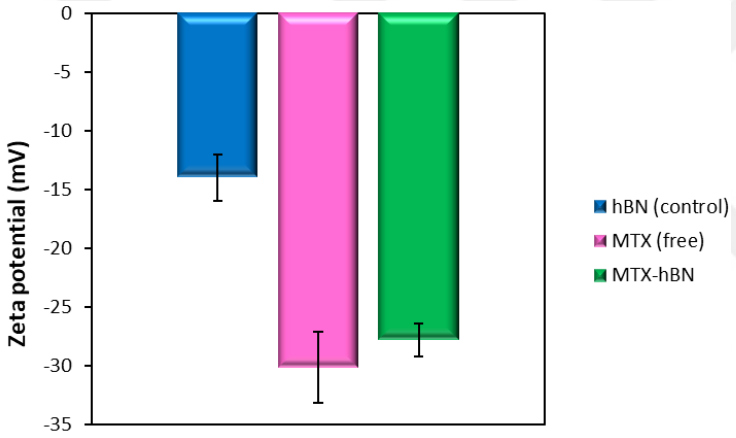

Figure 4.19 : Zeta potential measurements of hBN, MTX (free), and MTX-hBN.

According to results, in Table 4.4, it is clearly seen that while the hBN nanosystem was incipident stability before drug loading, MTX-hBN nanosystem approached moderate stability after drug loading.

Table 4.4 : Zeta potential values of hBN, MTX (free), and MTX-hBN samples.

Samples	hBN	MTX (free)	MTX-hBN
Zeta potential (mV)	-14.0 ± 1.95	-30.15 ± 3.04	-27.8 ± 1.41

Considering the electrostatic interactions that occur due to the repulsion of the same charges, after the negatively charged MTX (-30.15 mV) is loaded onto the negatively charged hBNs (-14.0 mV), the charge of the drug delivery system (MTX-hBN) is less negative (- 27.8 mV). Thus, the MTX-hBN interaction has become a much more stable system than hBN.

The size distribution can be calculated by intensity, volume and number. The Dynamic Light Scattering (DLS) analysis in Table 4.5 shows the data calculated by intensity. According to DLS analysis, the size of the hBNs before drug loading was 184.4, while the size of the MTX-hBN nanosystem after loading MTX was 566.9 (Table 4.5). An almost 5-fold increase in initial hBN size after drug loading indicates effective drug loading. The results confirm the Zeta potential data as the drug is effectively loaded.

Table 4.5 : Size and intensity parameters of hBN and MTX-hBN samples.

Samples	Size (d.nm)	Intensity (%)	PDI
hBN	184.4	26.4	0.06
MTX-hBN	566.9	90.4	0.03

The polydispersity index (PDI) is a value that helps in determining the heterogeneity of a material based on size. The PDI value is a value between 0-1. According to international standards, a PDI value less than 0.1 indicates that the material is monodispersed. On the other hand, if the PDI is greater than 0.1, then it is interpreted that the material is polydisperse [132]. According to Table 4.5, the PDI value for both systems is less than 0.1, indicating that the nanosystems are monodispersed.

4.3 Drug Release Studies

The release behavior of the MTX drug, described in detail in this section, can be controlled by pH, and regulation of the Zeta potential.

The reason for choosing the pH values is that the pH value of tumor tissues and tumor microenvironment is acidic (4.5-6.0); however, the blood pH is neutral (7.34-7.45) [42]. While the drug release experiments in the acidic medium represent the drug release in the tumor region, they represent the drug release in the blood in the neutral environment.

The recommended starting dose of Mitoxantrone in cancer treatment is 12-14 mg/m^2 (at 21-day intervals). Considering this data as the drug release target, although the amount of MTX dose used in this study is low compared to the treatment dose, it has been explained in the literature that this amount can be increased if desired [92].

In this study, drug release experiments were carried out in two different pH environments. Thus, the effect of medium pH on drug release of hBN nanoparticles

was investigated. At the same time, the reason for choosing two different pH values is that the cancer cell tissue is in the pH range of about 4.5-6.5, and the pH of healthy cell tissues and bloodstream is 7.4. Moreover, in a previous study [108] pH-dependent drug release kinetics was reported for MTX. According to the results of this study, approximately 50% and 8% release of MTX from carbon nanotubes was observed in pH 5.5 and 7.4 environments, respectively. It has been explained that the reason for almost 6 times more drug release at pH 5.5 compared to pH 7.4 medium is the amine groups in the MTX molecule. Amine groups play an important role in making MTX drug hydrophobic at higher pH and hydrophilic at lower pH. This showed that the binding of MTX anti-cancer drug to nanomaterials is pH-dependent.

In the cumulative drug release experiments conducted in this study (Figure 4.20), it was noticed that the drug release performance of hBN nanocarriers at pH 4.5 reached an equilibrium value after approximately 72 hours for prepared 2.5/3.0 MTX/hBN ratio, and after approximately 1 day for prepared 5.0/3.0 MTX/hBN ratio. In drug release experiments at pH 7.4, it was observed that the drug release performance of hBN nanocarriers reached an equilibrium value after approximately 1 day for 2.5/3.0 MTX/hBN, and after approximately 3 days for 5.0/3.0 MTX/hBN.

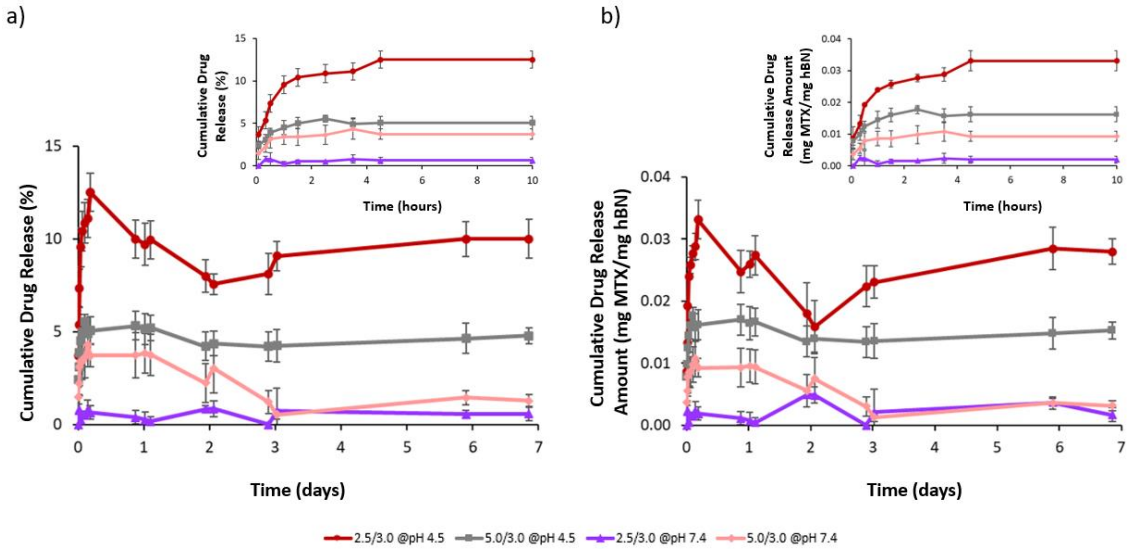

Figure 4.20 : Cumulative drug release at pH 4.5 and 7.4 mediums with different drug concentrations a) %release amount, b) mg/mg release amount (The results are given as mean ±SD, $p \leq 0.05$).

In these experiments performed for different MTX/hBN and different pH environments, maximum drug release performances for MTX-hBN nanosystems were found to be 12.5%, 5.5%, 0.9%, and 4.3%, for 2.5/3.0 (pH 4.5), 5.0/3.0 (pH 4.5),

2.5/3.0 (pH 7.4) and 5.0/3.0 (pH 7.4), respectively. The cumulative drug release amounts are 0.033 mg, 0.018 mg, 0.005 mg, and 0.011 mg per 1 mg hBN, respectively.

According to drug release data, the most suitable system for pH 4.5 medium was the 2.5/3.0 coded test system; because maximum drug release is desired in this pH 4.5 environment. Likewise, since the desired condition for the pH 7.4 environment is minimum drug release, the most appropriate system here was again the 2.5/3.0 coded test system. However, it seems clear that the low release of MTX from hBNs is owing to the low amount of MTX loaded on hBNs [62]. The drug release performance for all four systems was less than 50% for 168 hours, indicating strong π-π interactions of the drug with hBN [108]. As the strength of the π-π interactions between the aromatic rings of the MTX drug and the aromatic surface of the hBN nanocarriers increases, the amount of drug release will decrease. The system with the strongest π-π interaction in the MTX-hBN complex was the 2.5/3.0 system with a maximum release of 0.9% in pH 7.4 medium.

The most important finding to be determined in nanosystems studied for cancer treatment is the drug release performance in pH 7.4. Because if the drug loaded on the nanocarriers can not be released in the blood and other healthy organs until it reaches the tumor site but can be released at the desired location, it is stated that a successful nanosystem is designed, and it is extremely promising in future studies. In a study in the literature [42], since the release of paclitaxel from expansile nanoparticles at pH 7.4 is less than 10%, a "minimum release" interpretation has been made about this situation. The desired situation in the design of a drug delivery system in cancer treatment is that the cancer drug should be as stable as possible in the nanocarrier system, which is expected from drug delivery systems; however, it should not be released into the bloodstream except for a minimum drug leakage (<10%) [42]. Thus, when the drug in the drug-nanocarrier system reaches the cancerous tissues, it will be released from the nanocarrier with a particular increase due to the enhanced permeability and retention (EPR) effect and pH-dependent release performance with targeting delivery [133]. In this way, our drug release study had a <10% amount in the pH 7.4 PBS medium. The release of the 2.5/3.0 MTX/hBN nanosystem in the first 5 minutes is 0%, and the maximum value reached within 24 hours is 12.52% (0.033 mg/mg), which is considered a "minimum level of drug leakage" as stated in the literature. At the same time, this result once again proved that hBNs have very superior

drug loading capacity, as it is also due to the strong π-π interactions between MTX and hBN nanosurfaces. This implies that our study is extremely promising. In conclusion, it is predicted that our MTX-hBN nanosystem will be significantly successful in cancer treatment. All these results support the drug loading results and prove that the drug is loaded effectively.

4.3.1 Drug release kinetics models for MTX-hBN

FDA has defined the releases (Figure 4.21) such as immediate-release, modified-release, extended-release, and delayed-release; however, no definition is yet to be provided for targeted or controlled release [110].

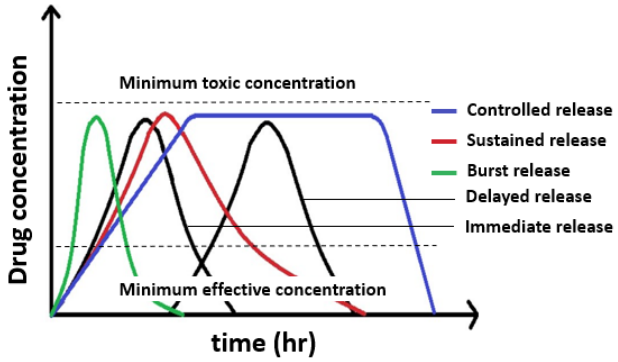

Figure 4.21 : Drug release kinetics [134].

The Zero Order Model is an ideal model for linear drug release profiles. In this model, drug release rate is independent of drug concentration. In addition, this model is usually used in transdermal, oral control release, osmotic pressure, and tablet with low solubility drug applications [109,110].

The First Order Model is attributed to the loaded-drug amount in the solution and depends on only the initial drug concentration. In addition, this model is favorable for sustained release systems. Moreover, this model has several drug applications, such as dissolution-controlled release, diffusion-controlled release, and sustained release systems [109,110].

The Higuchi Model is described as a diffusion process. It is also based on Fick's square root time-dependent law. This model, one of the first models to explain drug solubility from matrix systems after 1960, helps to identify the drug kinetics dispersed in a solid matrix. According to Higuchi Model, drug release occurs with Fickian diffusion [110].

The Korsmeyer-Peppas Model describes the exponential correlation between release and time in release kinetics. This model is often used to investigate drug delivery from sources like tablets, membranes, hydrogels, and fibers. The explanation of the value of n according to the drug transport mechanism is shown in Table 4.6 below [110].

Table 4.6 : Drug mechanism model by n value [135].

Exponent (n)	Drug Release Mechanism
$n \leq 0.45$	Fickian diffusion (Case I diffusional)
$0.45 < n < 0.89$	Anomalous (non-Fickian) diffusion
$n = 0.89$	Zero Order (Case II transport)
$n > 0.89$	Super case II transport

The Hixson-Crowell model is a kinetic model based on two assumptions. The first assumption is that drug release is limited only by drug dissolution rate. The second assumption is to keep the initial shape constant in matrix erosion and reduce the size of the matrix. In the Hixson-Crowell model, drug release does not occur by diffusion. Dissolution varies with surface area and particle diameter [110].

Mathematically modeling the release kinetics in this study helps to optimize existing drug delivery nanosystems and to design a polymer-based therapeutic systems in which the drug will be released at the required rate and concentration [134]. In this study, various kinetic models were used in order to interpret drug release mechanisms and kinetics mathematically. For this purpose, drug release data were adapted to 5 different drug release kinetic models. The parameters calculated for the Zero Order, First Order, Higuchi, Korsmeyer-Peppas, and Hixson-Crowell Models are shown in Table 4.7.

Table 4.7 : Parameters of kinetic models in drug delivery.

Kinetic Models	Parameters	Drug Delivery Systems (MTX/hBN ratio)			
		pH 4.5		pH 7.4	
		2.5/3.0	5.0/3.0	2.5/3.0	5.0/3.0
Zero Order	k_0	3.6201	1.6306	0.2007	1.2251
	R^2	0.8645	0.7477	0.3722	0.7683
First Order	k_F	3.6201	1.6306	0.2007	1.2251
	R^2	0.8698	0.7482	0.3718	0.7695
Higuchi	k_H	6.9135	3.2058	0.3918	2.3884
	R^2	0.9420	0.8615	0.4105	0.8679

Table 4.7 (continue) : Parameters of kinetic models in drug delivery.

Kinetic Models	Parameters	Drug Delivery Systems (MTX/hBN ratio)			
		pH 4.5		pH 4.5	
		2.5/3.0	2.5/3.0	2.5/3.0	2.5/3.0
Korsmeyer-Peppas	k_P	2.8032	2.0407	0.2445	1.3446
	R^2	0.9399	0.9195	0.2943	0.8997
	n	0.2703	0.1782	0.1826	0.2054
Hixson-Crowell	k_S	0.0974	0.1041	0.1088	0.1054
	R^2	0.8645	0.7477	0.3722	0.7683

When each data set was evaluated (Figure 4.22), it was found that the release mechanism at pH 4.5 for the 2.5/3.0 system could be explained by Higuchi (R^2=0.94) model. Since the highest R^2 value at pH 7.4 was 0.41, no release kinetic model in this study was suitable for the system. Furthermore, for the 5.0/3.0 system, both release mechanisms at pH 4.5 and 7.4 were explained by the Korsmeyer-Peppas model (R^2=0.92, R^2=0.90, respectively).

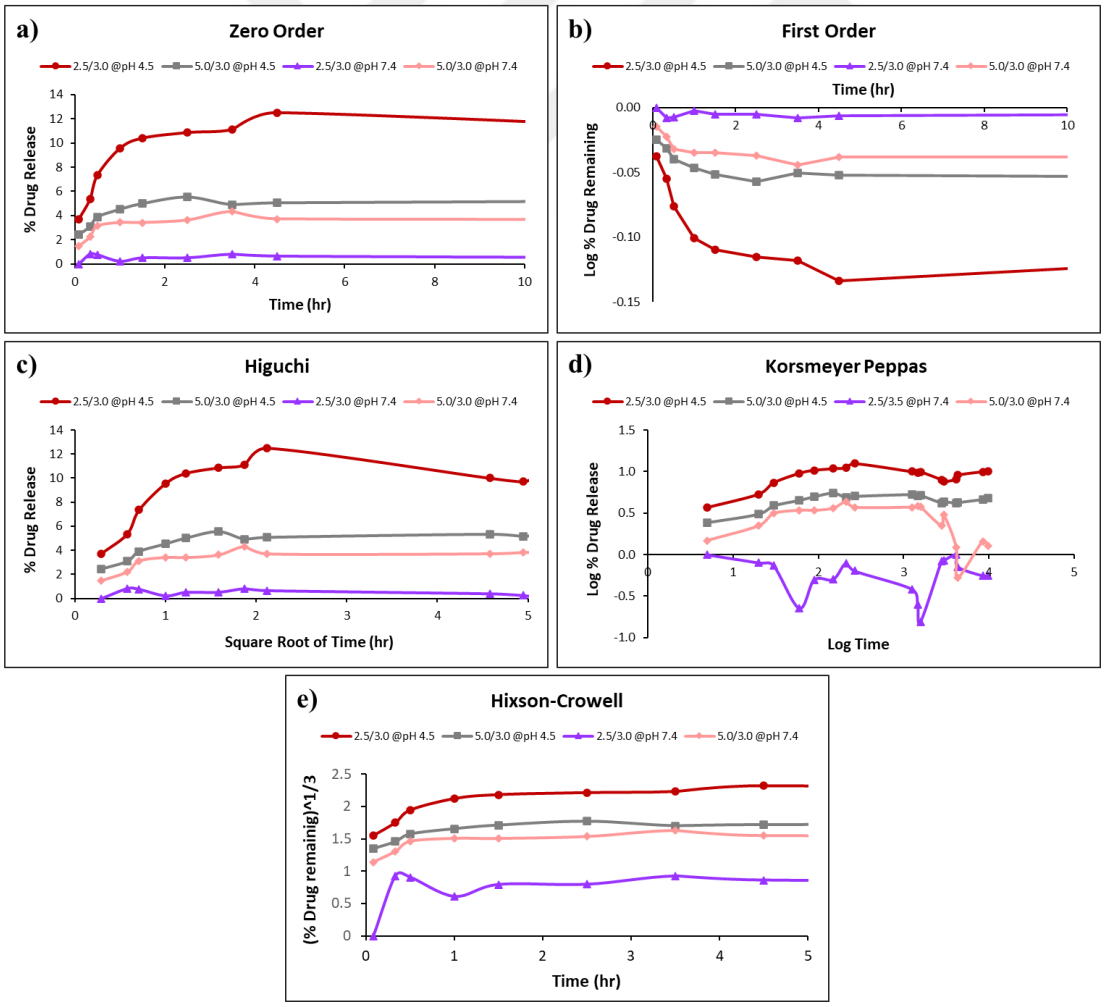

Figure 4.22 : Release kinetic models of MTX-hBN nanosystems; a) Zero Order, b) First Order, c) Higuchi, d) Korsmeyer-Peppas, and e) Hixson-Crowell.

In addition, the n value characterizing the release mechanism of the drug in the Korsmeyer-Peppas model was found to be less than 0.45 in all systems except the system (2.5/3.0) at pH 7.4 medium with the lowest R^2 value. In this case, the drug release mechanism of all systems corresponds to the diffusion mechanism obeying Fick's law and is compatible with the literature [109,135].

4.4 Statistical Analysis Results

Drug loading and release data were analyzed statistically, as demonstrated by one-way ANOVA analysis. Since $p>0.05$ according to drug loading data in pH 6.0 medium, there was no difference observed between the means of any groups. On the other hand, in the loading data in pH 9.0 medium, a statistically significant difference was found at a very high level, as it was much smaller than $p<0.05$. Likewise, all of the drug release data in pH 4.5 and 7.4 mediums were much smaller than $p<0.05$; therefore, a very high statistically significant difference was noticed. According to the one-way ANOVA test results, the t-test was performed to reveal the difference between which groups in the data with a statistically significant *p* value. When comparing the 2.5/3.0 versus 5.0/3.0 nanosystem in loading data at pH 9.0, there was no difference between them; however, at pH 4.5 and 7.4, there was a very high statistically significant difference between these nanosystems.

5. CONCLUSIONS

Cancer treatment is an area where many disciplines, such as genetics, medicine, biochemistry, and molecular biology, work together and aim to prevent millions of deaths. For an effective treatment, it is aimed that cancer drugs affect the tumor area in a minimum time and with maximum efficiency. At the same time, the damage to healthy tissues should be minimal. Hexagonal boron nitrides (hBN), which are nanosized and have a surface small enough to easily enter the targeted cell, are a structural analog of carbon-based graphene material, and draw attention with their non-toxicity when compared to other nanocarriers used in cancer treatment. However, according to some studies, since the biocompatibility of hBNs has not yet been determined and the biocompatibility varies according to the size, shape, and surface area of the nanomaterial, these materials may need to be functionalized.

In this study, drug transport and release performances of hBNs, which were successfully synthesized by Chemical Vapor Depotision (CVD) method and with high purity, were investigated in detail. The non-covalent interaction of hBNs with the Mitoxantrone anticancer drug chosen as the model drug, was investigated for the first time in this study, which made the study innovative.

The most important step in designing a drug delivery system in cancer therapy is the synthesis of the nanocarrier. The properties of each nanomaterial vary according to the raw materials and the synthesis method. After synthesizing hBNs with boric acid as a boron precursor, various characterization analyses were performed and their morphological and spectroscopic structures were extensively investigated. According to the analysis results, the synthesis was carried out successfully because the hBNs were of high purity, uniform, and similar to thrombocytes.

To design a drug-hBN nanosystem in cancer treatment, the drug loading capacity of hBNs in different pH mediums (6.0 ve 9.0) was investigated by UV/Vis spectroscopy by keeping the hBN amount constant at a different drug:hBN (1.25/3.0 mg/mg, 2.5/3.0 mg/mg, 5.0/3.0 mg/mg) ratios. Drug loading results were 6.0% (0.024 mg/mg), 4.6% (0.036 mg/mg), 6.3% (0.102 mg/mg) for pH 6.0 medium based on 1.25/3.0 mg/mg,

2.5/3.0 mg/mg and 5.0/3.0 mg/mg MTX/hBN ratios, respectively; 20% (0.111 mg/mg), 27.9% (0.284 mg/mg), 32.8% (0.657 mg/mg) for pH 9.0 medium, respectively, was performed. The amount of drug loading increased when the amount of the drug increased in loading solution. Thus, the optimum drug loading condition for the MTX-hBN system is the 5.0/3.0 MTX/hBN system in a pH 9.0 medium.

The peaks at about 778 and 1352 cm^{-1} observed in the FT-IR spectra of the MTX-hBN nanosystem corresponded to B-N-B and B-N vibrations from hBN, respectively. In addition, the slight peaks between at 1231-1021 cm^{-1} belong to the C-H bonds in the chain from MTX. Furthermore, a weak peak attributed to the -OH bond was observed for MTX-hBN at 3197 cm^{-1}. Moreover, the absence of any peaks in the functional group region (4000-1450 cm^{-1}) proved that there were not any functional groups in the MTX-hBN system.

It was clearly seen in SEM images that, the morphology of pure hBNs has completely changed after drug-loading process. That means, MTX molecules cover the hBNs surfaces and drug-loading was performed successfully.

In the size distribution analysis performed according to the DLS method, hBNs with a size of 184.4 before drug loading and a size of 566.9 after drug loading showed that an effective drug loading has occurred. In Zeta potential results, the MTX-hBN nanosystem, which was formed after the interaction of -14.0 mV loaded hBNs with -30.15 mV loaded MTX drug molecule, proved to be a more stable system than hBNs, with -27.8 mV load.

Cumulative drug release studies were observed by UV/Vis spectroscopy in two different pH mediums, which reflect the pH of the cancer cell (pH 4.5) and the healthy cell (pH 7.4) and bloodstream (pH 7.4). Based on the drug loading efficiency results, 2.5/3.0 and 5.0/3.0 MTX/hBN systems were selected for release studies. Drug release were 12.5% (0.033 mg/mg) and 5.5% (0.018 mg/mg) for the pH 4.5 medium and 0.9% (0.005 mg/mg) and 4.3% (0.011 mg/mg) for the pH 7.4 medium, based on the 2.5/3.0 mg/mg and 5.0/3.0 mg/mg MTX/hBN ratios, respectively. Accordingly, the drug release performance can be summarized as 2.5/3.0 @pH 4.5 > 5.0/3.0 @pH 4.5 > 5.0/3.0 @pH 7.4 > 2.5/3.0 @pH 7.4.

Moreover, it was determined that drug release was less than 50% in both systems, and MTX drug molecules formed a strong π-π interaction on the nanosurface of hBNs. In

addition, the stronger π-π interaction between hBNs and MTX in the 2.5/3.0 mg/mg nanosystem indicates that drug release occurs in a lower amount. Based on these results, the most successful MTX-hBN nanosystem showing both maximum release in pH 4.5 and minimum drug leakage in pH 7.4, was the 2.5/3.0 mg/mg nanosystem. When both drug loading and drug release performances are evaluated together, the optimum MTX-hBN medium is the drug-loaded MTX-hBN nanosystem at a ratio of 2.5/3.0 mg/mg in a pH 9.0 medium. For this reason, FT-IR, SEM, Zeta potential, and size distribution analyzes were performed for this nanosystem to examine the drug loading performance.

According to the drug kinetic models examined in detail with several release mechanisms, all drug releases except for the lowest R^2 value at pH 7.4 medium, corresponded to the diffusion mechanism obeying Fick's law as expected.

When all the data obtained are evaluated, it can be said that the MTX-hBN nanosystem, which is designed as an alternative treatment method for cancer disease, is significantly promising and will be played a very important role, especially in targeted cancer treatment.

In future studies, functionalization with appropriate biomaterials is envisaged in order to increase the drug-loading capacity and completely eliminate the limited uncertainty on the biocompatibility of hBNs. Although there is no functionalization requirement in the use of hBN as nanocarriers, functionalization can be made with various biomaterials in order to strengthen its structure, to make hBNs dispersed, to increase the loading-capacity, and to add appropriate targeting agent. For future studies, the functionalization of hBNs by sonication can be recommended as it is a cheaper method and does not involve any additional process for purification. Another suggestion is that according to studies in the literature, drug-loading efficiency increased almost 3 times after functionalization with Folic acid biomolecule which was chosen for the targeting agent. It is suggested that functionalization studies can be performed with various biomolecules such as Fmoc-Glycine, Fmoc-Cysteine, Fmoc-Tryptophan amino acids.

Moreover, a dispersion experiment can be performed to support Zeta potential results and to make a comment about the blood stay condition of the drug-loaded nanosystem. Furthermore, drug-loading capacity can also be increased by loading studies in cold

conditions. In addition, in order to save both time and material for the functionalization process, suitable simulation studies can be carried out before the experimental studies.

REFERENCES

[1] **A. Deb and R. Vimala,** "Natural and synthetic polymer for graphene oxide mediated anticancer drug delivery—A comparative study" *Int. J. Biol. Macromol.*, vol. 107, pp. 2320–2333, 2018.

[2] **R. Misra, S. Acharya, and S. K. Sahoo,** "Cancer nanotechnology: Application of nanotechnology in cancer therapy" *Drug Discov. Today*, vol. 15, no. 19–20, pp. 842–850, 2010.

[3] **U. Version and C. Articles,** "The Surface Properties of Cancer Cells: A Review" *Cancer Res.*, pp. 525–548, 1962.

[4] **S. Nie, Y. Xing, G. J. Kim, and J. W. Simons**, "Nanotechnology applications in cancer" *Annu. Rev. Biomed. Eng.*, vol. 9, pp. 257–288, 2007.

[5] **P. Kumari, B. Ghosh, and S. Biswas,** "Nanocarriers for cancer-targeted drug delivery" *J. Drug Target.*, vol. 24, no. 3, pp. 179–191, 2016.

[6] **H. Sung *et al.*,** "Global Cancer Statistics 2020: GLOBOCAN Estimates of Incidence and Mortality Worldwide for 36 Cancers in 185 Countries" *CA. Cancer J. Clin.*, vol. 71, no. 3, pp. 209–249, 2021.

[7]**Url-1,** [Online]. Available: <*https://www.drozdogan.com/turkiye-kanser-istatistikleri-2020*> date retrieved 03.08.2022.

[8] **J. E. Hulla, S. C. Sahu, and A. W. Hayes,** "Nanotechnology: History and future" *Hum. Exp. Toxicol.*, vol. 34, no. 12, pp. 1318–1321, 2015.

[9] **L. Zhang and T. J. Webster,** "Nanotechnology and nanomaterials: Promises for improved tissue regeneration" *Nano Today*, vol. 4, no. 1, pp. 66–80, 2009.

[10] **V. Grecchi and G. Turchetti,** "P and P′ from high-energy sum rules" *Nuovo Cim. A*, vol. 56, no. 3, pp. 786–789, 1968.

[11] **I. I. Lungu, A. M. Grumezescu, A. Volceanov, and E. Andronescu,** "Nanobiomaterials used in cancer therapy: An up-to-date overview", *Molecules*, vol. 24, no. 19, pp. 1–21, 2019.

[12] **S. Naz, M. Shamoon, R. Wang, L. Zhang, J. Zhou, and J. Chen,** "Advances in therapeutic implications of inorganic drug delivery nano-platforms for cancer" *Int. J. Mol. Sci.*, vol. 20, no. 4, pp. 1–17, 2019.

[13] **Z. Yang, Y. Ma, H. Zhao, Y. Yuan, and B. Y. S. Kim,** "Nanotechnology platforms for cancer immunotherapy" *Wiley Interdiscip. Rev. Nanomedicine Nanobiotechnology*, vol. 12, no. 2, pp. 1–28, 2020.

[14] **Farah Hamad Farah,** "Nanocarriers As Delivery Systems for Therapeutics Agents" *Int. J. Pharm. Sci. Res.*, vol. 10, no. 8, pp. 3487–3507, 2019.

[15] **K. Park,** "Controlled drug delivery systems: Past forward and future back" *J. Control. Release*, vol. 190, pp. 3–8, 2014.

[16] **M. N. Singh, K. S. Y. Hemant, M. Ram, and H. G. Shivakumar,** "Microencapsulation: A promising technique for controlled drug delivery" *Res. Pharm. Sci.*, vol. 5, no. 2, pp. 65–77, 2010.

[17] **H. Park, A. Otte, and K. Park,** "Evolution of drug delivery systems: From 1950 to 2020 and beyond" *J. Control. Release*, vol. 342, no. December 2021, pp. 53–65, 2022.

[18] **M. Ebadi, S. Bullo, K. Buskara, M. Z. Hussein, S. Fakurazi, and G. Pastorin,** "Release of a liver anticancer drug, sorafenib from its PVA/LDH- and PEG/LDH-coated iron oxide nanoparticles for drug delivery applications" *Sci. Rep.*, vol. 10, no. 1, pp. 1–19, 2020.

[19] **A. D. Nurhan,** "Dash, Murthy" *Polish Pharm. Soc.*, vol. 67, no. 3, pp. 217–223, 2010.

[20] **O. S. Fenton, K. N. Olafson, P. S. Pillai, M. J. Mitchell, and R. Langer,** "Advances in Biomaterials for Drug Delivery" *Adv. Mater.*, vol. 30, no. 29, pp. 1–29, 2018.

[21] **P. Selvam and S. K. Mohapatra,** "Synthesis , characterization and catalytic properties of mesoporous TiHMA molecular sieves : selective oxidation of cycloalkanes" vol. 73, pp. 137–149, 2004.

[22] **S. Mitragotri and P. Stayton,** "Organic nanoparticles for drug delivery and imaging" *MRS Bull.*, vol. 39, no. 3, pp. 219–223, 2014.

[23] **S. Y. Lim, W. Shen, and Z. Gao,** "Chem Soc Rev" pp. 362–381, 2015.

[24] **D. Bera, L. Qian, T. Tseng, and P. H. Holloway,** "Quantum Dots and Their Multimodal Applications: A Review" pp. 2260–2345, 2010.

[25] **S. K. Prajapati, A. Malaiya, P. Kesharwani, D. Soni, and A. Jain,** "Biomedical applications and toxicities of carbon nanotubes" *Drug Chem. Toxicol.*, vol. 45, no. 1, pp. 435–450, 2022.

[26] **Michael F. L.; De Volder, Sameh H.; Tawfick, Ray H.; Baughman, and A. John,** "Carbon Nanotubes: Present and Future Commercial Applications" *Science (80-.).*, vol. 339, no. 6119, pp. 535–539, 2013.

[27] **S. Iijima,** "Carbon nanotubes: past, present, and future" vol. 323, pp. 1–5, 2002.

[28] **C. Bárcena, A. K. Sra, and J. Gao,** "Applications of magnetic nanoparticles in biomedicine" *Nanoscale Magn. Mater. Appl.*, vol. 167, pp. 591–626, 2009.

[29] **A. Akbarzadeh, R. Rezaei-sadabady, S. Davaran, S. W. Joo, and N. Zarghami,** "Liposome : classification , preparation , and applications" pp. 1–9, 2013.

[30] **N. Filipczak, J. Pan, S. S. K. Yalamarty, and V. P. Torchilin,** "Recent advancements in liposome technology" *Adv. Drug Deliv. Rev.*, vol. 156, pp. 4–22, 2020.

[31] **H. M. Aliabadi and A. Lavasanifar,** "Polymeric micelles for drug delivery" *Expert Opin. Drug Deliv.*, vol. 3, no. 1, pp. 139–162, 2006.

[32] **Z. Ahmad, A. Shah, M. Siddiq, and H. B. Kraatz,** "Polymeric micelles as drug delivery vehicles" *RSC Adv.*, vol. 4, no. 33, pp. 17028–17038, 2014.

[33] **M. T. Chevalier, J. Gonzalez, and V. Alvarez,** "Biodegradable polymeric microparticles as drug delivery devices" *IFMBE Proc.*, vol. 49, pp. 187–190, 2015.

[34] **B. Begines *et al.*,** "Polymeric nanoparticles for drug delivery: Recent developments and future prospects" *Nanomaterials*, vol. 10, no. 7, pp. 1–41, 2020.

[35] **P. Kesharwani, K. Jain, and N. K. Jain,** "Dendrimer as nanocarrier for drug delivery" *Prog. Polym. Sci.*, vol. 39, no. 2, pp. 268–307, 2014.

[36] **R. Duncan and L. Izzo,** "Dendrimer biocompatibility and toxicity" *Adv. Drug Deliv. Rev.*, vol. 57, no. 15, pp. 2215–2237, 2005.

[37] **J. H. Lee and Y. Yeo,** "Controlled drug release from pharmaceutical nanocarriers" *Chem. Eng. Sci.*, vol. 125, pp. 75–84, 2015.

[38] **M. F. Attia, N. Anton, J. Wallyn, Z. Omran, and T. F. Vandamme,** "An overview of active and passive targeting strategies to improve the nanocarriers efficiency to tumour sites" *J. Pharm. Pharmacol.*, vol. 71, no. 8, pp. 1185–1198, 2019.

[39] **R. van der Meel,** *Targeted inhibiton of tumor growth and angiogenesis*. 2013.

[40] **H. Khodabandehloo, H. Zahednasab, and A. A. Hafez,** "Nanocarriers usage for drug delivery in cancer therapy" *Int. J. Cancer Manag.*, vol. 9, no. 2, 2016.

[41] **M. Karimi *et al.*,** "Temperature-Responsive Smart Nanocarriers for Delivery of Therapeutic Agents: Applications and Recent Advances" *ACS Appl. Mater. Interfaces*, vol. 8, no. 33, pp. 21107–21133, 2016.

[42] **W. Gao, J. M. Chan, and O. C. Farokhzad,** "reviews pH-Responsive Nanoparticles for Drug Delivery" vol. 7, no. 6, pp. 1913–1920, 2010.

[43] **W. Hong, C. C. Liu, H. Zhang, Z. Chen, M. Xiao, and L. Xu,** "Cancer Cell Preferential Penetration and pH-Responsive Drug Delivery of Oligorutin" *Biomacromolecules*, vol. 22, no. 9, pp. 3679–3691, 2021.

[44] **J. Z. Du, X. J. Du, C. Q. Mao, and J. Wang,** "Tailor-Made dual pH-sensitive polymer-doxorubicin nanoparticles for efficient anticancer drug delivery" *J. Am. Chem. Soc.*, vol. 133, no. 44, pp. 17560–17563, 2011.

[45] **P. Mi *et al.*,** "Hybrid Calcium Phosphate-Polymeric Micelles Incorporating Gadolinium Chelates for Imaging-Guided Gadolinium Neutron Capture Tumor Therapy" *ACS Nano*, vol. 9, no. 6, pp. 5913–5921, 2015.

[46] **Z. Zhen and H. Zhu,** *Structure and properties of graphene*. Elsevier Inc., 2017.

[47] **S. Iijima,** Helical microtubules of graphitic carbon. Nature. 1991; 354(6348):56-8.

[48] **S. Senapati, A. K. Mahanta, S. Kumar, and P. Maiti,** "Controlled drug delivery vehicles for cancer treatment and their performance" *Signal Transduct. Target. Ther.*, vol. 3, no. 1, pp. 1–19, 2018.

[49] **Z. Jia, Z. Wang, J. Liang, B. Wei, and D. Wu,** "Production of short multi-walled carbon nanotubes" *Carbon N. Y.*, vol. 37, no. 6, pp. 903–906, 1999.

[50] **H. He, L. A. Pham-Huy, P. Dramou, D. Xiao, P. Zuo, and C. Pham-Huy,** "Carbon nanotubes: Applications in pharmacy and medicine" *Biomed Res. Int.*, vol. 2013.

[51] **L. Feng and Z. Liu,** vol. 6, pp. 317–324, 2011.

[52] **A. K. Geim and K. S. Novoselov,** "The rise of graphene" *Nanosci. Technol. A Collect. Rev. from Nat. Journals*, pp. 11–19, 2009.

[53] **G. Ciofani and V. Mattoli,** *Boron nitride nanotubes in nanomedicine*. 2016.

[54] **A. Pakdel, C. Zhi, Y. Bando, and D. Golberg,** "Low-dimensional boron nitride nanomaterials" *Mater. Today*, vol. 15, no. 6, pp. 256–265, 2012.

[55] **V. Sharma, H. L. Kagdada, P. K. Jha, P. Śpiewak, and K. J. Kurzydłowski,** "Thermal transport properties of boron nitride based materials: A review" *Renew. Sustain. Energy Rev.*, vol. 120, no. October 2019, 2020.

[56] **J. Yin *et al.*,** "Boron Nitride Nanostructures: Fabrication, Functionalization and Applications" *Small*, vol. 12, no. 22, pp. 2942–2968, 2016.

[57] **A. Manuscript,** "Nanoscale," no. 207890, 2010.

[58] **M. Li *et al.*,** "Perspectives on environmental applications of hexagonal boron nitride nanomaterials" *Nano Today*, vol. 44, p. 101486, 2022.

[59] **X. Wang, C. Zhi, Q. Weng, Y. Bando, and D. Golberg,** "Boron nitride nanosheets: Novel syntheses and applications in polymeric composites" *J. Phys. Conf. Ser.*, vol. 471, no. 1, 2013.

[60] **D. Golberg *et al.*,** "Boron nitride nanotubes and nanosheets" *ACS Nano*, vol. 4, no. 6, pp. 2979–2993, 2010.

[61] **S. M. Sharker,** "Hexagonal boron nitrides (White graphene): A promising method for cancer drug delivery" *Int. J. Nanomedicine*, vol. 14, pp. 9983–9993, 2019.

[62] **M. Emanet, Ö. Şen, and M. Çulha,** "Evaluation of boron nitride nanotubes and hexagonal boron nitrides as nanocarriers for cancer drugs" *Nanomedicine*, vol. 12, no. 7, pp. 797–810, 2017.

[63] **A. Merlo, V. R. S. S. Mokkapati, S. Pandit, and I. Mijakovic,** "Boron nitride nanomaterials: Biocompatibility and bio-applications" *Biomater. Sci.*, vol. 6, no. 9, pp. 2298–2311, 2018.

[64] **S. Roy *et al.*,** "Structure, Properties and Applications of Two-Dimensional Hexagonal Boron Nitride" *Adv. Mater.*, vol. 33, no. 44, pp. 1–48, 2021.

[65] **C. Cazorla and T. Gould,** "Polymorphism of bulk boron nitride" *Sci. Adv.*, vol. 5, no. 1, pp. 1–6, 2019.

[66] **Y. Tsuji *et al.*,** "Adhesion of epoxy resin with hexagonal boron nitride and graphite" *ACS Omega*, vol. 4, no. 3, pp. 4491–4504, 2019.

[67] **X. F. Jiang *et al.*,** "Recent Progress on Fabrications and Applications of Boron Nitride Nanomaterials: A Review" *J. Mater. Sci. Technol.*, vol. 31, no. 6, pp. 589–598, 2015.

[68] **J. Wang, F. Ma, and M. Sun,** "Graphene, hexagonal boron nitride, and their heterostructures: properties and applications" *RSC Adv.*, vol. 7, no. 27, pp. 16801–16822, 2017.

[69] **R. Arenal and A. Lopez-Bezanilla,** "Boron nitride materials: An overview from 0D to 3D (nano)structures" *Wiley Interdiscip. Rev. Comput. Mol. Sci.*, vol. 5, no. 4, pp. 299–309, 2015.

[70] **T. E. Oconnor,** "Synthesis of boron nitride" *J. Am. Chem. Soc.*, vol. 84, no. 9, pp. 1753–1754, 1962.

[71] **R. Y. Tay,** *Chemical Vapor Deposition Growth and Characterization of Two-Dimensional Hexagonal Boron Nitride*. 2018.

[72] **V. Vatanpour, S. A. Naziri Mehrabani, B. Keskin, N. Arabi, B. Zeytuncu, and I. Koyuncu,** "A Comprehensive Review on the Applications of Boron Nitride Nanomaterials in Membrane Fabrication and Modification" *Ind. Eng. Chem. Res.*, 2021.

[73] **J. H. Ramirez Leyva *et al.*,** "Mechanism of Hierarchical Porosity Development in Hexagonal Boron Nitride Nanocrystalline Microstructures for Biomedical and Industrial Applications" *ACS Appl. Nano Mater.*, vol. 1, no. 9, pp. 4491–4501, 2018.

[74] **B. Y. Irem Culha Taskin, Ozlem Sen, Melis Emanet, Mustafa Culha,** "Biocompatibility evaluation of hexagonal boron nitrides on healthy mouse hippocampal cell line and their positive effect on stressed cells" pp. 0–20, 2019.

[75] **D. V. Shtansky, K. L. Firestein, and D. V. Golberg,** "Fabrication and application of BN nanoparticles, nanosheets and their nanohybrids" *Nanoscale*, vol. 10, no. 37, pp. 17477–17493, 2018.

[76] **H. Zhang, T. Yamazaki, C. Zhi, and N. Hanagata,** "Identification of a boron nitride nanosphere-binding peptide for the intracellular delivery of CpG oligodeoxynucleotides" *Nanoscale*, vol. 4, no. 20, pp. 6343–6350, 2012.

[77] **M. Emanet, Ö. Sen, I. Ç. Taşkin, and M. Çulha,** "Synthesis, Functionalization, and Bioapplications of Two-Dimensional Boron Nitride Nanomaterials" *Front. Bioeng. Biotechnol.*, vol. 7, no. December, 2019.

[78] **H. Zhang, S. Chen, C. Zhi, T. Yamazaki, and N. Hanagata,** "Chitosan-coated boron nitride nanospheres enhance delivery of CpG oligodeoxynucleotides and induction of cytokines" *Int. J. Nanomedicine*, vol. 8, pp. 1783–1793, 2013.

[79] **S. Mateti *et al.*,** "Biocompatibility of boron nitride nanosheets" *Nano Res.*, vol. 11, no. 1, pp. 334–342, 2018.

[80] **S. Feng *et al.*,** "Folate-conjugated boron nitride nanospheres for targeted delivery of anticancer drugs" *Int. J. Nanomedicine*, vol. 11, pp. 4573–4582, 2016.

[81] **X. Li *et al.*,** "Hollow boron nitride nanospheres as boron reservoir for prostate cancer treatment" *Nat. Commun.*, vol. 8, pp. 1–2, 2017.

[82] **I. V Sukhorukova, I. Y. Zhitnyak, A. M. Kovalskii, and A. T. Matveev,** "BN nanoparticles with petal-like surface as anticancer drug delivery system" pp. 1-26.

[83] **A. Salvetti *et al.*,** "In vivo biocompatibility of boron nitride nanotubes: Effects on stem cell biology and tissue regeneration in planarians" *Nanomedicine*, vol. 10, no. 12, pp. 1911–1922, 2015.

[84] **M. Jedrzejczak-Silicka, M. Trukawka, M. Dudziak, K. Piotrowska, and E. Mijowska,** "Hexagonal boron nitride functionalized with Au nanoparticles—properties and potential biological applications" *Nanomaterials*, vol. 8, no. 8, 2018.

[85] **T. Lu, L. Wang, Y. Jiang, Q. Liu, and C. Huang,** "Hexagonal boron nitride nanoplates as emerging biological nanovectors and their potential applications in biomedicine" *J. Mater. Chem. B*, vol. 4, no. 36, pp. 6103–6110, 2016.

[86] **M. Nurunnabi, M. Nafiujjaman, S. J. Lee, I. K. Park, K. M. Huh, and Y. K. Lee,** "Preparation of ultra-thin hexagonal boron nitride nanoplates for cancer cell imaging and neurotransmitter sensing" *Chem. Commun.*, vol. 52, no. 36, pp. 6146–6149, 2016.

[87] **M. Kıvanç, B. Barutca, A. T. Koparal, Y. Göncü, S. H. Bostancı, and N. Ay,** "Effects of hexagonal boron nitride nanoparticles on antimicrobial and antibiofilm activities, cell viability" *Mater. Sci. Eng. C*, vol. 91, pp. 115–124, 2018.

[88] **G. Ciofani,** "Potential applications of boron nitride nanotubes as drug delivery systems" *Expert Opin. Drug Deliv.*, vol. 7, no. 8, pp. 889–893, 2010.

[89] **F. Kar *et al.*,** "In Vivo Assessment of the Effect of Hexagonal Boron Nitride Nanoparticles on Biochemical, Histopathological, Oxidant and Antioxidant Status" *J. Clust. Sci.*, vol. 32, no. 2, pp. 517–529, 2021.

[90] **B. J. S. Sanderson, L. R. Ferguson, and W. A. Denny,** "Mutagenic and carcinogenic properties of platinum-based anticancer drugs" *Mutat. Res. - Fundam. Mol. Mech. Mutagen.*, vol. 355, no. 1–2, pp. 59–70, 1996.

[91] **P. Halterman, N. J. Vogelzang, A. Farabishahadel, and O. B. Goodman,** "Mitoxantrone" *Drug Manag. Prostate Cancer*, vol. 18, no. 6, pp. 125–131, 2010.

[92] **C. R. Lee and D. Faulds,** "Altretamine: A Review of its Pharmacodynamic and Pharmacokinetic Properties, and Therapeutic Potential in Cancer Chemotherapy" *Drugs*, vol. 49, no. 6, pp. 932–953, 1995.

[93] **J. Wu, M. Lin, X. Weng, G. Owens, and Z. Chen,** "Pre-adsorption and Fenton-like oxidation of mitoxantrone using hybrid green synthesized rGO/Fe nanoparticles" *Chem. Eng. J.*, vol. 408, no. July, p. 127273, 2021.

[94] **S. Preethi, H. Kumar, V. B. Rawal, R. Ajmeer, and V. Jain,** "Overview of Mitoxantrone-a Potential Candidate for Treatment of Breast Cancer" *Int. J. Appl. Pharm.*, vol. 14, no. 2, pp. 10–22, 2022.

[95] **J. A. Neidhart, D. Gochnour, R. Roach, D. Hoth, and D. Young,** "A comparison of mitoxantrone and doxorubicin in breast cancer" *J. Clin. Oncol.*, vol. 4, no. 5, pp. 672–677, 1986.

[96] **Q. Weng *et al.*,** "Highly water-soluble, porous, and biocompatible boron nitrides for anticancer drug delivery" *ACS Nano*, vol. 8, no. 6, pp. 6123–6130, 2014.

[97] **S. M. Sharker, M. A. Alam, M. C. Shill, G. M. S. Rahman, and H. M. Reza,** "Functionalized hBN as targeted photothermal chemotherapy for complete eradication of cancer cells" *Int. J. Pharm.*, vol. 534, no. 1–2, pp. 206–212, 2017.

[98] **M. Vatanparast and Z. Shariatinia,** "Hexagonal boron nitride nanosheet as novel drug delivery system for anticancer drugs: Insights from DFT calculations and molecular dynamics simulations" *J. Mol. Graph. Model.*, vol. 89, pp. 50–59, 2019.

[99] **J. Ruan, K. Wang, H. Song, X. Xu, J. Ji, and D. Cui,** "Biocompatibility of hydrophilic silica-coated CdTe quantum dots and magnetic nanoparticles" *Nanoscale Res. Lett.*, vol. 6, no. 1, pp. 1–13, 2011.

[100] **Ö. Ç. Yıldırım *et al.*,** "Boron Nitride Nanoparticles Loaded with a Boron-Based Hybrid as a Promising Drug Carrier System for Alzheimer's Disease Treatment" *Int. J. Mol. Sci.*, vol. 23, no. 15, 2022.

[101] **S. S. Suri, H. Fenniri, and B. Singh,** "Nanotechnology-based drug delivery systems" *J. Occup. Med. Toxicol.*, vol. 2, no. 1, pp. 1–6, 2007.

[102] **N. A. Matrose, K. Obikese, Z. A. Belay, and O. J. Caleb,** "Journal Pre of" *Sci. Total Environ.*, p. 135907, 2019.

[103] **S. Onsori and E. Alipour,** "A computational study on the cisplatin drug interaction with boron nitride nanocluster" *J. Mol. Graph. Model.*, vol. 79, pp. 223–229, 2018.

[104] **Url-2,** [Online] The Chemical Structure of Mitoxantrone Dihydrochloride, Available:<*https://lktlabs.com/product/mitoxantrone-dihydrochloride*>; date retrieved 25.09.2022.

[105] **Ö. Şen, M. Emanet, and M. Çulha,** "One-step synthesis of hexagonal boron nitrides, their crystallinity and biodegradation" *Front. Bioeng. Biotechnol.*, vol. 9, no. JUN, pp. 1–9, 2018.

[106] **M. Emanet Ciofani, Ö. Şen, and M. Çulha,** "Hexagonal Boron Nitride Nanoparticles for Prostate Cancer Treatment" *ACS Appl. Nano Mater.*, vol. 3, no. 3, pp. 2364–2372, 2020.

[107] **A. Salis and M. Monduzzi,** "Not only pH. Specific buffer effects in biological systems" *Curr. Opin. Colloid Interface Sci.*, vol. 23, pp. 1–9, 2016.

[108] **E. Heister, V. Neves, C. Lamprecht, S. R. P. Silva, H. M. Coley, and J. McFadden,** "Drug loading, dispersion stability, and therapeutic efficacy in targeted drug delivery with carbon nanotubes" *Carbon N. Y.*, vol. 50, no. 2, pp. 622–632, 2012.

[109] **M. Barzegar-Jalali *et al.*,** "Kinetic analysis of drug release from nanoparticles" *J. Pharm. Pharm. Sci.*, vol. 11, no. 1, pp. 167–177, 2008.

[110] **M. Rostamitabar, A. M. Abdelgawad, S. Jockenhoevel, and S. Ghazanfari,** "Drug-Eluting Medical Textiles: From Fiber Production and Textile Fabrication to Drug Loading and Delivery" *Macromol. Biosci.*, vol. 21, no. 7, 2021.

[111] **H. Aydin,** "Nanoyapılı Hegzagonal Bor Nitrür Üretimi ve Karakterizasyonu" *Fırat Üniv. Müh. Bil. Derg. Sci. Eng. J Fırat Univ*, vol. 30, no. 2, pp. 269–275, 2018.

[112] **J. A. RAVEN,** "Short- and Long-Distance Transport of Boric Acid in Plants" *New Phytol.*, vol. 84, no. 2, pp. 231–249, 1980.

[113] **S. Bhatia,** *Natural polymer drug delivery systems: Nanoparticles, plants, and algae*. 2016.

[114] **Z. Lin, Y. Liu, K. Moon, and C. Wong,** "Enhanced Thermal Transport of Hexagonal Boron Nitride Filled Polymer Composite by Magnetic Field-assisted Alignmen" pp. 1692–1696, 2013.

[115] **M. Enache, A. M. Toader, and M. I. Enache,** "Mitoxantrone-surfactant interactions: A physicochemical overview" *Molecules*, vol. 21, no. 10, pp. 1–17, 2016.

[116] **M. Enache and A. M. Toader,** "Spectroscopic study of the interaction of anticancer drug mitoxantrone with sodium cholate aggregates" *Rev. Chim.*, vol. 69, no. 5, pp. 1060–1065, 2018.

[117] **Y. Liu, M. Wei, Y. Hu, L. Zhu, and J. Du,** "An electrochemical sensor based on a molecularly imprinted polymer for determination of anticancer drug Mitoxantrone" *Sensors Actuators, B Chem.*, vol. 255, pp. 544–551, 2018.

[118] **M. Hrubý, Č. Koňák, and K. Ulbrich,** "Polymeric micellar pH-sensitive drug delivery system for doxorubicin" *J. Control. Release*, vol. 103, no. 1, pp. 137–148, 2005.

[119] **S. Feng, H. Zhang, S. Xu, C. Zhi, H. Nakanishi, and X. D. Gao,** "Folate-conjugated, mesoporous silica functionalized boron nitride nanospheres for targeted delivery of doxorubicin" *Mater. Sci. Eng. C*, vol. 96, no. November 2018, pp. 552–560, 2019.

[120] **L. G. Rossato *et al.*,** "The metabolic profile of mitoxantrone and its relation with mitoxantrone-induced cardiotoxicity" *Arch. Toxicol.*, vol. 87, no. 10, pp. 1809–1820, 2013.

[121] **I. R. Stenglová-Netíková, L. Petruzelka, M. Stastny, and V. Stengl,** "Anthracycline antibiotics derivate mitoxantrone - Destructive sorption and photocatalytic degradation" *PLoS One*, vol. 13, no. 3, pp. 1–15, 2018.

[122] **H. Miller, M. H. Nathanson, and G. C. Griffith,** "The action of procaine amide in cardiac arrhythmias" *J. Am. Med. Assoc.*, vol. 146, no. 11, pp. 1004–1007, 1951.

[123] **Arslan, M. B.,** İlaç Taşıyıcı Sistem Olarak Kullanılacak PEG Kaplı Karbon Nanotüplerin Sentezi ve İlaç Taşıma Performanslarının Belirlenmesi (M.Sc. Thesis), 2021, Istanbul Technical University, Graduate School, Istanbul.

[124] **Kılıç, S.,** Fmoc-Aa Türevleri ve MTX Molekülünün Tek Duvarlı Karbon Nanotüp ile Etkileşimlerinin Moleküler Dinamik Simülasyonları Kullanılarak İncelenmesi (M.Sc. Thesis), 2022, Istanbul Technical University, Graduate School, Istanbul.

[125] **F. He, W. Cai, J. Lin, B. Yu, G. Owens, and Z. Chen,** "Reducing the impact of antibiotics in wastewaters: Increased removal of mitoxantrone from wastewater by biosynthesized manganese nanoparticles" *J. Clean. Prod.*, vol. 293, p. 126207, 2021.

[126] **Sigma Aldrich,** "IR Spectrum Table & Chart," *IR Spectrum Table & Chart*, *<https://www.sigmaaldrich.com/TR/en/technical-documents/technical-article/analytical-chemistry/photometry-and-reflectometry/ir-spectrum-table>* 2022.

[127] **Z. Xia, V. Rozyyev, A. U. Mane, J. W. Elam, and S. B. Darling,** "Surface Zeta Potential of ALD-Grown Metal-Oxide Films" *Langmuir*, vol. 37, no. 39, pp. 11618–11624, 2021.

[128] **P. G. Smith, M. N. Patel, J. Kim, K. P. Johnston, and T. E. Milner,** "Electrophoretic mobility measurement by differential-phase optical coherence tomography" *J. Phys. Chem. C*, vol. 111, no. 6, pp. 2614–2622, 2007.

[129] **A. Sze, D. Erickson, L. Ren, and D. Li,** "Zeta-potential measurement using the Smoluchowski equation and the slope of the current-time relationship in electroosmotic flow" *J. Colloid Interface Sci.*, vol. 261, no. 2, pp. 402–410, 2003.

[130] **S. Honary and F. Zahir,** "Effect of zeta potential on the properties of nano-drug delivery systems - A review (Part 1)" *Trop. J. Pharm. Res.*, vol. 12, no. 2, pp. 255–264, 2013.

[131] **K. Pate and P. Safier,** "Chemical metrology methods for CMP quality" *Adv. Chem. Mech. Planarization*, pp. 1–325, 2016.

[132] **R. Personal,** *Surfactants and Lipids*, Second Edi. Elsevier Inc., 2003.

[133] **B. Chang, X. Sha, J. Guo, Y. Jiao, C. Wang, and W. Yang,** "Thermo and pH dual responsive, polymer shell coated, magnetic mesoporous silica nanoparticles for controlled drug release" *J. Mater. Chem.*, vol. 21, no. 25, pp. 9239–9247, 2011.

[134] **N. Goonoo, A. Bhaw-Luximon, R. Ujoodha, A. Jhugroo, G. K. Hulse, and D. Jhurry,** "Naltrexone: A review of existing sustained drug delivery systems and emerging nano-based systems" *J. Control. Release*, vol. 183, no. 1, pp. 154–166, 2014.

[135] **M. P. Paarakh, P. A. N. I. Jose, C. M. Setty, and G. V Peter,** "Release Kinetics – Concepts and Applications" *Int. J. Pharm. Res. Technol.*, vol. 8, no. 1, pp. 12–20, 2019.

APPENDICES

APPENDIX A: UV Spectra

APPENDIX A

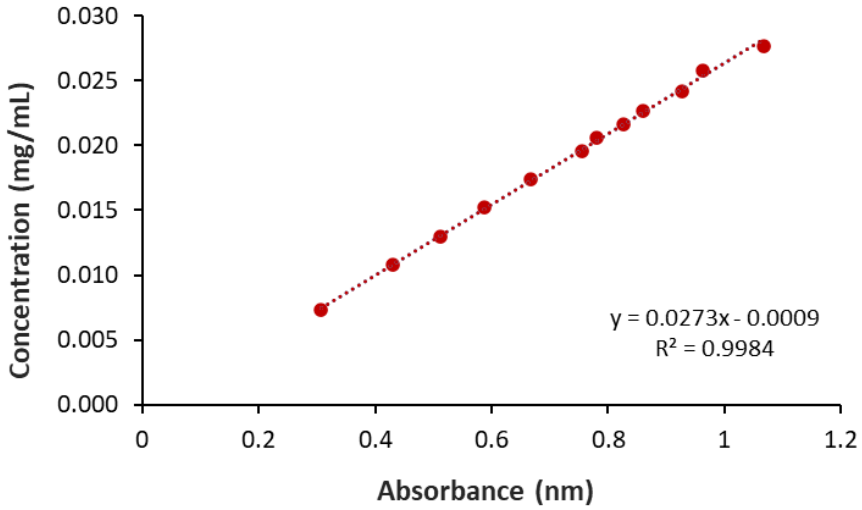

Figure A.1 : pH 6.0 medium Mitoxantrone molecule calibration curve.

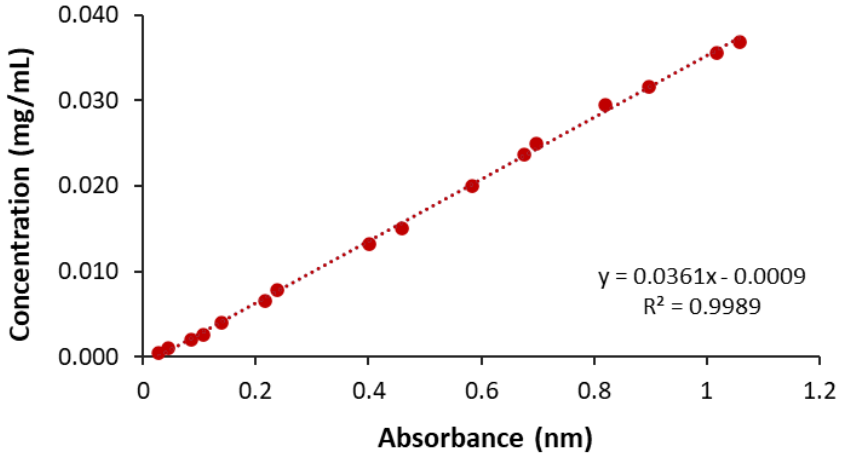

Figure A.2 : pH 9.0 medium Mitoxantrone molecule calibration curve.

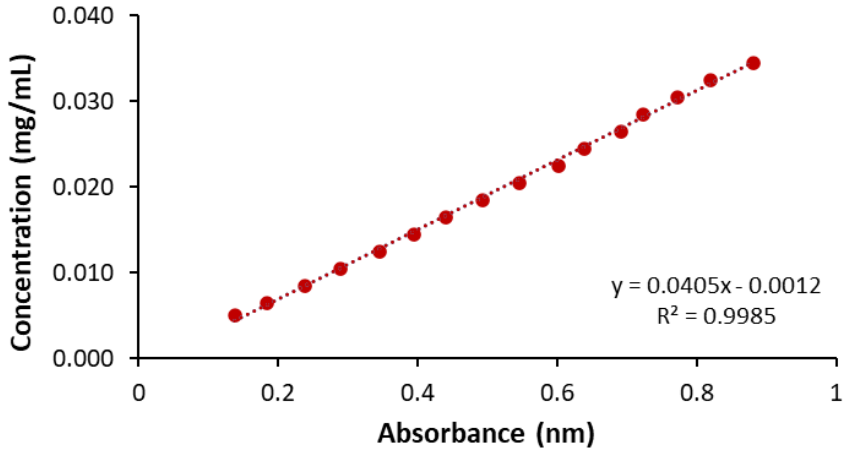

Figure A.3 : pH 8.0 medium Mitoxantrone molecule calibration curve.

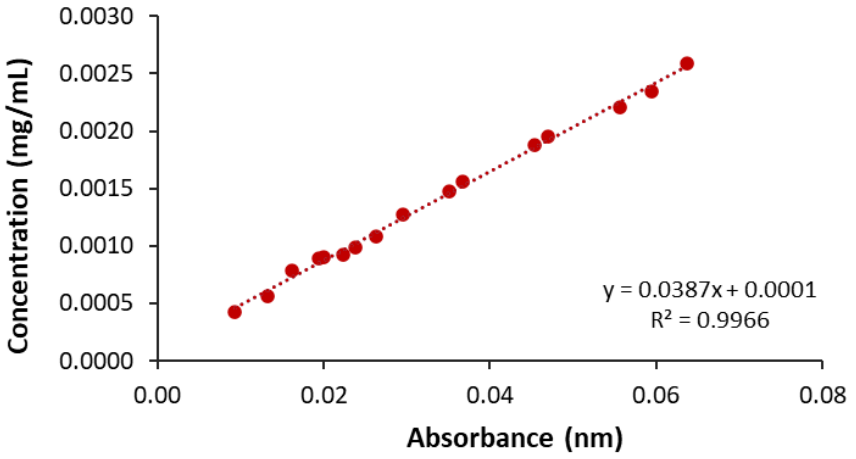

Figure A.4 : pH 4.5 medium Mitoxantrone molecule calibration curve.

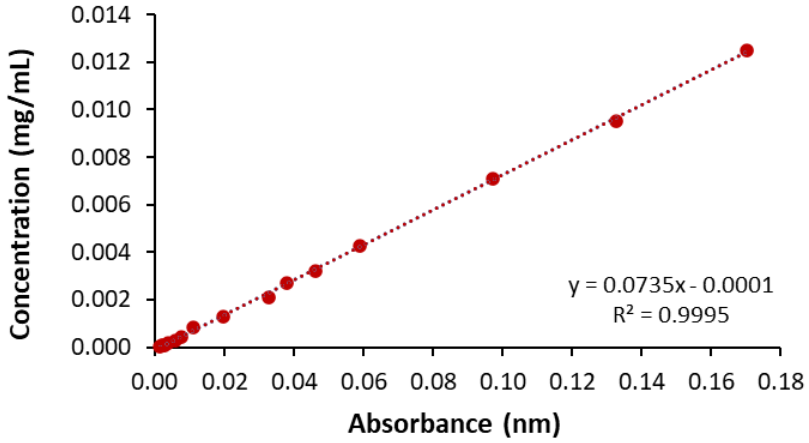

Figure A.5 : pH 7.4 medium Mitoxantrone molecule calibration curve.

CURRICULUM VITAE

Name Surname **:** Mısra YAMANSAVAŞÇILAR NAGANLU

EDUCATION

- **B.Sc.:** 2018, Istanbul University-Cerrahpaşa, Faculty of Engineering, Chemical Engineering Department
- **M.Sc.:** 2022, Istanbul Technical University, Faculty of Chemical and Metallurgical Engineering, Chemical Engineering Department

PROFESSIONAL EXPERIENCE AND REWARDS:

- 2022-present, Junior Regulatory Specialist, REACHLaw Turkey
- 2021-present, General Researcher, Istanbul Technical University Scientific Research Projects, General Research Project (BAP)
- 2018, Production Engineering Intern, Ali Raif İlaç Sanayi A.Ş.
- 2016, Laboratory Intern, Istanbul University-Cerrahpaşa Medical Faculty, Biochemistry Department

PUBLICATIONS, PRESENTATIONS AND PATENTS ON THE THESIS:

- **Yamansavascilar M.,** Kocaaga B., Cobandede Z., Yilmaz H., and Guner S. 2022: Bahcesehir University 8th International Drug Design Education Congress December 15-17, 2022 Istanbul, Turkey. (Short-talk presentation)